

**A BIG RESPONSE TO A “SMALL” PROBLEM: IDENTIFYING THE
OXIDATIVE POTENTIAL OF NANOPARTICLES AND THE
PHYSICOCHEMICAL CHARACTERISTICS THAT PLAY A ROLE**

A Dissertation

by

JAMES MICHAEL BERG

Submitted to the Office of Graduate Studies of
Texas A&M University
in partial fulfillment of the requirements for the degree of

DOCTOR OF PHILOSOPHY

December 2011

Major Subject: Toxicology

A Big Response to a “Small” Problem: Identifying the Oxidative Potential of
Nanoparticles and the Physicochemical Characteristics That Play a Role

Copyright 2011 James Michael Berg

**A BIG RESPONSE TO A “SMALL” PROBLEM: IDENTIFYING THE
OXIDATIVE POTENTIAL OF NANOPARTICLES AND THE
PHYSICOCHEMICAL CHARACTERISTICS THAT PLAY A ROLE**

A Dissertation

by

JAMES MICHAEL BERG

Submitted to the Office of Graduate Studies of
Texas A&M University
in partial fulfillment of the requirements for the degree of

DOCTOR OF PHILOSOPHY

Approved by:

Chair of Committee,
Committee Members,

Intercollegiate Faculty Chair,

Christie M. Sayes
Weston Porter
Stephen Safe
Andreas Holzenburg
Weston Porter

December 2011

Major Subject: Toxicology

ABSTRACT

A Big Response to a “Small” Problem: Identifying the Oxidative Potential of Nanoparticles and the Physicochemical Characteristics That Play a Role.

(December 2011)

James Michael Berg, B.S., Baylor University

Chair of Advisory Committee: Dr. Christie M. Sayes

Nanotechnology as a science is emerging rapidly. As materials are synthesized and utilized at the nanometer size scale, concerns of potential health and safety effects are arising. In this work, an effort to elucidate the physicochemical characteristics of nanoparticles influential in toxicological studies, surface properties of metal oxide and carbonaceous nanoparticles are measured. These properties include zeta potential, dissolution and surface-bound chemical components. Subsequently, the role of these properties in oxidative stress is examined *in vitro*.

This work identifies the influence that pH has on the zeta potential of nanoparticles. The zeta potential has the ability to alter colloidal stability, as the largest nanoparticle agglomerate is seen at or near the isoelectric point for each of the particles tested. Furthermore, it is observed that metal oxide nanoparticles, which exhibit a charged surface at physiological pH, lead to decreased *in vitro* cellular viability as compared to those that were neutral. Thus, nanoparticle zeta potential may be an important factor to consider when attempting to predict nanoparticle toxicity.

Real world exposure to nanoparticles is a mixture of various particulates and organics. Therefore, to simulate this particle mixture, iron oxide (Fe_2O_3) and engineered carbon black (ECB) are utilized in combination to identify potential synergistic reactions. Following *in vitro* exposure, both nanoparticle types are internalized into endosomes, where liberated Fe^{3+} reacts with hydroquinone moieties on the ECB surface yielding Fe^{2+} . This bioavailable iron may then generate oxidative stress through intracellular pathways including the Fenton reaction.

As oxidative stress is common in particulate toxicology, a comparison between the antioxidant defenses of epithelial (A549) and mesothelial (MeT-5A) cell lines is made. The A549 cell line exhibits alterations in the NRF2-KEAP1 transcription factor system and therefore retains high basal levels of phase II antioxidants. Both cell types are exposed to 33 nm silica where intracellular oxidant generation, coupled with markers of oxidative stress, are observed. While the MeT-5A cells exhibit a decrease in cell viability, the A549 cell line does not. Therefore, proper characterization of both material and biological systems prior to toxicity testing may help to further define the risks associated with the use of nanotechnology.

ACKNOWLEDGEMENTS

First and foremost, I would like to thank my committee chair, Dr. Christie Sayes, for her advice, mentorship, and guidance throughout the course of my studies at Texas A&M. Additionally, I would like to thank my committee members, Dr. Stephen Safe, Dr. Weston Porter, and Dr. Andreas Holzenburg, for their excellent teaching ability and dedication to graduate student education.

Furthermore, I would like to thank the toxicology program at Texas A&M University, including the faculty, staff, and graduate students, who helped to integrate multiple scientific fields necessary for the advancement of toxicology. The graduate students of the Texas A&M Toxicology program, past and present, were influential in the learning of novel techniques as well as scientific collaboration throughout my course of study.

I would also like to thank my collaborators who have provided influential input on multiple projects throughout the past years. The faculty and staff at the Texas A&M Microscopy Imaging Center, including Dr. Andreas Holzenburg, Dr. Christos Savva, Dr. Hansoo Kim, and Ms. Ann Ellis, were influential in my understanding of the electron microscope and microscopy specimen preparation. Additionally, Dr. Robert Burghardt and Dr. Ross Payne of the Image Analysis Lab, provided the resources and knowledge necessary for a variety of microscopy techniques.

With regard to nanoparticle synthesis and characterization, Dr. Bing Guo was influential in the preparation and analysis of Fe₂O₃ nanoparticles utilized in multiple

published studies from Dr. Christie Sayes' lab. Also influential in these analyses were Drs. Manual Soriaga and Kyle Cummins, who analyzed the surface of our nanostructures with x-ray photoelectron spectroscopy. Dr. Robert Taylor provided insight into, and experimental techniques with regards to trace metal analysis in nanoparticle samples.

The attitude throughout graduate school is often determined by the people who work alongside you. Therefore, I would like to thank my fellow co-workers, Amelia Romoser, Aishu Soores, and Ahmed Ridha, for their help and collaboration in every aspect of life.

Last, but not least, I would like to thank my family for their enduring support. My wife, Dr. Sarah Berg, has provided love, support, and encouragement throughout my research endeavors. Additionally, I would like to thank my mother and father for their love and endurance throughout this process.

TABLE OF CONTENTS

	Page
ABSTRACT	iii
ACKNOWLEDGEMENTS	v
TABLE OF CONTENTS	vii
LIST OF FIGURES	ix
LIST OF TABLES	xi
1. INTRODUCTION.....	1
1.1 Sources of Exposure to Engineered Nanoparticles and Their Mixtures.....	7
1.2 Physicochemical Properties Relevant to Nanoparticle Mixtures	15
1.3 Cell and Nanoparticle Interactions as a Preliminary Step in Toxicity	27
1.4 Oxidant Production	36
1.5 Summary	53
2. THE RELATIONSHIP BETWEEN pH AND ZETA POTENTIAL OF ~30 NM METAL OXIDE NANOPARTICLE SUSPENSIONS RELEVANT TO <i>IN VITRO</i> TOXICOLOGICAL EVALUATIONS.....	55
2.1 Introduction	55
2.2 Experimental Procedures.....	59
2.3 Results	63
2.4 Discussion	66
3. INTERNALIZATION OF CARBON BLACK AND MAGHEMITE IRON OXIDE NANOPARTICLE MIXTURES LEADS TO OXIDANT PRODUCTION	72
3.1 Introduction	73
3.2 Experimental Procedures.....	77
3.3 Results	83

	Page
3.4 Discussion	97
4. CELLULAR RESPONSE IS ASSOCIATED WITH ANTIOXIDANT ABILITY: A COMPARISON BETWEEN HUMAN PULMONARY EPITHELIAL AND MESOTHELIAL CELLS EXPOSED TO SiO ₂ NANOPARTICLES	103
4.1 Introduction	104
4.2 Experimental Procedures.....	108
4.3 Results	114
4.4 Discussion	130
5. CONCLUSIONS.....	136
REFERENCES.....	141
APPENDIX A	165
VITA	170

LIST OF FIGURES

FIGURE	Page
1.1 Internalization and oxidant production of nanoparticle mixtures.	6
1.2 Reductive ability of carbonaceous nanostructures	14
1.3 Fourier transform infrared spectroscopy of native and silane coated SiO ₂	21
1.4 Hierarchical model of oxidative stress	38
2.1 Schematic diagram of the effects of pH on a metal oxide nanoparticle.....	57
2.2 Titration of nanoparticles in ultrapure water	62
2.3 Alterations in zeta potential over time	65
2.4 Cellular viability after nanoparticle exposure	67
3.1 Intracellular nanomaterial localization analyses	87
3.2 Intracellular metal analysis of lung epithelial cells	89
3.3 Lysosomal characterization.....	91
3.4 Intracellular oxidant production	93
3.5 Cellular proliferation and viability	96
4.1 Cellular antioxidant characterization.....	115
4.2 Dose-response relationships to hydrogen peroxide.....	117
4.3 Characterization of SiO ₂ nanoparticles	119
4.4 Intracellular oxidant production and dose-response relationship.....	120
4.5 Glutathione depletion following exposure to SiO ₂ nanoparticles	122
4.6 NRF2 translocation schematic	123

FIGURE	Page
4.7 Time-dependent NRF2 protein expression	125
4.8 Stabilization of NRF2 transcription factor	126
4.9 mRNA levels of <i>nrf2</i> transcript	127
4.10 Cell line dependent induction of catalase.....	129

LIST OF TABLES

TABLE	Page
1.1 Inhalational exposure to nanoparticles and their mixtures.....	8
1.2 Physicochemical parameters influencing nanoparticle uptake.....	29
1.3 Dyes utilized to monitor the production of reactive oxygen species	44
1.4 Biological markers of oxidative stress and analytical techniques.....	48
2.1 Prediction of metal oxide nanomaterial properties in various pharmacodynamic environments	69
3.1 Characterization of Fe ₂ O ₃ , ECB, and ox-ECB nanoparticles.....	85

1. INTRODUCTION

Human health effects stemming from exposure to engineered nanoparticles is currently a researched topic in nanotechnology. Engineered nanoparticles are defined as particulates engineered to have at least one dimension measuring 1 nm to 100 nm and exhibit novel properties which differ from their bulk-phase, micrometer scale counterparts of identical chemical composition (NSTC 2011; TRS 2004). While the presence of ambient and incidental particles less than 100 nm is not a new occurrence, the intentional manipulation of matter at this scale and subsequent release into the environment has not occurred before the 20th century (Feynman 1992).

Engineering novel materials at the nanometer size scale results in unique physicochemical properties (e.g. enhanced electrical conductivity, increased insulating ability, a high surface area to volume ratio). These properties are often desirable in technology driven products ranging from “self-cleaning” surfaces to scratch resistant glass, medical devices, image contrast reagents and sunscreens (Richardson 2010). A more comprehensive list of “nano-enabled” products can be found online at www.nanotechproject.org (Nanotechproject 2011). Nanotechnology driven products are generating a new industrial revolution with expected revenues between \$2.6 trillion and \$3.1 trillion by the years 2014 and 2015, respectively (Dai 2010; Schmidt 2009).

While the incorporation of nanomaterials into products is enhancing our daily lives, mounting concerns of health and safety are rising to the surface. These health concerns have been attributed to the fact that nanoparticles often behave according to

This dissertation follows the style of Nanotoxicology.

very different physical and chemical laws than their micrometer size counterparts. Therefore, it is not unreasonable to expect an altered biological response following cellular or organism exposure to nanoparticles (Donaldson et al. 2002; Donaldson et al. 2001; Oberdorster 2001).

These physical laws, or so called “nano-effects”, rule the behavior and properties of particles at the nanometer size scale. In fact, the standard definition of a nanoparticle (as described previously) has been modified by Auffan et al. (2009) in order to place greater emphasis on altered physicochemical properties seen at the nanometer size scale, which they suggest to be more prolific at particle sizes of 30 nm or less (Auffan et al. 2009).

While this modified definition emphasizes the quantum properties at the nanometer size scale, it does not take into account the extrinsic (passive) properties (e.g. size) that enable events such as alveolar deposition. For example, particles in this size range (<100 nm) are increasingly respirable and hence, retain the ability penetrate into the deepest components of the lung. As another example, nanoparticles are often observed to pass through the blood brain barrier, diffuse through the cellular membrane, translocate to sites different from that of the exposure, and retain the potential to elicit adverse effects unless cleared from the bloodstream by the reticular endothelial system (Kreyling et al. 2002; Oberdorster et al. 2004; Oberdorster et al. 2002; Brigger et al. 2002).

Due to the increased ability for nanoparticles to penetrate into the alveolar region of the respiratory tract and translocate to alternate sites of action, exposure to nanometer

size particles may lead to adverse pathophysiological effects. While engineered nanoparticles are a relatively new class of materials, human exposure to ultrafine particles (i.e. in the nanometer range, but not engineered) is not a new occurrence. Ultrafine particles may be either anthropogenic or natural in origin. For example, natural ultrafine particles are generated in heat driven processes such as forest fires and volcanoes. Nonetheless, incidental anthropogenic ultrafine particles may be due to incomplete combustion of hydrocarbon fuels, through the welding process, or through cigarette smoking. Due to the close relationship with ultrafine particle toxicology, the emergence of nanotoxicology as a subdivision of ultrafine toxicology has been suggested (Oberdorster et al. 2005).

Increased exposure to ultrafine particles has been linked to a variety of diseases. Epidemiological studies suggest that these maladies range from the decreased peak expiratory flow and increased use of medication in asthmatics to potentially fatal respiratory and cardiovascular malignancies (von Klot et al. 2002). For example, Dockery et al. noted statistical significance between mortality and ambient air pollution associated with increased concentrations of fine particulates. This increase in mortality is linked to both lung cancer and cardiopulmonary disease (Dockery et al. 1993).

While large amounts of epidemiological data exist for ambient ultrafine or incidental particles; little to none exists following exposure to engineered nanoparticles. To date, one manuscript has been published linking engineered nanoparticles to increased health problems and mortality; however, the severe limitations of the study combined with the lack of particle characterization lead to alarm among many scientists

(Song et al. 2009). This lack of epidemiological data in nanotoxicology is attributed to a variety of factors including: enormity of nanoparticle compositions, heterogeneity within single composition nanoparticles (i.e. differences in size and/or shape), temporal relationship, and endpoint measurements (Schulte et al. 2009). Increased standardization in analytical and characterization methods across the nanotoxicology field pertaining to measured properties (e.g. particle number concentration) and potential disease endpoints are necessary prior to the development of epidemiological data.

The nanotoxicology literature is dominated with studies delineating the effects stemming from a single nanoparticle-type; when in fact, exposure to engineered nanoparticles is often a complex scenario involving a multitude of materials albeit engineered or incidental. Shulte et al. (2009) emphasizes that exposure to nanoparticles is often as mixtures and describes this as a major limitation to future epidemiological efforts (Schulte et al. 2009). On the other hand, Sharma (2010) concludes that while nanoparticles almost always exist as a mixture, single composition nanoparticle exposures *may* be found in the workplace (Sharma 2010). While the ideal scenario involving a single workplace exposure to an engineered nanoparticle *may* exist, multiple simulated occupational exposure scenarios demonstrate otherwise. With few exceptions, activity-based monitoring has been performed in environments where significant background nanoparticle populations are present (Demou et al. 2008; Demou et al. 2009; Park et al. 2009; Brouwer et al. 2009).

Exposure to multiple material-types, including both engineered nanoparticles and/or ultrafine particles, often complicates the risk assessment paradigm. This is

because interactions between a nanoparticle (including organic and inorganic components) and biological entities may lead to alterations in the predicted biological response. Both hazard identification and exposure assessment are confounded by the presence of multiple, often unidentified material types. It is for this reason that current exposure assessments for simulated occupational exposures rarely yield precise results and often draws the conclusion that a certain activity did or did not indicate nanoparticle release (Brouwer et al. 2009). Similarly, recent work in our lab has demonstrated that a mixture of nanoparticles with different compositions may yield a toxicological response greater than what was observed for each single particle-type alone (Berg et al. 2010). This non-additive effect, observed for combinations of carbon black and maghemite iron oxide nanoparticles, involved intracellular colocalization of particles in an acidified vesicle thereby leading to the dissolution and reduction of Fe^{2+} and increasing the potential for generation of intracellular reactive oxygen species (ROS) (Figure 1.1). If this scenario is applied to the occupational exposure, hazard data may be grossly underestimated due to the fact that nanoparticle co-exposures may be more deleterious than exposure to a single chemical entity or particulate alone.

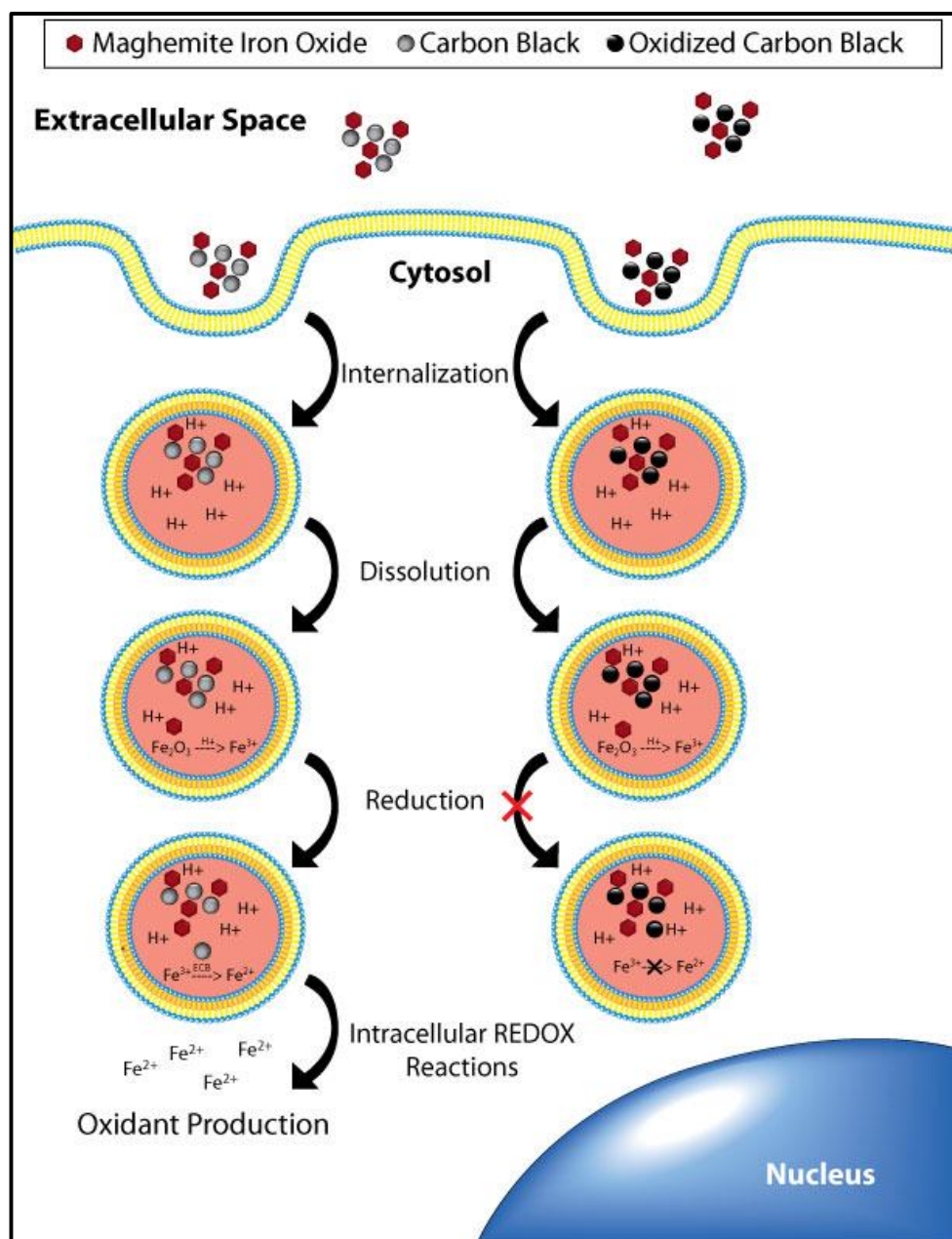


Figure 1.1 Internalization and oxidant production of nanoparticle mixtures.

1.1 Sources of Exposure to Engineered Nanoparticles and Their Mixtures

The life cycle of engineered nanoparticles provides multiple opportunities for these materials to come into contact with workers who produce them or the consumer who utilizes a derived product. A variety of dosimetries have been suggested for measuring nanoparticles in the workplace. These metrics often include number, mass, or surface-area based concentrations. Nanoparticles have an extremely high surface area: volume ratio with which to interact with biological substrates. To capitalize on this increased surface area, Maynard and others (2004) have suggested the surface area parameter is often the best dosimetric for nanoparticle inhalation studies (Maynard et al. 2004). However, while surface area dosimetries may have a higher correlation with health effects, mass-based measurements continue to dominate the *in vitro* toxicology literature (Maynard and Zimmer 2002).

1.1.1 Nanoparticle Exposure via Synthesis

Nanoparticle synthesis methods are often generalized into multiple categories consisting of mechanical, liquid phase, vapor deposition and gas phase synthesis (Demou et al. 2008; Aitken et al. 2004). Although each synthetic method may lead to an increased risk of nanoparticle exposure, only gas phase synthesis released nonagglomerated primary particles (Aitken et al. 2004). Liquid phase synthesis may also lead to nanoparticle release; however in liquid phase synthesis released nanoparticles remain highly agglomerated (Park et al. 2009).

Table 1.1 Inhalational exposures to nanoparticles and their mixtures

<i>Action</i>	<i>Component #1</i>	<i>Component #2</i>	<i>Background Particulates Present</i>	<i>Method of Reporting</i>	<i>Other Sources</i>	<i>Reference(s)</i>
Synthesis Gas Phase	NaCl, TiO ₂ , Pt/Ba/Al ₂ O ₃	Not Applicable	Present	SMPS, CPC	Not Identified	Demou, E (2008), Demou, E (2009)
	Fullerenes	Not Applicable	Present	SMPS, CPC, LDMA, NDMA, PAS	Vehicular	Yeganeh ,B (2008)
	Fullerenes	Not Applicable	Present	SMPS, OPC, SEM	Industrial Origin	Fujitani, Y (2008)
	MWCNT	Fe, Ni, Mn, Si	Present	SMPS, UCPC, APS, Aethalometer, STEM-EDS	Metals used as catalyst, insulation	Han, J (2008)
Synthesis Liquid Phase	Ag	Not Applicable	Present	SPMS-LDMA, TEM	Not Identified	Park, J (2009)
Bagging / Handling	Fumed SiO ₂	Not Applicable	Present	TEM, ELPI	Not Identified	Brouwer, D (2009)
	Li ₄ Ti ₅ O ₁₂	Mn	Present	CPC, OPC, TEM, SEM	Welding	Peters, T (2009)
	SWCNT	Fe, Ni	Not Present	TEM, ICP-AES, SPMS, CPC, APS	Metals used as catalyst	Maynard (2004)
	ECB	Not Applicable	Present	SPMS, APS	Combustion powered forklifts or heaters or traffic	Kuhlbusch, T (2006) Kuhlbusch, T (2010)
Pouring or Transferring by Spatula	Ag, Al ₂ O ₃	Not Applicable	Present	SMPS, TEM, STEM	Not Identified	Tsai (2008)

Table 1.1 Cont.

<i>Action</i>	<i>Component #1</i>	<i>Component #2</i>	<i>Background Particulates Present</i>	<i>Method of Reporting</i>	<i>Other Sources</i>	<i>Reference(s)</i>
Milling, Grinding or Cutting for Industrial Application	Steel, Hardwood, Al	Possible Al ₂ O ₃	Not Present	SPMS, APS	Al ₂ O ₃ coated grinding wheel, electric motor	Maynard, A (2002)
	CNT, Al ₂ O ₃	Present -- Not Identified	Present	CPC, TEM	Not Identified	Bello, D (2009)
Abrasion Simulating Wear Resistance	ZnO	Al, Si, Ti	Not Present	TEM, EDS, SMPS, CPC	Abrasion Test Wheel	Vorbau, M (2009)

While these released nanoparticles are assumed to be due to the synthesis or handling process, it is necessary to conduct further materials characterization to ensure that the nanoparticles released are representative of the chemical composition of the process occurring.

Current occupational monitoring suggests that synthesized nanoparticles are not the only nanometer sized particulates present in local ambient environments (Table 1.1). Monitoring of industrial plants in which nanoparticles of a single composition were synthesized, revealed that multiple ambient or background nanoparticles were also present (Park et al. 2009; Demou et al. 2008; Yeganeh et al. 2008; Demou et al. 2009). While these background particles may not be engineered nanoparticles, they can potentially alter the toxicological profile of the synthesized particle. For example, carbonaceous ultrafine particles, often derived from incomplete combustion, are a primary source of background nanoparticles. These particles are produced during processes such as the operation of forklifts, heaters and nearby traffic (Yeganeh et al. 2008; Kuhlbusch et al. 2010; Kuhlbusch and Fissan 2006; Fujitani et al. 2008). In Berg et al. (2010), engineered carbon black (ECB) was utilized as a surrogate for elemental carbon found in the ambient atmosphere (Cass et al. 2000; Berg et al. 2010). It was further suggested that this carbon could act upon other particles present and increase their cellular, toxicological response.

While a variety of simulated occupational activity studies do exist, the decreased attention to background chemical composition provides a potential source of ambiguity. For example, Demou et al. (2008 & 2009) did not chemically differentiate the particles

prior to measurement and hence, speculate that measured particles in a similar size range are derived from other sources such as traffic, industrial sources, or outdoor activities (Demou et al. 2008; Demou et al. 2009). Similarly, multiple studies note the presence of unidentified nanoparticles during the course of carbon nanotube (CNT) synthesis and further suggest that these unidentified particles may originate from either outdoor sources or the carbon brushes in a vacuum motor as has been observed elsewhere (Maynard et al. 2004; Fujitani et al. 2008; Bello et al. 2008).

1.1.2 The Importance of Background Particle Determination

The determination of background nanoparticle composition may lead to increased epidemiological insights as well. Few studies that monitor nanoparticle synthesis and handling utilize current analytical methods, such as inductively couple plasma-mass spectroscopy (ICP-MS) and scanning transmission electron microscopy-energy dispersive spectrometry (STEM-EDS) to further identify and characterize background particulates present. Careful characterization of such background particles may further help to differentiate between the health-risks associated with engineered nanoparticle exposure from that of the background particulate. For example, Han and others (2008) identified the presence of chrysotile asbestos-like fibers in their multiwall carbon nanotube (MWCNT) samples using electron microscopy (Han et al. 2008). It was hypothesized that these fibers were not a product of MWCNT synthesis, but released from the equipment or high-temperature furnace used for the chemical vapor deposition process.

The use of novel analytical techniques such as ICP-MS or STEM-EDS as a means to characterize chemical components can be applied to nanoparticles as well. Peters and others (2009) undertook the responsibility to determine the composition of the particles released from the production of both their synthesized $\text{Li}_4\text{Ti}_5\text{O}_{12}$ particles and the nearby incidental particles which often dominate the airborne number concentration (Peters et al. 2009). Utilizing these techniques, they determined that the particle numbers measured by condensation particle counter (CPC) and optical particle counter (OPC) often contained manganese which originated from a nearby welding source. This background particle identification may help to separate the effect of background particle-based health effects, such as “metal fume fever” from that of the engineered nanomaterial themselves.

Maynard and others (2004) address a similar situation stemming from the use of iron and nickel as catalysts in high pressure carbon monoxide (HiPCO) synthesis of multi-walled carbon nanotubes (MWCNT) (Maynard et al. 2004; Bronikowski et al. 2001). They suggest that while alveolar deposition of the MWCNT is unlikely due to agglomerate size, a number of materials (i.e. Ni) used as catalysts have been associated with adverse long-term health effects (Feron et al. 2001). The use of transition metals as catalysts in the production of CNT provides yet another source of nanoparticle mixtures. These catalysts often comprise up to 30% by mass of the final carbonaceous product, exist as ultrafine (~5 nm) particles, and may be detected in the final CNT composition via EDS (Han et al. 2008). While these metals are often carbon coated, little is known about their decomposition once inside a cellular environment and hence, interaction

between the MWCNT and transition metals is possible. Using a colorimetric reductive capacity assay, work in our lab had determined that carbon structures such as CNT, fullerenes, and ECB may act to reduce the transition metal in an acidic *ex vivo* environment (Figure 1.2). Each of these carbonaceous materials may become incorporated into consumer products thus providing the potential for material release and exposure at the processing or consumer level.

1.1.3 Release of Nanoparticles During Post-Synthesis Processing for Industrial Use

At the forefront of nanotechnology-driven product generation is the post-synthesis processing of nanoparticle containing materials. This process often includes milling, grinding, cutting, or abrasion of nanoparticle-containing composites. Currently, there are concerns regarding particle release from nanoparticle-containing substrates; however, it remains undetermined if the quantities of particles released are sufficiently high to be a risk. For example, Vorbau (2009) suggests that individual nanoparticles were not liberated from nanoparticle-containing composites, but alternatively incorporated into micrometer size particles as analyzed by TEM (Vorbau et al. 2009). Alternatively, the simple act of both high-speed grinding and dry cutting of metal substrates or carbon composites leads to nanoparticle generation regardless of their incorporation into the original product (Maynard and Zimmer 2002; Bello et al. 2008). Throughout these processes, generated nanoparticles may be released from the processed substrate (material being milled), the processing implement (blade or grinding wheel) or the machinery utilizing the processing implement (i.e. electric saw or high-speed grinder).

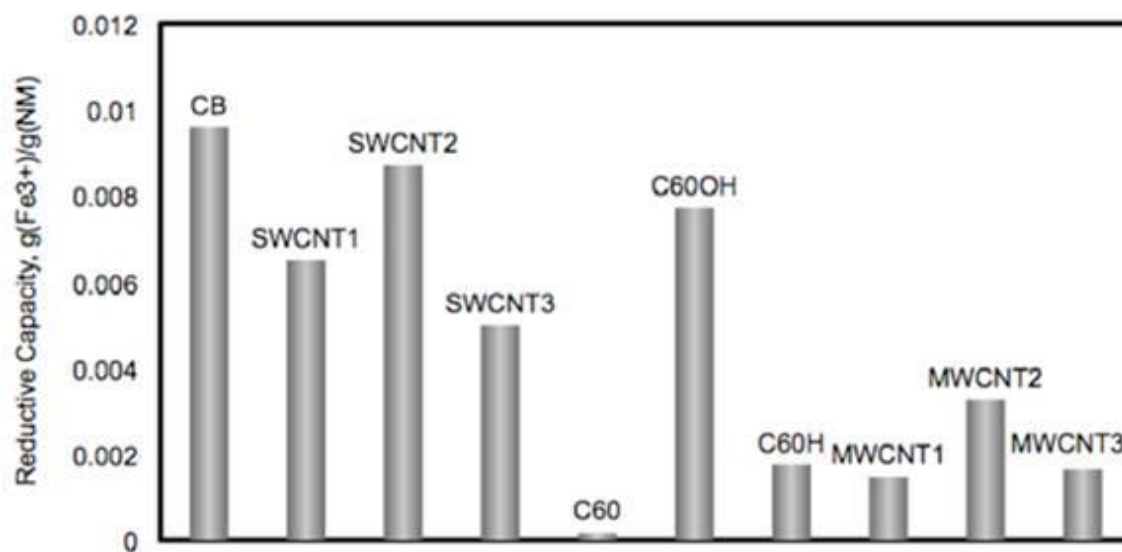


Figure 1.2 Reductive ability of carbonaceous nanostructures. Carbonaceous nanostructures including carbon black, fullerenes, and nanotube are able to reduce Fe^{3+} to Fe^{2+} in solution.

Albeit nanoparticle synthesis, handling, or processing, identifying exposure to both nanoparticles and their mixtures will remain an important factor in the advancement of nanoparticle containing products. While it is obvious that nanoscientists are nowhere near completing a comprehensive risk assessment, identifying knowledge gaps and opportunities for future directed efforts can be determined with careful characterization and thoughtful experimental design.

1.2 Physicochemical Properties Relevant to Nanoparticle Mixtures

Engineered nanoparticles are synthesized with various physicochemical properties in an effort to yield specific structural or functional features. It remains a distinct possibility that the same physicochemical properties which are beneficial to product development may elicit a negative biological response, in either *in vitro* or *in vivo* test systems. Under the basis of “precautionary principle”, it is necessary to determine what physicochemical characteristics of an individual nanoparticle or a mixture of nanoparticles may be important for potential toxicological consideration. There has been an effort in the nanotoxicology field to utilize a structure activity relationship generated from gathered nanoparticle toxicological data in order to possibly predict nanoparticle toxicology through the use of *in silico* techniques (Sayes and Ivanov 2010). While the list of recommended physicochemical properties is undergoing constant morphological changes, the properties of composition, size, zeta potential, crystallinity (or lack thereof), and surface chemistry have been hypothesized to play a critical role in the development of toxicological conditions.

1.2.1 Chemical Composition

While a nanoparticle is classically defined by both its size and unique properties, the current definition says nothing about its chemical composition. This lack of chemical description has often lead to vagueness and criticism in the field. For example, a recent study in the *European Journal of Respiratory Health* related nanoparticles that were used in an occupational setting to adverse health effects including pleural granulomas and subsequent mortality of two subjects (Song et al. 2009). However, the authors of this study performed little physicochemical characterization and the composition of the particles was not examined to determine if a link to the workplace exposure did exist.

Many toxicological parameters have been linked to a nanoparticle's chemical composition. While particles are intentionally comprised of certain elements (i.e. SiO₂ is comprised of silicon and oxygen) oftentimes unintentional elements may be present at low concentrations (Vallyathan et al. 1988; Limbach et al. 2007; Fubini et al. 1990). For example, transition metal impurities such as Fe, Co, Mn, and Ti in a primary matrix of SiO₂ lead to greater oxidant production following incubation in a cellular environment than pure SiO₂ alone (Limbach et al. 2007). Additionally, trace iron impurities on the surface of silica particles are often implicated in free radical release (Fubini et al. 1990; Vallyathan et al. 1988). These impurities may be unintentional by-products of the nanoparticle synthesis process. For example, both Fe and Ni are present in carbon nanotubes at up to 30% mass in ultrafine particle form (Bronikowski et al. 2001; Maynard et al. 2004). Because transition metal impurities are not obvious and may not

be reported by the manufacturer, in-house elemental confirmation ICP-MS or EDS is recommended.

In addition to trace metal contaminants, organics modifying the surface may also lead to altered toxicological profiles. Sodium citrate is often used as the reducing agent and colloidal stabilizer for nanoparticle synthesis (Dadosh 2009; Lee and Meisel 1982). Residual sodium citrate adhered to the nanoparticle surface after synthesis has been shown to impact cellular processes including metabolic activity, cellular proliferation, and lactate dehydrogenase (LDH) release (Uboldi et al. 2009).

Nanoparticle composition also influences particle dissolution. Many studies suggest that particle dissolution is responsible for negative effects following exposure to nanoparticles of a certain composition (Brunner et al. 2006; Franklin et al. 2007; Nel et al. 2006; Xia et al. 2008a). For example, ZnO nanoparticles rapidly dissolve in cell culture media to form Zn^{2+} ions which may generate cellular stress through an oxidative pathway (Xia et al. 2008a). In contrast, insoluble nanoparticles (i.e. TiO_2 or SiO_2) may be less cytotoxic in the short term than their soluble counterparts (Brunner et al. 2006). Both TiO_2 and SiO_2 can generate a refractory oxide shell in the presence of acidic environments and this enables them to withstand dissolution under harsh (acidic and/or oxidizing) conditions. However, while low dissolution rates may be advantageous over the short term, this characteristic may lead to increased biopersistence and *in vivo* residence times. Therefore, highly soluble particles must be thoroughly tested for their short-term toxicity while highly insoluble particles should be monitored for their long term responses. Synthesizing a nanoparticle which maintains this delicate balance of

both retention and dissolution may provide an appropriate means to manage the risk associated with the use of nanoparticle containing products.

1.2.2 Crystalline Structure

Nanoparticles may be synthesized in either a crystalline or amorphous form. Moreover, different crystalline forms exist for nanoparticles of different composition. For example, while the toxicology of the most common forms of titanium dioxide including anatase, rutile, and brookite, are the most studied; other forms of TiO₂ also exist. Many toxicological comparisons between anatase TiO₂ and rutile TiO₂ demonstrate that there are stark differences in their cytotoxicity, inflammation, and oxidant production. For example, in acellular assays utilizing oxidant reactive dyes, anatase generates greater oxidant production than anatase/rutile mixtures or rutile alone (Jiang et al. 2008a; Sayes et al. 2006). Sayes et al. (2006) concluded that the anatase crystal phase was 100 times more toxic than TiO₂ in the rutile crystal phase according to cytotoxicity assays using calcein AM and ethidium homodimer (Sayes et al. 2006). On the other hand, Bradydich-Stolle and others (2009) suggest that crystalline state is only one mediator of TiO₂ toxicity and identified different cellular responses including necrosis and apoptosis for the anatase and rutile crystal phases respectively (Braydich-Stolle et al. 2009). In the animal model, mixtures of 80% anatase: 20% rutile are more inflammogenic than exposure to rutile alone (Warheit et al. 2007a; Warheit et al. 2007b).

Similarly, amorphous forms of traditionally inert material may become biologically active at the nanometer size scale. For example, both amorphous TiO₂ and amorphous SiO₂ generate both oxidant production and oxidative stress in both acellular

and cellular environments at the nanometer size scale (Jiang et al. 2008a; Lin et al. 2006; Chang et al. 2007). This increased activity of the amorphous form may be due to the increased surface defect density which enhances interactions with the external environment (Carp et al. 2004). Furthermore, an increase in the surface density of functional groups may contribute to the generation of oxidants. Thus, it is considered that changes in crystalline form may alter both the surface chemistry of a particle and its toxicological effects.

1.2.3 Surface Chemistry

While many components are expected to contribute to nanoparticle toxicity, decreasing nanoparticle diameter leads to exponential increases in particle surface molecules (Oberdorster et al. 2005). These exponential increases in surface area make the nanoparticle unique from bulk material. In fact, it has been suggested that particle surface characteristics may be more important than particle size when determining nanoparticle cytotoxicity (Warheit et al. 2007a; Warheit et al. 2007b). As an example, the increased surface area of nanometer size particles provide an enhanced ability to unintentionally bind contaminants such as organics, transition metals or even biomolecules (Donaldson et al. 2001). Taken a step further, these surface-adhered macromolecules may further dictate particle uptake or distribution *in vitro* or *in vivo* (Lundqvist et al. 2008). While unintentional macromolecule surface modification may lead to unwanted distribution, intentionally coating nanoparticles with various polymers, including polyethylene glycol (PEG) for medicinal techniques, may increase their residence time and help avoid macrophage clearance (McNeil 2005).

Surface chemistry can be determined using a variety of techniques including x-ray photoelectron spectroscopy (XPS) or Fourier transform infrared spectroscopy (FTIR). XPS, otherwise known as electron spectroscopy for chemical analysis (ESCA) utilizes a focused x-ray beam to emit electrons from the surface (~15 nm) of the materials which may then be analyzed for elemental composition (Murdock et al. 2008). Furthermore, XPS may be utilized to detect surface labeling of nanoparticles using fluorescent dyes (Hens et al. 2008). In addition to XPS measurements, FTIR may be used to verify the presence of surface functional groups. For example, FTIR may be used to show surface functional groups in SiO₂ and subsequent amine functionalization following surface modification as shown in Figure 1.3. While XPS and FTIR are analytical tools that provide elemental and functional composition at the nanoparticle surface, the Vitamin C assay may be utilized to determine surface reactivity. The Vitamin C yellowing test has been previously developed as a means to correlate the surface reactivity of the nanoparticle to its chemical stability. Available evidence indicates that the color change mechanism is the formation of a charge transfer complex between ascorbic acid-6-palmitate and the “active sites” on the nanoparticle surface (Warheit et al. 2007b; Rajh et al. 1999).

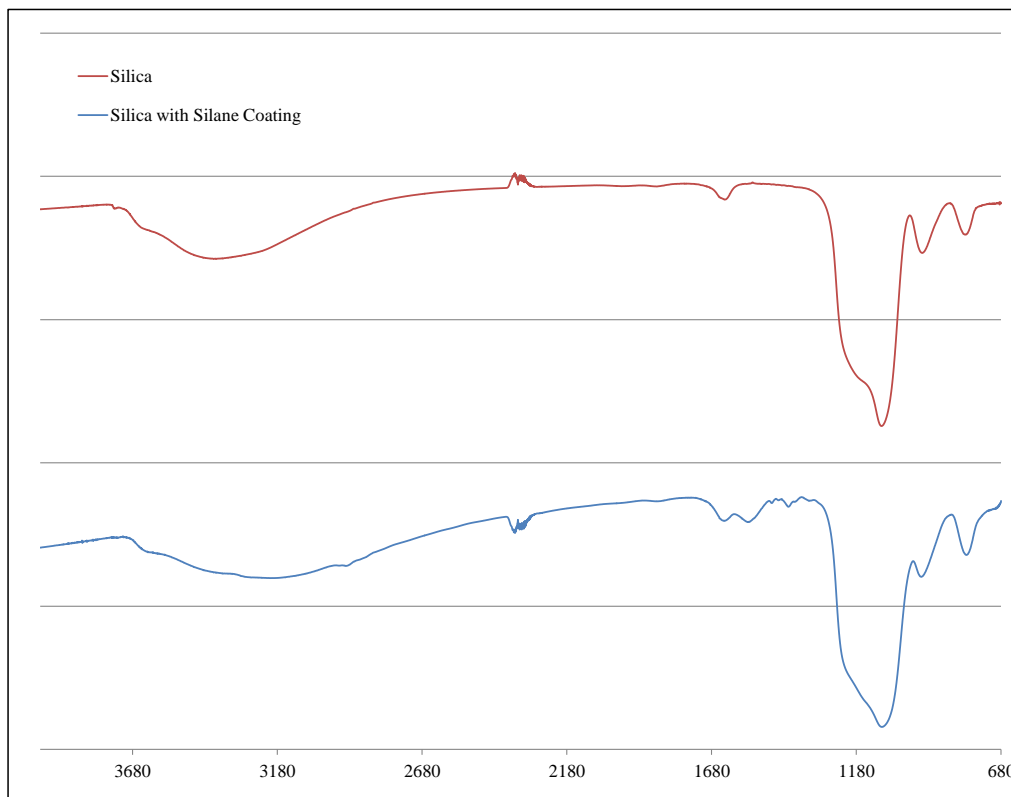


Figure 1.3 Fourier transform infrared spectroscopy of native and silane coated SiO_2 . Native SiO_2 (red) elicits characteristic peaks of 801, 954, and 1093 cm^{-1} associated with Si-O, Si-OH, and Si-O-Si bonding. Upon reaction with 3-aminopropyl triethoxysilane (blue), disappearance of the peak at 3749 cm^{-1} associated with surface silanol groups is coupled with an increase in transmittance at $\sim 1552 \text{ cm}^{-1}$ often associated with an amino group vibrational mode.

1.2.4 Redox Chemistry

The introduction of reduction and oxidation (redox) chemistry and biology to the nanotoxicology field allows an enhanced understanding of interactions taking place at the chemical level. For example, recent work by our lab, has evaluated the usefulness of XPS by analyzing the surface of carbon black both prior to and after surface oxidation (Berg et al. 2010). Following surface oxidation of engineered carbon black, the surface quinone:hydroquinone ($Q_{(s)}:HQ_{(s)}$) ratio was circa 5000 times greater than in the unoxidized carbon black. Furthermore, we identified potential redox cycling involving liberated Fe^{3+} from Fe_2O_3 nanoparticle and the surface of carbon black, thus potentially identifying the reducing component of particulate matter (PM) that may play a role in hydroxyl radical generation in response to PM_{10} (Donaldson et al. 1997).

1.2.5 Other Physicochemical Properties Relevant to Toxicology

While the previous physicochemical parameters are necessary measurements for nanoparticle mixtures, the following properties of nanoparticles should also be measured.

1.2.5.1 Nanoparticle Size

Many materials typically inert at the micron scale, gain the ability to induce a biological response at the nanometer size scale at both the cellular and organism level (Li et al. 2008b; Li et al. 1999; Kaewamatawong et al. 2005; Nemmar et al. 2003). These size-dependent effects may be attributed to increased surface area: volume ratio, increased particle number concentrations per unit mass, altered surface atomic composition, or discontinuous crystal planes which may increase the presence of

structural defects on the surface of the particle (Vallyathan et al. 1988). Size-dependent effects are often well defined within the nanometer size range itself as many biological dependent mechanisms, such as nanoparticle internalization and cellular signaling, often respond to slight differences (i.e. 45 nm vs. 10 nm) in nanoparticle size (Jiang et al. 2008b; Chithrani et al. 2006). While size-dependent mechanisms of nanoparticle induced toxicity dominate the literature, numerous studies suggest other factors that play a role. For example, Warheit et al. (2007) suggests that particle surface characteristics may be more important for toxicological purposes than nanoparticle size when utilizing both fine and nanometer sized quartz (Warheit et al. 2007a). Alternatively, Wagner et al. (2007) suggests that particle composition in combination with particle surface area are more influential in the toxicity of Al₂O₃ nanoparticle than size alone (Wagner et al. 2007).

Nanoparticle size is reported in a variety of ways including primary particle size, aerodynamic diameter, hydrodynamic diameter, and agglomerate size (Hwang et al. 2008; Wuelfing et al. 1999; Zhang et al. 2005; Pauluhn 2009). Although each of these measurements assumes that nanoparticles are spherical in diameter, each may lend itself to a different reported diameter. Primary particle size is often obtained through the use of electron microscopy or calculated through surface area analysis using the Brunauer, Emmett and Teller (BET) method (Brunauer et al. 1938). The aerodynamic diameter is often utilized to measure the size of an aerosolized nanoparticle powder. This aerodynamic size is important in inhalational studies as particles size in this form defines their impaction and travel within the lower levels of the respiratory tract. If individual

nanoparticles reach the lower level of the respiratory tract (i.e. not ciliated), particle clearance may be hindered since various nanoparticles decrease alveolar clearance mechanisms (Renwick et al. 2001). Hydrodynamic diameter, measured via dynamic light scattering in a suspension, gives a measure of the nanoparticle size at the nanoparticle slipping plane. The nanoparticle slipping plane is comprised of the nanoparticle core with the surrounding layer of water and adsorbed ions (Murdock et al. 2008). Both the aerodynamic and hydrodynamic measurements are subject to alteration through a process termed nanoparticle agglomeration. Agglomerates of nanoparticles occur when individual primary particles are held together by weak intermolecular forces including solvation forces, van der Waals forces, electrostatic attractions, and hydrophobic interactions (Hakim et al. 2007; Min et al. 2008; Fichthorn and Qin 2008).

In addition to primary particle size as described above, nanoparticle agglomerate size may also provide an additional property worthy of consideration in nanotoxicological studies (Pauluhn 2009; Mayer et al. 2009). In an effort to distinguish the toxicological effects of nanoparticle agglomerates from that of the individual primary particle size, research involving the synthesis and deagglomeration of particles using biologically compatible colloidal stabilizers, such as bovine serum albumin (BSA) or diphenylphosphatidylcholine (DPPC), has become widely prevalent (Thomassen et al. 2009; Bihari et al. 2008; Vippola et al. 2009; Brigger et al. 2002; Sager et al. 2007; Porter et al. 2008). Therefore, as further research into the deagglomeration of nanoparticles takes place, an increased understanding of the role of primary particle size may become more apparent.

1.2.5.2 Nanoparticle Surface Charge

Nanoparticle surface charge, often measured as zeta potential, is a dynamic characteristic often dependent upon the microenvironmental conditions in which the particle is suspended. The zeta potential of the nanoparticle represents the charge of the nanoparticle at the slipping plane of the electric double layer. This double layer is influenced by the surrounding ions in solution (Malvern 2008). Nanoparticle zeta potential is measured using dynamic light scattering combined with phase analysis light scattering (Berne and Pecora 1976). Because the zeta potential measurement is influenced by the surrounding ions in solution, the characteristics of the suspension medium such as pH, ionic strength, and/or presence of surfactants may all influence the zeta potential (Tiyaboonchai and Limpeanchob 2007; Mayer et al. 2009; Berg et al. 2009; Handy et al. 2008). Alterations in the zeta potential will, in effect, lead to modification of other physicochemical characteristics such as changes in the agglomeration state (Berg et al. 2009). The largest nanoparticle agglomeration state is theoretically present at the nanoparticles isoelectric point. The isoelectric point is defined as the pH at which the net zeta potential is equal to 0 mV. In fact, zeta potential values greater than +30 mV or less than -30 mV allow increased nanoparticle stabilization following deaggregation using sonication techniques (Murdock et al. 2008). However, sonication alone does not alter the nanoparticle zeta potential.

Alterations in the zeta potential of a nanoparticle will lead to different biological effects providing that the remaining physicochemical properties remain the same. It has been suggested that surface protein adsorption is significant to the toxicological

characteristics of the particle (Lundqvist et al. 2008). This protein adsorption is often mediated by the surface parameters of the individual particles including surface charge. Beyond protein modification, surface charge has been shown to play a role in internalization and distribution of nanoparticles. For example, nanoparticle zeta potential plays an important role in delivery across the blood brain barrier (Lockman et al. 2004; Fenart et al. 1999). Similarly, alterations in the zeta potential may mediate the route of cellular internalization (Dausend et al. 2008; Harush-Frenkel et al. 2008). For example, when using an amiloride inhibitor of macropinocytosis, Dausend et al. (2008) noted that only positively charged particles were blocked from cellular entrance while negatively charged particles were unaffected (Dausend et al. 2008). The zeta potential of a nanoparticle should be considered in nanotoxicology studies.

While this discussion of the physicochemical characteristics of nanoparticle is not exhaustive, they represent a basic set of physicochemical parameters that influence the toxicity of nanoparticles. Future work can utilize these characteristics to develop mathematical quantitative structure activity relationships (QSARs) which determine the contributions of these physicochemical properties to biological responses (Sayes and Ivanov 2010).

1.2.6 The Characterization of Nanoparticle Mixtures

The characterization of nanoparticles and their mixtures is extremely important and will facilitate future determination of health impacts following nanoparticle exposure. Characterizing nanoparticles and their mixtures uses several techniques to measure both particle *exposure* limits as well as the composition of the particles.

Natural or incidental nanoparticles may often interfere with measurements of nanoparticle parameters in an occupational setting. In an effort to eliminate these background particles, sampled activities can be monitored for potential nanoparticle release through the use of a high-efficacy HEPA filter in combination with task-based isolation as discussed elsewhere (Yeganeh et al. 2008; Maynard and Zimmer 2002; Maynard et al. 2004; Vorbau et al. 2009). Furthermore, the identification and characterization of background particles should be addressed through the use of current analytical techniques. As an example, both ICP-MS and STEM-EDS have been utilized in an effort to identify background nanoparticle sources from incidental sources (Peters et al. 2009; Maynard et al. 2004; Han et al. 2008). Current efforts utilizing the Nanoparticle Emission Assessment Technique (NEAT), proposed by Methner at NIOSH, involve specific combinations of particle measurements with careful chemical characterization using filter based techniques to provide the most appropriate characterization of the materials (Methner et al. 2010b; Methner et al. 2010a).

1.3 Cell and Nanoparticle Interactions as a Preliminary Step in Toxicity

Interaction of nanoparticles with biological systems occurs on a size scale similar to those observed with the entrance of viral pathogens into a cellular system (Diaz-Griffero et al. 2002; McClure et al. 1990). Similar to viruses, nanoparticles uniquely access intracellular components both intentionally (e.g. medicinally) or unintentionally (e.g. occupationally) (Xia et al. 2008b; Ferrari 2008). Viral and bacterial pathogens at the nanometer size scale infiltrate cellular systems through various endocytic pathways as a primary means of eliciting cellular or subcellular dysfunction. In this respect,

nanoparticles are similar to pathogens; however, while multiple pathways for the internalization of nanoparticles have been hypothesized, the results are conflicting. This discrepancy in the data has been attributed to many factors – the most common being the lack of physicochemical characterization of the particle-types tested (Dausend et al. 2008). It has been postulated that many of the physical parameters of nanoparticles can affect their uptake in cells either through specific or non-specific pathways (Jiang et al. 2008b). Thus far, the most documented particle characteristics that influence internalization are nanoparticle size, charge, and surface modification as indicated in Table 1.2 (Zhang and Monteiro-Riviere 2009).

1.3.1 Influence of Size on Nanoparticle Uptake

Endocytosis is responsible for the sorting, processing, and degradation of internalized cargo (Gould and Lippincott-Schwartz 2009; Qaddoumi et al. 2003). This process, which is often tightly regulated, consists of multiple receptor- and non-receptor mediated routes that are limited by size constraints and may be applicable to the internalization of nanoparticles. For example, Qaddoumi and others (2004) observed an inverse relationship between nanoparticle size and quantity of particle internalization (Qaddoumi et al. 2004). Hence, particulates approaching the nanometer scale may retain the ability to utilize endocytic routes not available for use by larger particulates.

Table 1.2 Physicochemical parameters influencing nanoparticle uptake

<i>Endocytic Pathway</i>	<i>Physicochemical Property</i>	<i>Reference(s)</i>
Receptor-mediated endocytosis	<ul style="list-style-type: none"> • Strong positive or negative charge • <200 nm primary particle size • Likely to be protein and/or surface modified • Moderate aspect ratio and moderate degree of curvature • Non-agglomerated • Most efficient when particle size ~50 nm 	<ul style="list-style-type: none"> • (Osaki et al. 2004) • (Harush-Frenkel et al. 2008) • (Jiang et al. 2008b) • (Chithrani et al. 2006) • (Zhang and Monteiro-Riviere 2009) • (Yuan et al. 2008) • (Ferrari 2008) • (Kim et al. 2006)
Macropinocytosis	<ul style="list-style-type: none"> • Hydrophobic • >200 nm in primary particle size • May be highly agglomerated 	<ul style="list-style-type: none"> • (Schoepf et al. 1998) • (Osaki et al. 2004) • (Qaddoumi et al. 2003)
Diffusion	<ul style="list-style-type: none"> • Amphiphilic • Peptide Modified • Non-agglomerated 	<ul style="list-style-type: none"> • (Nativo et al. 2008) • (Rothen-Rutishauser et al. 2006) • (Verma et al. 2008)
Absorptive endocytosis	<ul style="list-style-type: none"> • Biodegradable • <200 nm 	<ul style="list-style-type: none"> • (Qaddoumi et al. 2004) • (Qaddoumi et al. 2003)

Multiple forms of receptor-mediated endocytosis, including both clathrin- and caveolin-dependent mechanisms, are subject to size restrictions. Clathrin-mediated endocytosis, the most common form of receptor-mediated endocytosis, is size restricted to particles of approximately 200 nm due to protein scaffolding lining the budding membrane surface. Similarly, uptake via caveolae-mediated endocytosis is limited to particles ~ 60 nm in diameter due to thermodynamic constraints. However, nanoparticles with dimensions less 60-200 nm can utilize these pathways as a means of cellular entrance. Theoretical calculations, based on size-dependent receptor-mediated endocytosis, have shown most efficient particle uptake when particle radii are ~25-30 nm (Gao et al. 2005; Aoyama et al. 2003). These theoretical calculations have been confirmed via experimentation (Jiang et al. 2008b; Chithrani et al. 2006; Osaki et al. 2004; Nakai et al. 2003).

In addition to receptor mediated pathways, receptor independent pathways, such as macropinocytosis, are an alternate route for both individual nanoparticles and their corresponding agglomerates to enter the cell. Particles internalized via macropinocytosis range from approximately 200 nm to 5 μ m and this process is a more non-specific route for nanoparticle internalization (Swanson and Watts 1995). Macropinocytosis is characterized by membrane ruffling which is generated by newly polymerized actin filaments. As ruffles rejoin the membrane surface, they encapsulate extracellular nutrients and alternatively provide a way for either single nanoparticle or their agglomerates to enter the cell. For example, one report suggests that both particles and fibers can adhere non-specifically to the external cellular membrane (Boylan et al.

1995). Non-selective membrane ruffling may retain the capacity to accidentally internalize nanoparticles and agglomerates up to 5 μm with potentially deleterious results. This pathway has been observed for internalization of polymer-based positively charged nanoparticles (Harush-Frenkel et al. 2008).

Size-dependent limitations may not occur with nanoparticles less than ~ 60 nm due to their ability to traverse the receptor- and non-receptor-mediated routes. Moreover, the uptake of nanoparticles with specific surface properties may not require an active process to occur (Rothen-Rutishauser et al. 2006; Geiser et al. 2005).

1.3.2 Influence of Charge on Nanoparticle Uptake

While size-restrictions may limit the specific route of uptake, it has been suggested that charge, rather than size, is the prominent factor for both the route and quantity of nanoparticle uptake (Kemp et al. 2008). For example, charged nanoparticles often exhibit increased uptake compared to neutrally-charged nanoparticles (Zhang and Monteiro-Riviere 2009). This has been readily observed by the increase in uptake of negatively charged (-COOH coated) quantum dots by a keratinocyte cell line (HEK) over either neutral (polyethylene glycol (PEG) coated) or positively charged (PEG-amine coated) quantum dots (Zhang and Monteiro-Riviere 2009). Similar results were obtained by Kemp and others (2008), where up to 75% of cells in culture internalized carboxylate-modified latex particles (Kemp et al. 2008). Charge-directed internalization of nanoparticles may be influenced by surface modifications via culture media components; for example, negatively charged gold nanoparticles bind proteins in culture

media which not only act as colloidal stabilizer, but also may influence endocytosis (Chithrani et al. 2006).

Results of several studies suggest that generalizations regarding endocytosis of nanoparticles cannot be made. Previously described studies indicate increased uptake of negatively charged nanoparticles (Zhang and Monteiro-Riviere 2009; Kemp et al. 2008), whereas other studies do not confirm this observation (Harush-Frenkel et al. 2008). Since nanoparticle charge is often modified by the addition of specific functional groups, the ability to chemically modify the surface of the nanoparticle is a potential source of discrepancy among studies.

1.3.3 Influence of Surface Modifications on Nanoparticle Uptake

Slight modifications in the surface parameters of a nanoparticle may lead to large alterations in nanoparticle uptake route and efficacy. These surface modifications may be made in the form of non-specific adsorption of proteins or through intentional surface modification with either biological (e.g. ligands) or synthetic (PEG) compounds. Changes in these surface properties may not only alter the cellular uptake, but may also modify the intracellular localization of the particle once inside the cell.

Many studies suggest that nanoparticles may adsorb components from serum, cell culture media and lung fluid in the cellular environment. This coating may influence both the nanoparticle agglomeration state as well as route of internalization (Lundqvist et al. 2008; Chen et al. 2006; Chen et al. 2005; Huang et al. 2007; Schellenberger et al. 2008). For example, vitronectin, a major adhesive protein found in serum, leads to enhanced internalization of asbestos fibers and it is likely that proteins

such as vitronectin could adsorb onto a nanoparticle surface and enhance their internalization (Boylan et al. 1995).

The potential toxicological effects of nanoparticles of similar size or chemical composition are often dependent on their surface functional groups. For example, protein absorption may be enhanced by the adsorbed ionic stabilizers often found in commercial nanoparticle products and PEG-modified surfaces protect native surface from further modifications (Nativo et al. 2008). Interestingly, PEGylating the nanoparticle surface can also limit nanoparticle uptake, suggesting a link between protein adsorption and internalization (Ferrari 2008; Kanaras et al. 2002). Modification of nanoparticle surfaces by ligands such as folate, transferrin, or cholesterol may target particles to the clathrin-dependent pathway (Yuan et al. 2008; Anderson 1998; Rodal et al. 1999; Damke et al. 1994). Nanoparticles may also be modified with either cell-penetrating peptides or nuclear localization sequences to direct their internalization to a specific pathway or bypass the endocytic machinery altogether (Nativo et al. 2008; Levy et al. 2004).

1.3.4 Intracellular Trafficking of Nanoparticles

Nanoparticle entrance into the cell is important for determining the level of exposure or dose; however, intracellular trafficking of nanoparticles may also influence toxicity. These adverse effects may proceed via alterations of the physicochemical properties of nanoparticles thereby leading to events such as nanoparticle deagglomeration, release into the intracellular environment, or dissolution into ions.

Nanoparticle uptake into a cell may occur rapidly following an exposure. For instance, Kemp and others (2008) observed a rapid increase in cellular fluorescence within the first 15 minutes following exposure (Kemp et al. 2008). In most cases reported, this rapid increase in intracellular uptake is an energy dependent process capable of inhibition by eliminating cellular ATP stores, f-actin polymerization, or low temperature (4° C) incubation (Qaddoumi et al. 2003). Following the initial surge in particle uptake, differences in particle uptake kinetics are dependent upon the internalization route. Chithrani and others (2006) observed a plateau phase in uptake after 4-7 hrs and reported that uptake occurred through a receptor-mediated event. (Chithrani et al. 2006). In contrast, uptake of dextran-coated iron oxide exhibited relatively linear, non-saturable uptake over the time course studied and this is characteristic of a non-receptor mediated route of internalization (Schoepf et al. 1998).

Internalization of nanoparticles through energy-dependent endocytosis leads to accumulation of nanoparticles in various endosomal stages and subsequently, lysosomal transfer. Zhang and Montierro-Riviere (2009) monitored the uptake of fluorescent CdSe-COOH quantum dots following cellular exposure and observed early endosomal accumulation (colocalization with EEA1) followed by late endosomal transfer (colocalized with CD63) and ultimately lysosomal accumulation (colocalized LAMP1) (Zhang and Monteiro-Riviere 2009). This lysosomal accumulation has also been observed for ligand-coated, surface modified, and uncoated particles, suggesting common pathways (Jiang et al. 2008b; Nativo et al. 2008; Uboldi et al. 2009; Rothen-Rutishauser et al. 2007). While lysosomal fate is common, it is possible to avoid this

endosomal pathway through the use of liposomal incorporation or surface modification using cell penetrating peptide moieties (Nativo et al. 2008).

Thus, it may be possible that route of endocytosis and subsequent intracellular trafficking play an important role in cellular damage in response to nanoparticle exposure. Multiple studies indicate that the lysosomal environment may alter the surface properties of nanoparticles. For example, CdTe quantum dots alter their surface charge when in the lysosomal environment, as the drop in pH alters the nanoparticle zeta potential (Berg et al. 2009; Nabiev et al. 2007). Similarly, ZnO nanoparticles undergo dissolution following lysosomal incorporation (Xia et al. 2008a).

However, while lysosomal conditions offer protection from foreign pathogens under typical cellular situations, in the context of exposure to nanoparticles, it may yield adverse effects. Nanoparticle uptake may lead to lysosomal rupture through a variety of mechanisms. For example, it has been suggested that surface modified CdTe quantum dots may act as lysosomotropic agents by enabling the rupture of the lysosome through the sequestration of protons identified as the “proton sponge effect” thereby releasing lysosomal contents into the cytosolic milieu. Additionally Navio (2008) suggested that the peptide modification of nanoparticles can disrupt the endosomal membrane and lead to release of its contents.

The ultimate intracellular fate of nanoparticles may provide a preliminary glimpse into the toxic effects of individual nanoparticles. For nanoparticles internalized into endosomes and/or lysosomes, it has been postulated that either lysosomal incorporation or mitochondrial sequestration may cause or accelerate production of

intracellular reactive oxygen species (ROS) (Guo et al. 2009; Lamb et al. 2009; Miller et al. 2007).

1.4 Oxidant Production

Nanoparticle-induced ROS has been reported for carbonaceous, metal-based, and ceramic nanoparticles in both cellular and acellular environments (Sayes et al. 2004; Rancan et al. 2002; Wilson et al. 2002; Li et al. 2003; Brown et al. 2001; Brown et al. 1999; Li et al. 1996). The mechanisms linking the generation of reactive oxygen species, a cumulative name for highly reactive oxygen-containing molecules (e.g. H_2O_2 , $\text{O}_2^{\cdot-}$, HO^{\cdot} , ROO^{\cdot}), to the cellular oxidative stress response are unclear; however multiple hypotheses currently exist. First, a variety studies indicate that “nano-specific” effects, such as increased surface area and alterations in surface chemistry, may facilitate induction of ROS by nanoparticles (Schins 2002; Jiang et al. 2008a). Secondly, cellular-based reactions involving nanoparticles or their remnants (in the case of dissolution) may also increase oxidative stress through intracellular reactions due, in part, to the recruitment of inflammatory mediators which themselves act to produce ROS (Brunner et al. 2006; Xia et al. 2008a).

Increases in intracellular oxidants may lead to alterations in cellular reduction and oxidation state. For example, generation of oxidative products in the cell will lead to a shift in the reduced glutathione: oxidized glutathione (GSH:GSSG) ratios, which is often utilized as a means to assess cellular redox state (Peters et al. 2009). Moreover, a hierarchical oxidative stress model (Figure 1.4) previously defined by Halliwell and Gutteridge (1999), suggests that shifts in the reduced glutathione: oxidized glutathione

(GSH: GSSG) ratios will lead to various cellular responses ranging from cellular quiescence to proliferation to cellular death via either an apoptotic or necrotic pathways (Manna et al. 2005; Bello et al. 2008; Peters et al. 2009).

1.4.1 Linking Physicochemical Properties to Oxidant Production

The physicochemical properties of nanoparticles set them apart from their bulk counterparts of identical composition. However, a variety of physicochemical properties including surface chemistry, crystalline structure, and chemical composition may influence the generation of reactive oxygen species.

The surface of nanoparticles is a primary source of oxidant production in the acellular environment and as the nanoparticle diameter decreases, there is an exponential increase in surface area which can interact with the external environment. The surface area-dependent increase in oxidative potential has been measured for a variety of nanoparticles including traditionally inert materials such as carbon black, amorphous or colloidal silica, and polystyrene (Lin et al. 2006; Kaewamatawong et al. 2005; Stone et al. 1998; Brown et al. 2001).

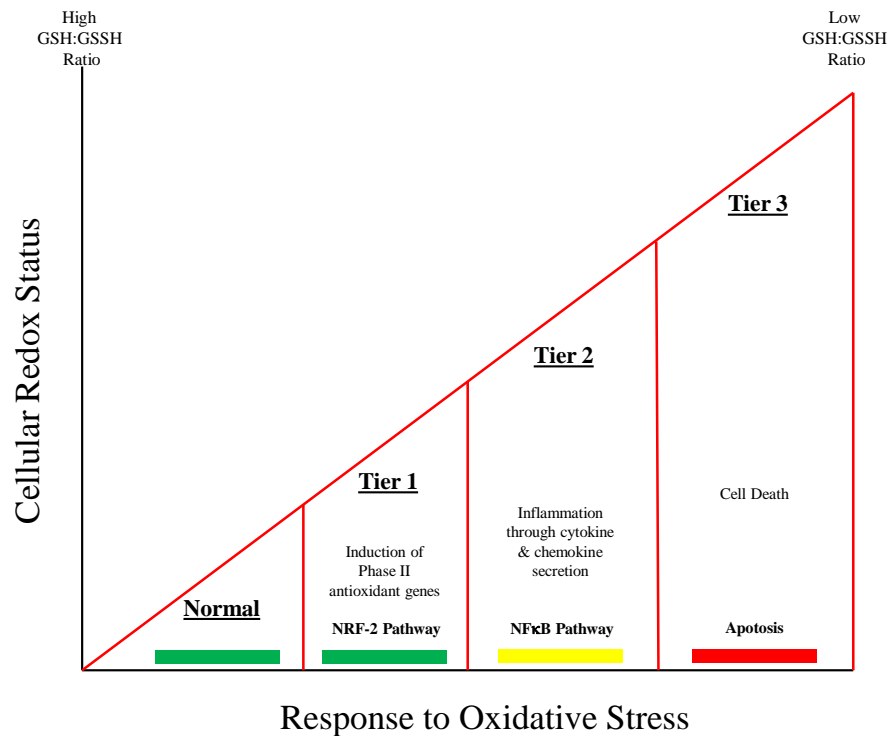


Figure 1.4 Hierarchical model of oxidative stress. At low levels of oxidative stress, cytoprotection occurs through the induction of phase II responses and inflammation; however at higher amounts of oxidative stress, characterized by a low GSH:GSSG ratio, cellular death via apoptosis or necrosis will occur. Cell survival is indicated by colored bar where green represents completely viable, yellow represents cell viability that may proceed to either a viable or nonviable state and red represents cell death. Adapted from Nel et al. (2006).

Similarly, novel materials such as the fullerene C_{60} , also generate both superoxide anions and hydroxyl radicals in cell free conditions which may be further enhanced by physiological reductants such as NADH and UV light (Sayes et al. 2005; Sayes et al. 2004; Rancan et al. 2002). The surface of a nanoparticle may donate or accept electrons or bind organic molecules (e.g. quinones) which may increase surface redox cycling in the presence of transition metals (Dockery et al. 1993; Berg et al. 2010). The ability for carbon black to synergistically modify the toxic effects of transition metals has been attributed to this reductive ability (Wilson et al. 2007; Wilson et al. 2002).

While many nanoparticles induce ROS without additional cofactors (e.g. light, UV, and/or transition metals), induction of ROS by other nanoparticles may require additional cofactor input (Oberdorster et al. 2005). A prime example is the UVA light-dependent heterolytic cleavage of water by TiO_2 to yield the hydroxyl radical (Shen et al. 2006). This reaction does not occur in the absence of light (Limbach et al. 2007). However, while a majority of TiO_2 nanoparticles are photocatalytically active, alterations in crystal phases can result in large differences in ROS production. For example, TiO_2 in the anatase crystal phase yields a significantly greater quantity of reactive oxygen species than TiO_2 in the rutile crystal phase (Sayes et al. 2006; Warheit et al. 2007b). This difference in ROS production is attributed to differences in the band gap energies of anatase and rutile (3.2 eV and 3.0 eV, respectively). Interestingly, the amorphous form of TiO_2 generates greater ROS than that of anatase TiO_2 and this has been attributed to

increases in surface defect densities (Jiang et al. 2008a). Such surface defects may isolate transition metals and hence increase their catalytic activity.

The use of transition metal-containing nanoparticles as additives or catalysts plays a large role in the generation of reactive oxygen species in both the cellular and acellular environment. The role of transition metals in particle toxicology has evolved from their previous association with diesel exhaust particles, coal fly ash, and other ambient atmospheric particulates (Cass et al. 2000; Dreher et al. 1997). The effect of transition metal incorporation, albeit on purpose or accidental, has the potential to alter the oxidative potential of the particle. This topic was recently investigated through the intentional incorporation of transition metals into colloidal silica which resulted in increased oxidant production *ex vivo* (Limbach et al. 2007). The results suggested that Fe-doped silica significantly increased *in vitro* oxidant production compared to an acellular-based reaction suggesting that the intracellular generation of oxidants proceeds through both particle-mediated and biologically-mediated routes.

An alternate particle-dependent route of oxidant production stems from the dissolution of metal ions from the nanoparticle surface. Nanoparticle dissolution may be enhanced upon co-exposure to other oxidative compounds. For example, the dissolution of silver nanoparticles is increased in the presence of H₂O₂, which then leads to a synergistic effect on the cytotoxicity *in vitro* (Ho et al. 2010). In effect, any cofactor which retains the ability to elicit H₂O₂ generation may lead to increased particle dissolution. In addition to oxidative dissolution, other environmental factors (e.g. pH), retain the potential to alter the nanoparticle dissolution. For example, ZnO nanoparticles

are highly soluble at acidic pH and hence, have been shown to rapidly dissolve in cell culture media and lysosomal fluid (Xia et al. 2008a). Liberated Zn^{2+} ions are sequestered into the mitochondria where membrane damage increases the release of electrons from the electron transport chain. These leaky electrons facilitate the generation of free radicals (Fujitani et al. 2008). Therefore, the release of free metal ions from transition-metal doped or transition metal-containing nanoparticles may increase metal bioavailability thus providing a particle-dependent means from which to damage cellular substrates.

1.4.2 Cellular-Mediated Generation of Oxidants

While the inherent physicochemical properties of nanoparticles may lead to the generation of intracellular oxidants, adverse effects stemming from cellular exposure to nanoparticles of various compositions may lead to increased oxidant generation over what has been reported *ex vivo*. Multiple nanoparticles have been reported to induce oxidant generation and subsequent oxidative stress in cellular systems (Brown et al. 2001; Foucaud et al. 2007; Li et al. 2003). This intracellular oxidant generation is likely to be a cell dependent process resulting from intracellular redox cycling or mitochondrial dysfunction.

Transition metal cations, such as ferrous iron and the cuprous ion, are excellent electron sources for the reduction of intracellular dihydrogen peroxide. Hence, nanomaterials which contain ions with similar characteristics to Fe or Cu, may lead to the intracellular generation of increasingly toxic oxygen species (e.g. OH^{\bullet}). Increased bioavailability of transition metals may generate intracellular oxidants through multiple

well-characterized reactions. First, ferrous (Fe^{2+}) ions, in the presence of hydrogen peroxide, may lead to the formation of more potent oxygen species such as the hydroxyl radical. This process, discovered in 1894, is known as the Fenton reaction (Fenton 1894). A simple addition to the Fenton reaction allows redox cycling of the Fe^{3+} . This process, termed the Haber-Weiss reaction, provides additional hydroxyl radical generation through the reduction of ferric (Fe^{3+}) iron to ferrous iron (Fe^{2+}) by the superoxide anion (Farber 1994). While the general formation of oxidant species in many cellular organelles is commonplace (e.g. peroxisomes and mitochondria), the potential for adverse effects following nanoparticle exposure may be raised, as the discrete size of nanoparticles may allow the distribution of iron into different cellular compartments not normally accessed by iron ions (Brunner et al. 2006).

A second means of intracellular oxidant production occurs in response to mitochondrial damage following exposure to nanoparticles. Multiple reports suggest that nanoparticles may preferentially partition to the mitochondria where they induce major structural damage to both the mitochondrial membrane and cristae (Li et al. 2003). For example, both fullerene particles and micellular nanocontainers have demonstrated passive distribution into mitochondria (Foley et al. 2002; Savic et al. 2003). This mitochondrial partitioning of nanoparticles may have the ability to interfere with mitochondrial metabolism and thus ROS amplification may be a consequence of either stimulation of mitochondrial respiration or decreased mitochondrial membrane efficiency (Wilson et al. 2002; Driscoll et al. 2002). This alteration of mitochondrial

function may result in excess superoxide anion radical formation thereby leading to resultant oxidative stress.

1.4.3 Cellular and Acellular Methods to Determine Oxidant Production

Linking nanoparticle physicochemical properties to oxidant production in both the cellular and acellular environment may help to define and identify novel properties associated with particle-induced oxidative stress. Fluorescence-based dyes are often a great alternative to analytical techniques such as electron spin resonance (ESR) or electron pair resonance (EPR) as a means of observing oxidant production (Sayes and Warheit 2009). The reactivity of these dyes, as depicted in Table 1.3, range from very broad (e.g. DCFH) to very specific (e.g. APF). In the nanotoxicology literature, the dichlorofluorescein diacetate (DCFH-DA) is the most common means to measure intracellular oxidant production and has been adapted for use in microplate format (Wang and Joseph 1999). Briefly, a permeable DCFH-DA molecule passes through the cell membrane where it is hydrolyzed to DCFH. Upon reaction with various intracellular oxidants (e.g. H_2O_2 , HO^\bullet , or ROO^\bullet) DCFH is oxidized to the fluorescent DCF (Gomes et al. 2005). Similarly, the DCFH-DA assay may additionally be modified for use in cell free-assays (Limbach et al. 2007). A variety of dihydrodyes (including dihydrorhodamine 123, dihydrocalcein, hydroethidium) react in a similar manner with slight alteration in their selectivity (Soh 2006). However, limitations of these dyes include their relatively non-specificity as well as their ability to undergo autooxidation.

Table 1.3 Dyes utilized to monitor the production of reactive oxygen species

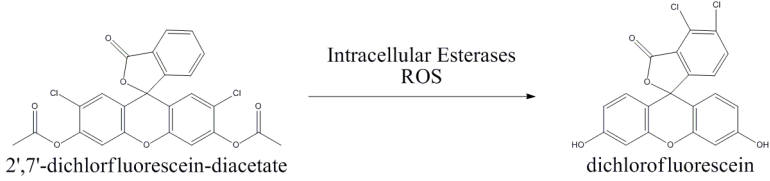



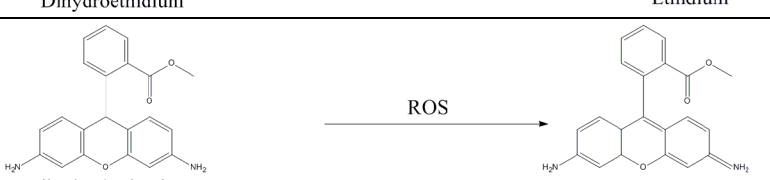
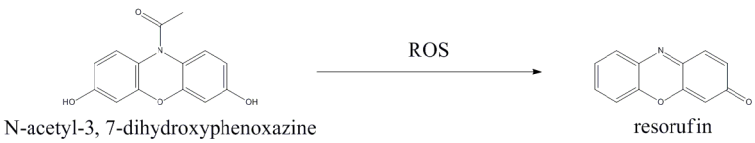

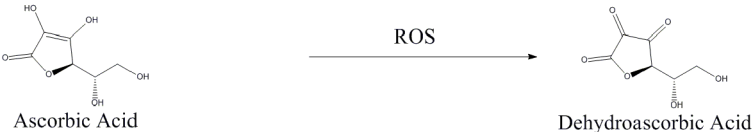
<i>ROS Probe</i>	<i>Acronyms</i>	<i>Chemical Reaction</i>	<i>Sensitivity</i>
2',7'-Dichlorofluorescein-diacetate	DCFH-DA	 <p>2',7'-dichlorofluorescein-diacetate → dichlorofluorescein</p>	Non-Specific
Aminophenyl fluorescein	APF	 <p>APF → Fluorescein Derivative</p>	OH^\bullet ONOO^- $^1\text{O}_2$ $-\text{OCl}$
Hydroxyphenyl fluorescein	HPF	 <p>HPF → Fluorescein Derivative</p>	OH^\bullet ONOO^- $^1\text{O}_2$
DiHydroethidium	DHE	 <p>Dihydroethidium → Ethidium</p>	$\text{O}_2^{\bullet -}$ ONOO^-
Dihydrorhodamine	DHR123	 <p>Dihydrorhodamine → Rhodamine</p>	$\text{O}_2^{\bullet -}$ ONOO^- $-\text{OCl}$

Table 1.3 Cont.

<i>ROS Probe</i>	<i>Acronyms</i>	<i>Chemical Reaction</i>	<i>Sensitivity</i>
N-acetyl-3,7-dihydroxyphenoxazine	Amplex Red	 <p>N-acetyl-3, 7-dihydroxyphenoxazine</p> <p>resorufin</p>	H ₂ O ₂
3-Aminophthalhydrazide	Luminol	 <p>3-aminophthalhydrazide</p> <p>Ground State Dianion</p>	-OCl OCl ONOO ⁻ OH [•]
Ascorbic Acid	Vitamin C	 <p>Ascorbic Acid</p> <p>Dehydroascorbic Acid</p>	Non-specific

To address these issues of autooxidation and non-specificity, aminophenyl fluorescein and hydroxyphenyl fluorescein are often utilized. These dyes are increasingly selective ($\text{OH}\cdot, \text{ONOO}^-$) in their reactivity and have been shown to be more resistant to autooxidation. While these fluorescent dyes comprise a large portion of nanoparticle-generated oxidant studies, Table 1.3 is by no means comprehensive. A great review of fluorescent dyes utilized for oxidant production and their sensitivities may be found elsewhere (Soh 2006; Gomes et al. 2005).

While fluorescent dyes are highly utilized among the nanotoxicology community, issues have arisen with nanoparticle compatibility. For example, the presence of liberated transition metals may alter the fluorescent properties of dyes such as dihydrocalcein. The presence of metal ions such as Fe^{3+} , Co^{2+} , Ni^{2+} , and Cu^{2+} have been reported to quench the fluorescence of dihydrocalcein. In an effort to further elucidate these potential interferences, Griffiths and Singh (2011) have described the potential for ultrafine dextran-coated iron oxide nanoparticle to alter the background in both absorbance and fluorescence-based assay and suggest that appropriate controls be applied (Griffiths et al. 2011).

1.4.4 Hierarchical Modeling of Oxidative Stress

All aerobically active cells generate low levels of intracellular oxidants resulting in by-products of cellular respiration. The potency of these intracellular oxidants is, under normal circumstances, ameliorated by both enzymatic and non-enzymatic cellular defenses. However, the aforementioned situations involving particle-generated oxidant production may pose a problem if the production of oxidants is greater than can be mediated by the cellular antioxidant system. For example, ultrafine carbon black, which retains greater free radical activity than micrometer size carbon black, leads to intracellular GSH level depletion upon cellular exposure (Stone et al. 1998). Furthermore, upon depletion or saturation of cellular antioxidant defense mechanisms, cellular damage can occur. The main biochemical targets of cellular oxidation are proteins, lipogenous membranes, nucleic acids and mitochondrial function. A variety of techniques have been utilized to assess these toxicological endpoints as seen in Table 1.4.

Table 1.4 Biological markers of oxidative stress and analytical techniques

Biological Response	Indicator	Reference(s)
Protein Oxidation	Carbonyl Content <ul style="list-style-type: none"> Indicator most commonly used Derivatives of P, K, R, T oxidation Easy detection using ELISA based format 	<ul style="list-style-type: none"> (Oberdorster 2004) (Murray et al. 2009) (Tedesco et al. 2008)
	3-Nitrotyrosine <ul style="list-style-type: none"> Covalent protein modification of tyrosine Indicator for oxidative stress Biomarker for peroxynitrite formation 	<ul style="list-style-type: none"> (Yokel et al. 2009) (Niu et al. 2007)
	GSH Oxidation <ul style="list-style-type: none"> Tripeptide oxidized as immediate response to ROS GSH oxidized to GSSG 	<ul style="list-style-type: none"> (Yu et al. 2009) (Yang et al. 2008) (Park and Park 2009) (Lin et al. 2006) (Stone et al. 1998)
DNA Oxidation	8-OHdG <ul style="list-style-type: none"> Product of oxidative damage by DNA Available for detection in tissue, serum, plasma, and urine 	<ul style="list-style-type: none"> (Trouiller et al. 2009) (Bhattacharya et al. 2009) (Inoue et al. 2006)
	COMET Assay <ul style="list-style-type: none"> Known as single cell gel electrophoresis Detects both single and double strand DNA breaks 	<ul style="list-style-type: none"> (Yang et al. 2008) (Barnes et al. 2008) (Reeves et al. 2008)
Mitochondrial Disruption	Mitox <ul style="list-style-type: none"> Detects mitochondrial superoxide Often utilized for live cell imaging 	<ul style="list-style-type: none"> (Long et al. 2006) (Xia et al. 2008a)
	MTT Assay <ul style="list-style-type: none"> Conversion to colorimetric product my mitochondrial metabolism Variety of related tetrazolium salts assays exist 	<ul style="list-style-type: none"> (Sayes et al. 2005) (Berg et al. 2009) (Oberdorster 2004)
Lipid Peroxidation	Malondialdehyde <ul style="list-style-type: none"> Oxidative degradation products of polyunsaturated lipids Often measure with the TBARS assay Can initiate multiple oxidation reactions 	<ul style="list-style-type: none"> (Yang et al. 2008) (Li et al. 2004) (Eom and Choi 2009)
Transcription Factor Activation	NRF2 <ul style="list-style-type: none"> Cytosolic stabilization and nuclear translocation Upregulation of phase II antioxidant genes <ul style="list-style-type: none"> Increased GSH synthesis Genes include: NQO1, HO-1, and GPX 	<ul style="list-style-type: none"> (Xia et al. 2008a) (Li et al. 2004) (Eom and Choi 2009)
	NFκB <ul style="list-style-type: none"> Nuclear Translocation of NFκB subunits Increased cytokine and chemokine expression Activated by a variety of cellular stressors 	<ul style="list-style-type: none"> (Xia et al. 2008a) (Manna et al. 2005) (Shukla et al. 2000)

The cellular response to oxidative stress reflects a delicate balance of cellular processes undertaken in direct response to the quantity of oxidative stress present. For example, at low to moderate levels of oxidative stress, cell proliferation or senescence may occur; while high levels of oxidative stress may direct cells to either apoptotic or necrotic pathways (Martindale and Holbrook 2002). A variety of cellular pathways are implicated upon the induction of cellular stress, however; both the NF-E2-related factor 2 (NRF2) and the NF κ B pathways have been identified to play a regulatory role in the cellular antioxidant and inflammatory response following stimulation by ROS. The NRF2 transcription factor is involved in the regulation and induction of multiple phase II antioxidant genes. Similarly, the NF κ B transcription factor plays a crucial role in the regulatory mechanism of the immune response.

The transcription factor NF-E2-related factor 2 (NRF2) is identified as an essential regulator of a variety of phase II antioxidant enzymes (Itoh et al. 1997). Metabolism by phase II enzymes typically result in large increases in compound hydrophilicity through conjugation with a variety of cofactors (e.g. glutathione; mercapturic acid synthesis) which promote compound excretion. Generating *nrf2* knockout mice, Itoh and Chiba (1997) have suggested that procarcinogens may be metabolized by phase I metabolism to carcinogens (e.g. Benzo(a)pyrene). These carcinogens may build up and exert an increased response in *nrf2*-/*nrf2*- mice (Itoh et al. 1997). However, while expression of NRF2 is typically beneficial, its regulation has been described as promising target for chemotherapeutic targeting as a means of altering drug toxicodynamics (Kensler and Wakabayashi 2010; Wang et al. 2008).

With few exceptions, the expression of NRF2 is highly ubiquitous. Under basal conditions, the NRF2 transcription factor is repressed by KEAP1 in the cytosolic compartment through sequence-specific binding to the Neh2 domain of NRF2 (Itoh et al. 1999). Under these conditions rapid proteosomal degradation of NRF2 leads to a relatively short protein half-life (McMahon et al. 2003). Upon direct stimulation by either electrophiles or indirect stimulation by kinases (e.g. protein kinase C) at serine 40, NRF2 is released from the repressor KEAP1 (Jaiswal 2004). This act reveals a nuclear localization signal and hence, nuclear translocation of NRF2 follows. Once in the nucleus, NRF2 dimerizes with sMAF proteins and binds to antioxidant response elements (ARE), otherwise known as electrophilic response element (EpRE), located in the promoter regions of numerous phase II genes (Itoh et al. 1997). Numerous genes have been shown to contain an ARE and thus may be subject to regulation by NRF2. Included in these genes are most notably NAD(P)H: quinone oxidoreductase 1 (NQO1), heme oxygenase 1 (HO-1), glutathione-s-transferase (GST), and glutamate cysteine ligase (GCL) and catalase (CAT) (Zhu et al. 2008).

As previously mentioned, NRF2 may provide a current target for chemotherapeutics, as upregulation of NRF2 often leads to enhanced ability to detoxify chemicals (Wang et al. 2008). A recent study by Singh and Misra (2006) demonstrates that a variety of non-small-cell lung cancer cell lines yield mutations in the NRF2 repressor, KEAP1 (Singh et al. 2006). Included in these non-small-cell derived cancers is the type II lung carcinomatic-derived epithelial cell line A549. Thus, it is suggested that A549 demonstrates increased NRF2 nuclear localization and transcriptional control

over non-cancerous cell lines. While the A549 cell line is continuously utilized in the literature as a model epithelial cell line, it is hence, suggested that other non-cancerous cell lines be utilized in tandem.

As oxidative stress accumulates, the cellular pool of GSH:GSSH further shifts to the oxidized state (Nel et al. 2006). This tier II response may lead to the activation of the NF κ B family of transcription factors, which enhances the release of inflammatory cytokines in a response to recruit inflammatory mediators. NF κ B is a key regulator of inflammatory cytokines such as TNF- α , Il-1, Il-6 and Il-8. Similar to NRF2 activation, the NF κ B pathway is posttranscriptionally regulated through a ubiquitin-dependent pathway.

The ability for nanoparticles to modulate inflammation has been reported to be mediated through the NF κ B pathway (Romoser et al. 2011; Brown et al. 2001; Manna et al. 2005). For example, Brown and others (2006) observed increased levels of Il-8, a major inflammatory mediator, following exposure to nanometer sized polystyrene. Similar Il-8 secretion has been observed with anatase TiO₂ in the A549 cell line; however, reported results suggest that activation is cell-line dependent (Sayes et al. 2006). Further implicating the NF κ B pathway as a mediator of nanoparticle induced inflammatory response, Manna and others (2005) report activation of the NF κ B pathway by SWCNT, which is dependent upon MAPK (Manna et al. 2005). This secretion of cytokines may lead to an inflammatory response *in vivo*.

Inflammation, typically a response to protect the body from foreign pathogens or stressors, may retain the potential to yield adverse pathological insults following

inhalational exposure to nanoparticles. Particles with low solubility retain the potential to induce a more potent inflammatory response compared with particles of higher solubility (Warheit et al. 2007a). This may be due, in part, to their increased biopersistence coupled with the ability to decrease macrophage uptake efficacy (Renwick et al. 2001). The inflammatory response *in vitro* may be measured by an influx of inflammatory mediators (e.g. neutrophils) to the site of insult. For example, Brown and others (2001) noted significantly more neutrophil influx in the rat lung following exposure to 64 nm polystyrene particles than was observed following exposure to either 202 nm or 505 nm particles (Brown et al. 2001). Additionally, nanometer-sized colloidal silica has been reported to have elicit greater neutrophil influx in lung alveoli than fine sized colloidal silica (Kaewamatawong et al. 2005). This influx of polymorphonuclear neutrophils in broncioalveolar lavage fluid may be associated with increases in oxidative surface potential (Stoeger et al. 2009). While this inflammation is typically beneficial in the response to foreign pathogens, it retains the possibility to be deleterious in situations of particulate exposure.

In response to low solubility particles that retain the ability to decrease macrophage clearance, excessive and persistent inflammation can occur; often with negative consequences to biological organisms. This effect is due to the fact that inflammatory mediators may produce a secondary oxidative insult which has been reported to increase the genotoxicity of particles (Schins 2002; Oberdorster 1995; Driscoll et al. 2002). This secondary genotoxicity effect, noted as the “respiratory burst”, is associated with increased consumption of oxygen coupled with production of

the superoxide anion and NO. The ability to produce this secondary oxidative toxicity is highlighted as the production of oxygen radicals by macrophages and neutrophils following exposure to either asbestos or crystalline silica (Quinlan et al. 1994; Fubini and Hubbard 2003). These effects are conserved at the nanometer size scale as well. For example, Driscoll and others (2002) noted that ultrafine carbon black increased mutation frequency in type II cells in the presence of polymorphonuclear neutrophils which was preventable by antioxidant addition (Driscoll et al. 2002).

Oxidative stress plays a role in a variety of cell processes ranging from cell signaling to inflammation to cell death. While nanotechnology retains the ability to be harnessed, it may be possible to decrease the ability of nanoparticle to produce ROS through surface oxidation as has been reported with carbonaceous compounds (Sayes et al. 2004; Berg et al. 2010). The development of both cellular and acellular assays to measure ROS production will play a crucial role in the health and safety of the nanotechnology field. For this reason, future efforts should require that nanoparticles destined for occupational use be analyzed for the potential to generate oxidant production in either the acellular and cellular-based environment.

1.5 Summary

The novel physicochemical parameters seen at the nanometer size scale, while often desirable in product development, have the potential to yield adverse effects following incidental exposure occurring throughout the product lifecycle. Often times, these exposures are not to a single particle alone, but in essence, a mixture comprised of multiple particle types and organics. These mixtures have the potential to elicit an

increased toxicological response which is often attributed to the physicochemical characteristics of the nanoparticle surface. Subsequently, physicochemical characteristics often define the particle and its uses. Simple alterations in physicochemical properties may lead to large differences in toxicity. Toxicity in particulates is often synonymous with increased oxidative stress and both cellular and acellular assays report the generation of reactive oxygen species by nanoparticle which is different on a nanoparticle basis. Subsequently, the oxidative stress may lead to a variety of cellular responses ranging from the induction of phase II enzymes to inflammation, and even cell death. Deciphering the nanoparticle physicochemical characteristics which play a role in oxidative stress and subsequent cellular toxicity combined with the identification of *actual* exposure values, will help to further define the risks associated with nanoparticle use.

2. THE RELATIONSHIP BETWEEN pH AND ZETA POTENTIAL OF ~30 NM METAL OXIDE NANOPARTICLE SUSPENSIONS RELEVANT TO *IN VITRO* TOXICOLOGICAL EVALUATIONS*

Zeta potential measurements are common in nanotoxicology. This research probes the effects of pH and time on nanoparticle zeta potential, agglomerate size, and cellular viability. The nanoparticles TiO_2 , Fe_2O_3 , Al_2O_3 , ZnO , and CeO_2 , were titrated from pH 12.0 to 2.0. The isoelectric points (IEP) of the nanoparticles were near neutral with the exception of TiO_2 (IEP=5.19) and Fe_2O_3 (IEP=4.24). Nanoparticle agglomerates were largest at the IEP. TiO_2 and Fe_2O_3 increased in zeta potential and agglomerate size over time; while Al_2O_3 and ZnO displayed little change. CeO_2 increased in zeta potential; however, the net charge remained negative. Cytotoxicity studies revealed that TiO_2 and Fe_2O_3 caused decreasing cellular viability over 48 hrs. Al_2O_3 , ZnO , and CeO_2 cellular viability remained similar to control. Results indicate that alterations in the pH have a large effect on zeta potential and agglomerate size which may be used as a predictive measure of nanotoxicity.

2.1 Introduction

Within the nanotoxicology field, increased findings demonstrate the ability of nanoparticle charge (zeta potential) to influence corresponding cellular responses ranging from particulate endocytosis to cytotoxicity (Nan et al. 2008; Lundqvist et al.

* “Reproduced with permission from Berg, J.M., Romoser, A., Banerjee, N., Zebda, R. and Sayes, C. 2009. The relationship between pH and zeta potential of ~ 30 nm metal oxide nanoparticle suspensions relevant to *in vitro* toxicological evaluations. *Nanotoxicology* 3(4): 276-283. Copyright © [2009] Informa UK Ltd.”

2008; Xia et al. 2006). Reviews of current literature suggest a need for careful characterization of all classes of nanomaterials including metal colloids, metal oxides, and carbonaceous particles, prior to their use in toxicity testing (Handy et al. 2008; Karakoti et al. 2006). The relationship between zeta potential and ambient conditions surrounding the nanoparticles remains a largely unexplored area which will require researchers from many scientific disciplines to answer. This research probes the effects of pH on nanoparticle zeta potential and size using ~30 nm particles in aqueous suspension. The nanoparticles include titanium dioxide (TiO_2), iron oxide (Fe_2O_3), aluminum oxide (Al_2O_3), zinc oxide (ZnO), and cerium dioxide (CeO_2). In these nanoparticle systems, which include both the nanoparticle and the suspension medium, features such as agglomeration, dispersion, and suspension stability may be influenced by external factors such as the flux of hydrogen ions (H^+) in solution.

The zeta potential represents the charge of a nanoparticle in relation to the surrounding conditions. Nevertheless, the zeta potential is not an actual measurement of the individual molecular surface charge; rather, it is a measurement of the electric double layer produced by the surrounding ions in solution (i.e. counter ions) (Instruments 2008). These counter ions play a role in the calculation of zeta potential measurement (Figure 2.1). All particle systems in an aqueous media carry an electric charge which may be positive, negative, or neutral. For surface-derived nanoparticles, dissociation of an acidic group, such as a carboxylic acid moiety on a nanoparticle surface will yield a negatively charged surface; while dissociation of a basic group on a nanoparticle surface will yield

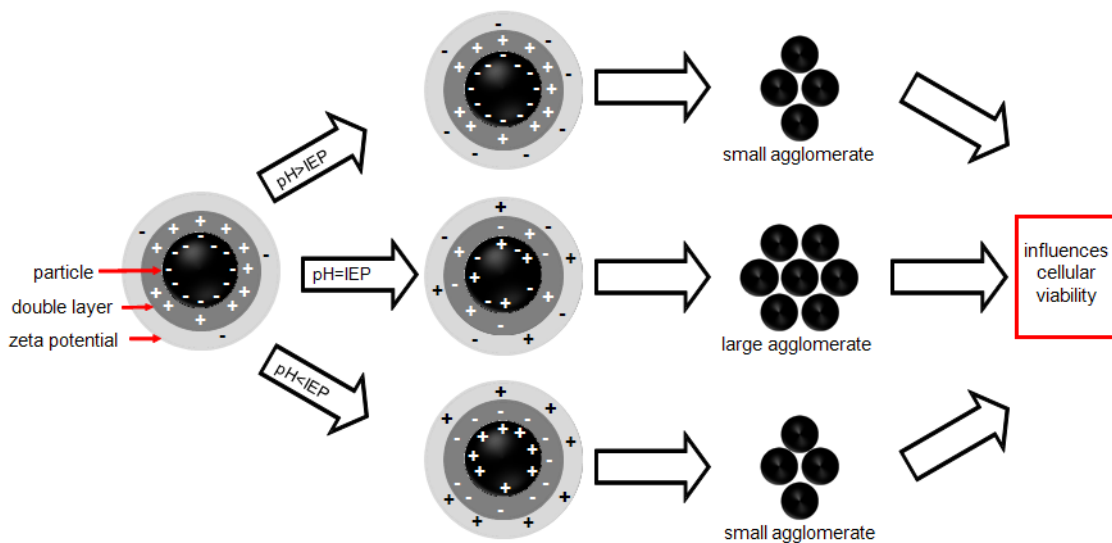


Figure 2.1 Schematic diagram of the effects of pH on a metal oxide nanoparticle. The zeta potential plane is measured as the primary indicator of surface charge. Surface charge is altered when the pH is increased or decreased. The downstream effect of altered zeta potential is a change in agglomeration state, which influences the cytotoxicity.

a positively charged surface. For unmodified nanoparticles, the individual atoms that comprise the surface of the particle dictate its charge.

2.1.1 Relevance to Toxicology

Agglomeration of nanoparticles occurs when individual particles are held together by weak inter-particle interactions including solvation forces, van der Waals forces, electrostatic attractions, and hydrophobic interactions (Fichthorn and Qin 2008; Hakim et al. 2007; Min et al. 2008). In most instances, agglomeration state is reversible, but only if additional entropy (e.g. sonication or homogenization) or ions (changing H^+) are added to the system. It is suspected that this methodology could be used to size select for certain nano-populations within a particle suspension. Limitations of utilizing changes in pH for biological applications are that the resultant suspension could have a pH that is outside of the physiological range (7.35-7.45), may alter chemistry of drug delivery vehicles, or change conditions in cell culture media for *in vitro* use (Klaassen and Watkins 2003). Further, this methodology could yield insights into the fate and transport of nanoparticle aggregates after an exposure has occurred.

A likely exposure to nanoparticles may occur orally (Gatti et al. 2009). This route of exposure would ensure that nanoparticles enter an environment yielding a wide range of pH values. Initially, the nanoparticle would be exposed to a low pH in the stomach (pH= ~2) (Rodriguez et al. 1999; Beak et al. 2006). Following acidic conditions in the stomach, the environment is once again altered in the intestinal tract, yielding a more basic pH combined with peristaltic movement. Under these physiological situations, physical properties of the agglomerates such as size, surface

area, and zeta potential will change. This alteration in physical properties will yield nanoagglomerates of differing size and may increase likelihood that these nanoparticles could translocate through the endothelial lining and enter the circulatory system. This in turn may induce a systemic and/or chronic effect (Semmler-Behnke et al. 2007; Panessa-Warren et al. 2008; Lockman et al. 2004; Oberdorster 2007; Santhanam et al. 2008).

Altering the pH of the medium in which the nanoparticle is suspended will also yield differences in nanoparticle dissolution into ions or alter the surface chemistry of a nanoparticle (Guo et al. 2009). Altering the surface chemistry of nanoparticles may in turn effect how a nanoparticle binds cellular substituents such as proteins, and may affect the mechanisms by which these nanoparticles enter cells (Al-Jamal et al. 2008; Lundqvist et al. 2008).

Discovering the fundamental relationships between the properties of nanomaterials and certain toxicological responses will require the separation of the complex kinetics of nanoparticle delivery *in vitro* from the dynamics of response. This could be made possible by integrated computational and experimental dose-response analyses.

2.2. Experimental Procedures

2.2.1 Particle Preparation

Titanium dioxide (TiO₂, ~27 nm, 99.8%) particles were acquired from Evonik, Hanau-Wolfgang, Germany. Aluminum oxide, zinc oxide, and cerium dioxide (Al₂O₃, <50 nm, 99.5%; ZnO, <50 nm, 99.5%; CeO₂, <25 nm, 99.5%) nanoparticles were

purchased from Sigma Aldrich, St. Louis, Missouri, USA. Iron oxide (Fe_2O_3 , 23-35 nm, 98%) nanoparticles were synthesized using a flame synthesis method that has been described in detail elsewhere (Guo and Kennedy 2007; Yang et al. 2001). The stock solutions of each of the five ~ 30 nm particles were prepared in Milli-Q ultrapure water (18.2 m Ω). The resultant suspensions were bath sonicated for 30 min prior to material characterization and *in vitro* exposures. Nanoparticle size was visualized using dynamic light scattering (DLS). Zeta potential was measured via electrophoretic light scattering (ELS) combined with phase analysis light scattering (PALS) (Malvern Zetasizer Nano ZS). Size and zeta potential parameters were measured over various time points ranging from t=0 hrs to t=1 wk.

2.2.2 Titration

Nanoparticle titration was performed using the Malvern MPT-2 Autotitrator in parallel with the Malvern Zetasizer Nano-ZS. This combination allowed automated titration over a wide pH range and thus made it possible to determine the isoelectric point (IEP). Nanoparticles were titrated from basic pH (pH=12) to an acidic pH (pH=2) utilizing HCl and NaOH. At every pH unit (± 0.2 U) the zeta potential and size were determined. The IEP was determined using the Malvern Software Version 5.03. The concentration of the nanoparticles used was dependent upon the turbidity of the sample. The zeta potential and agglomerate size of ZnO, Al_2O_3 and CeO_2 were measured at a concentration of 200 ppm (mg/L); TiO_2 was measured at a concentration of 50 ppm (mg/L); and Fe_2O_3 was measured at a concentration of 25 ppm (mg/L).

The differences in nanoparticle concentration for IEP measurements were necessary due to the refractive indices of the nanoparticles probed; however, as a note, a higher concentration of nanoparticles would facilitate increased incidence of collision, thus leading to agglomeration when compared to a lower concentration of nanoparticles.

2.2.3 Cytotoxicity

Cytotoxicity studies were performed by dosing cultured mouse hepatocytes (AML12, American Type Tissue Collection, Manassas, VA, USA) with 10 mg/L nanoparticles in 24-well plates. Dosed wells differed only by the type of nanoparticles used and not the concentration of nanoparticles. A control was added for comparison. DMEM/F-12 media was used for all cells. The dosed-cell plates were incubated at 37°C. Cell viability was determined using a Countess Automated Cell Counter (Invitrogen Corp., Carlsbad, CA, USA) in combination with trypan blue dye at 1 hrs, 24 hrs, and 48-hrs post-exposure time points. Dead cells exhibit a compromised membrane, which allows the dye to penetrate, providing for differentiation from live cells.

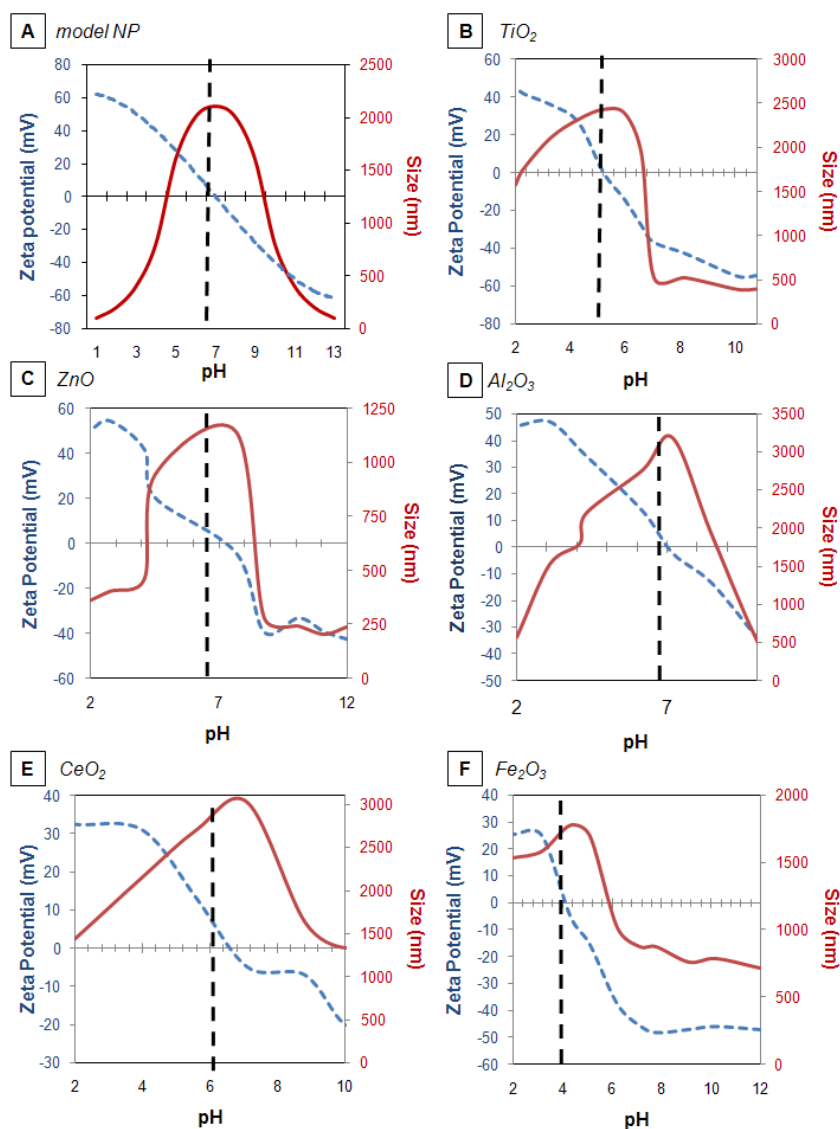


Figure 2.2 Titration of nanoparticles in ultrapure water. (A) In a model nanoparticle system, the largest aggregate size would be observed at its isoelectric point (zeta potential=0 mV). The farther the zeta potential deviates from 0 mV, the smaller the particle agglomerate due to increasing repulsive forces. Titrations of (B) TiO_2 , (C) ZnO , (D) Al_2O_3 , (E) CeO_2 , and (F) Fe_2O_3 from basic (pH>10) to acidic (pH<3) conditions. All nanoparticles exhibit an isoelectric point (IEP). Results indicate that zeta potential and size are dependent upon pH. Dashed vertical line represents isoelectric point.

2.3 Results

Results indicate that the pH has a pronounced effect on the zeta potential of each nanoparticle tested in this study. The change in zeta potential was found to alter the stability of the nanoparticle suspension. Figure 2.2 B-E illustrates the titration curves of TiO₂, ZnO, Al₂O₃, CeO₂, and Fe₂O₃. A hypothetical model nanoparticle exhibits the largest agglomerate size at the point where its zeta potential is 0 mV (Figure 2.2A), as was determined empirically for the remainder of the tested nanoparticles (Figure 2.2B-E). The point at which the nanoparticle exhibits no net charge is termed the isoelectric point (IEP). ZnO, Al₂O₃, and CeO₂ each display an IEP (IEP = 7.13, 7.06, and 6.71 respectively) at a pH relevant to interstitial fluid, bronchoalveolar lavage fluid, lymph, and blood (Klaassen and Watkins 2003). However, this trend does not continue for TiO₂ and Fe₂O₃ nanoparticles. The TiO₂ and Fe₂O₃ nanoparticles exhibited an IEP at pH 5.19 and 4.24, respectively. The largest nanoparticle agglomerate size was dependent upon chemical composition and ranged from $1,772 \pm 47.56$ nm in the Fe₂O₃ sample to $3,185 \pm 541.0$ nm in the Al₂O₃ suspension. Further, the smallest agglomerate size throughout each nanoparticle suspension existed at the pH where the nanoparticle displayed a strongly charged surface. The intense charge on the surface increases the charge-charge repulsions between the particles, thus maintaining a more stable and monodisperse suspension. The smallest nanoparticle size was found in the ZnO sample (203.8 nm). This size is indicative of the hydrodynamic radius of the nanoparticle. In addition to changes in pH, the zeta potential of a nanoparticle changes over time when held in aqueous suspension. Figure 2.3 demonstrates that the nanoparticles tested

demonstrate a wide range of agglomeration states and zeta potentials over a time period $t=1$ hrs to $t=1$ wk. Over the course of this experiment, TiO_2 and Fe_2O_3 nanoparticles displayed a large zeta potential increase, which consequently affected their agglomeration state. TiO_2 and Fe_2O_3 nanoparticles originally exhibited zeta potentials of -29 mV and -32 mV respectively; however, after the 1 week time point, the zeta potential rose to -15 mV. As witnessed in both of these nanoparticles, a more neutral surface charge led to larger agglomeration state. On the contrary, ZnO and Al_2O_3 nanoparticles retained their negative surface charge over time. In these samples, stability was due to the strongly negative-charged zeta potential and the lack of agglomeration. CeO_2 nanoparticles demonstrated a slight increase in zeta potential over the 1 week time course. Interestingly, this slight increase still led to a very negative zeta potential of -27.8 mV. Because the zeta potential remained close to -30 mV, a number commonly used to indicate solution stability, the agglomeration state of the nanoparticles decreased slightly.

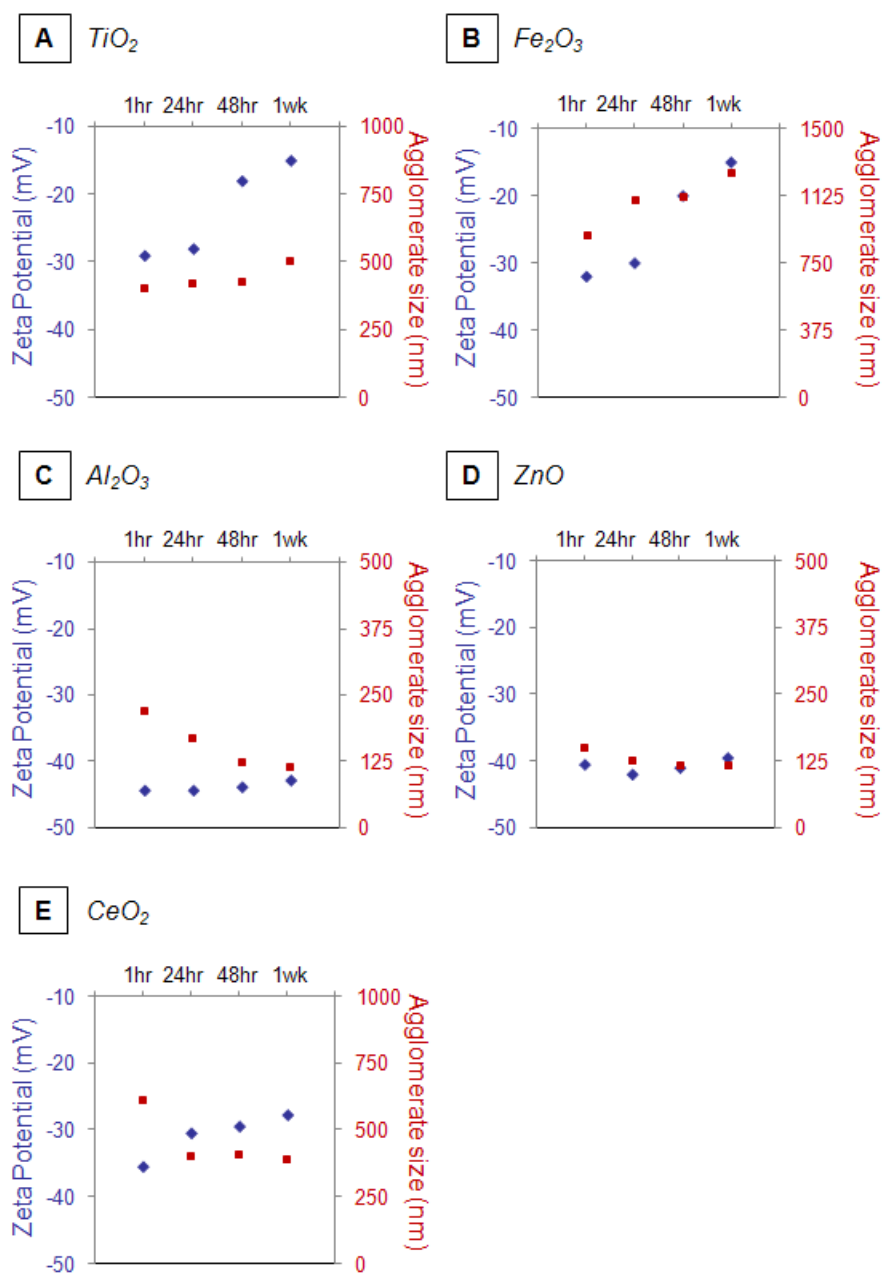


Figure 2.3 Alterations in zeta potential over time. The zeta potential of various metal oxide nanoparticles were measured over a time period of $t=0$ to $t=1$ week. Here, the TiO₂ nanoparticles (A) and the Fe₂O₃ nanoparticles (B) had an increasing zeta potential value (smaller absolute value). This increasing zeta potential corresponds with an increase in aggregate size. Both the Al₂O₃ nanoparticles (C) and the ZnO nanoparticles (D) remained highly negative, thus their aggregate size remained the same or decreased. CeO₂ nanoparticles (E) tend to decrease in size slowly over time despite the apparent small increase in zeta potential (smaller absolute value).

Cellular viability in the AML12 mouse liver hepatocyte was examined at 24 and 48hrs (Figure 2.4 A-F). It was noted that while the TiO_2 and Fe_2O_3 dosed samples exhibited heightened cellular viability at 1 hrs, they showed a decrease in viability each time thereafter. The ZnO and Al_2O_3 samples displayed increasing cell viability at 48 hrs, with viability of 91.5% and 91.75% respectively. This percentage is compared to the control cell viability of 96.0% after 48 hrs. CeO_2 nanoparticles, which exhibited only a slight change in cell viability, initially yielded 85.25% with a final 48 hrs post-exposure time point viability of 90%.

2.4 Discussion

Results indicate that alterations in the pH have a large effect on zeta potential and agglomerate size which may be used a predictive measure of nanoparticle toxicity. The suspension stability is dependent upon physical characteristics of both the suspended nanoparticles and their suspension medium. One of the major factors involved in the agglomeration process is electrostatic stabilization. Altering the zeta potential to the point at which it exhibits zero net charge, or the IEP of the nanoparticle, decreases stabilization forces and promotes agglomeration.

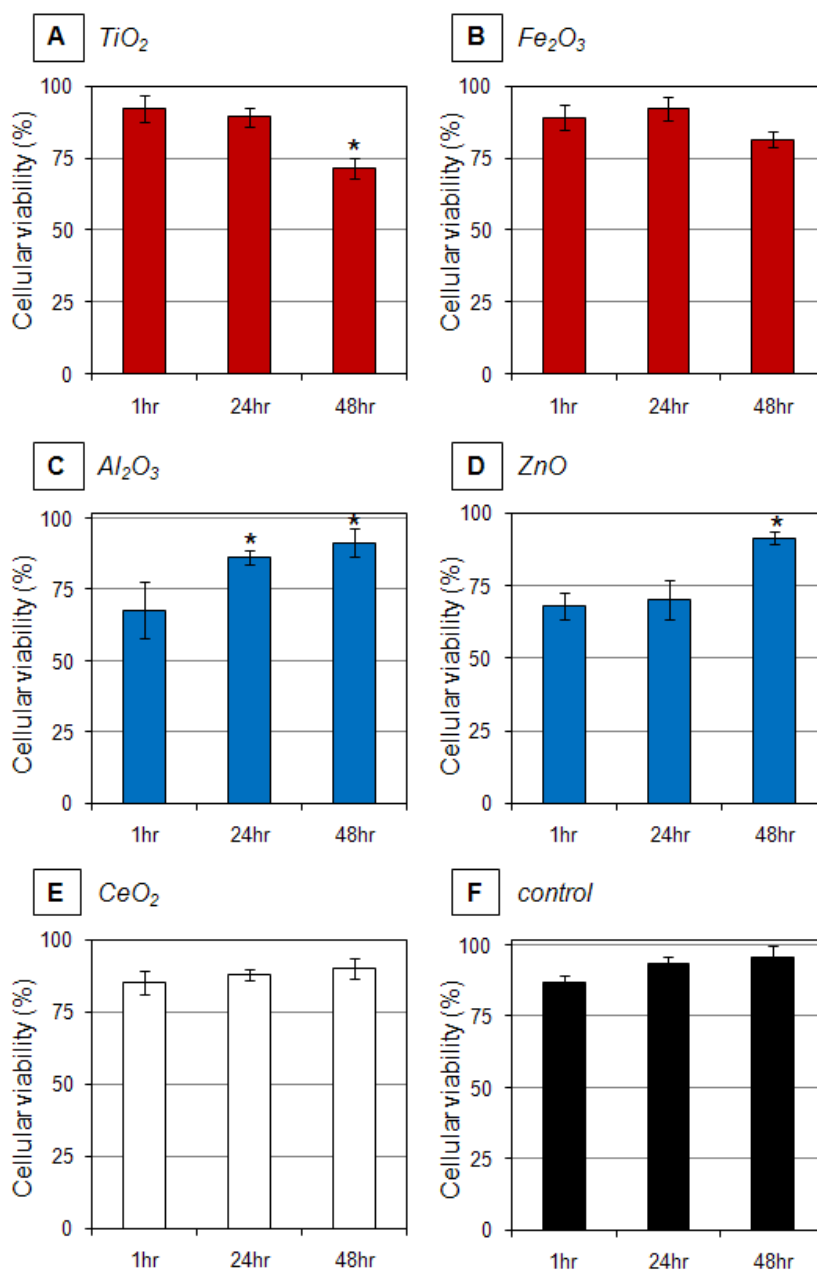


Figure 2.4 Cellular viability after nanoparticle exposure. Cellular viability correlates with the nanoparticle aggregation trend. AML12 cells were analyzed for cellular viability at times $t=0$ to $t=48$ hrs post exposure. Both the TiO_2 nanoparticles (A) and the Fe_2O_3 nanoparticles (B) displayed a decrease in cell viability until 48 hrs. This contrasts the Al_2O_3 (C) and the ZnO (D) nanoparticle data, which implies that cell viability increases over time. CeO_2 nanoparticles (E) displayed no significant change in viability. Control cells increased in cellular viability. * $p < 0.05$ vs. 1hrs post-exposure time point within the same graph.

In accordance with Figure 2.2, all of the nanoparticles tested displayed unique isoelectric points. While the ZnO, CeO₂, and Al₂O₃ nanoparticles possessed IEP at a physiologically-relevant pH, such as blood or interstitial fluid (pH=7.4), Fe₂O₃ and TiO₂ nanoparticles possessed IEP at acidic conditions. Conversely, the Fe₂O₃ and TiO₂ nanoparticles exhibited a charged surface at pH=7.4. This data, when compared with the difference in cellular viability seen in Figure 2.4, suggests that the presence of a charged surface on the nanoparticle agglomerate at physiological pH of 7.4 may correlate with a decrease in cellular viability in hepatocytes.

The study is pertinent due the possibility that many environments present in the body such as gastric secretions, urine, and lysosomal fluid are known to have a varying degree of pH which correlate with our findings regarding nanoparticle surface charge. Table 2.1 shows the representative pH of various bodily compartments which the particle would potentially be exposed to over the course of the pharmacodynamic process. Specifically, a pH of 2 present in the acidic gastric secretions from parietal cells, would likely alter the agglomeration state of the nanoparticles which have been examined in this study. Physiological conditions such as these would yield the smallest nanoparticle agglomerates seen by the body. In addition, for many of the nanoparticles tested, a strongly positive zeta potential may further yield electrostatic or covalent interactions with cellular components such as DNA or proteins as well as determine the specific route of uptake into the cell (Dausend et al. 2008).

Table 2.1 Prediction of metal oxide nanomaterial properties in various pharmacodynamic environments

Metal oxide nanomaterials	pH			
	<2.00	4.50	5.00	7.40
TiO ₂	+46.0/1573	+22.0/1860	+7.00/2390	-37.0/460
ZnO	+50.0/360	+44.0/945	+16.0/1200	-3.00/1170
Al ₂ O ₃	+45.0/561	+38.0/1750	+27.0/2400	-4.00/3050
CeO ₂	+32.6/1440	+26.0/2340	+20.0/2590	-6.00/2850
Fe ₂ O ₃	+25.4/1800	-9.00/1740	-15.0/1700	-47.0/830

*reported as zeta potential (mV) / average agglomerate size (nm)

Table 2.1 indicates that agglomerate size varies significantly, depending upon a variety of factors, including both pH and nanoparticle chemical composition. One possible condition not explored in this paper is the influence of ionic strength due to the addition of Na⁺ and Cl⁻ ions introduced during the titration. Increasing the ionic strength of the suspension medium may lead to an altered agglomeration state through possible charge shielding and condensation of the charge at the electric double layer (Handy et al. 2008; Tiyaboonchai and Limpeanchob 2007). This often poses a challenge when working with a biocompatible suspension medium. In addition, a buffered suspension medium (such as phosphate buffered saline) influences the particle agglomeration state (Sager et al. 2007). While these agglomerate sizes seen in the nanoparticle titration are representative of what would be seen in an aqueous suspension, it is important to note that both *in vitro* and *in vivo* conditions contain biomaterial, such as proteins and/or lipids that may coat the nanoparticle surface, altering both the chemistry and agglomeration state. This emerging hypothesis has proven valuable as shifts in the zeta potential and the isoelectric point have been reported after proteins adsorb onto the

particle surface (Cael et al. 2003; Xia et al. 2006). It has been suggested that this protein adsorption is just as significant to toxicology as the inherent physicochemical characteristics of the nanoparticles themselves (Lundqvist et al. 2008). Even in an *in vivo* model, specific nanoparticle-protein interactions will not only influence the agglomeration state of nanoparticles, but also provide a possible route of entry into cells. Although many reports have cited interactions at the nanomaterial-biological interface, these dynamic properties are influenced by the zeta potential and agglomeration state. This research strives to make a connection between these physicochemical characteristics as a predictive measure of nanomaterial toxicity.

Cellular viability was influenced by a variety of factors including zeta potential and agglomeration state. Results indicate that, of the nanoparticles tested, cellular exposure to Fe_2O_3 and TiO_2 yielded a decrease in viability over time. This alteration in cellular viability correlates with the charged surface and altered agglomeration state demonstrated by only these nanoparticles. It is hypothesized that the potential toxicity of nanoparticles is due to not just one, but many characteristics of the nanoparticle system. Our data suggests that both pH and agglomeration state show an association with cytotoxicity. Figure 2.3 shows that these nanoparticles increase in agglomeration size over time, coupled with a zeta potential trending towards neutral. These experiments were carried out in ultrapure water (pH=5.9). When suspended in a solution where pH=7.4, as that which is seen in cell culture media, Fe_2O_3 and TiO_2 were the only materials which were found not to be at or near their IEP. These results indicate that surface charge has the potential to influence cell viability.

Overall, it is important that nanoparticles be classified as an entire system that encompasses the nanoparticle, its suspension medium, and the ions in solution. This careful characterization is necessary to interpret which components of a nanoparticle may contribute to alterations in surface charge and toxicological effects. We have shown that factors such as pH can influence the zeta potential of different nanoparticles. Additionally, it was observed that changes in zeta potential lead to a change in cellular viability. In the future it will be important for researchers to carefully observe the conditions under which the zeta potential is measured when reporting results.

3. INTERNALIZATION OF CARBON BLACK AND MAGHEMITE IRON OXIDE NANOPARTICLE MIXTURES LEADS TO OXIDANT PRODUCTION*

Potential human exposure to mixed nanomaterials in consumer, occupational, and medicinal settings is increasing as nanomaterials enter the both the workplace and the marketplace. In this study, the toxicity of mixed engineered carbon black (ECB) and maghemite iron oxide (Fe_2O_3) nanoparticles was investigated in a cellular system in order to understand the mechanism of toxicity and potential methods of toxicity mitigation. Lung epithelial cells (A549) were exposed to mixed Fe_2O_3 and ECB nanoparticles, mixed Fe_2O_3 and ECB nanoparticles with addition of L-ascorbic acid, and mixed Fe_2O_3 and surface-oxidized engineered carbon black (ox-ECB) nanoparticles. The nanoparticles were characterized using transmission electron microscopy, nitrogen adsorption surface area measurement (BET), x-ray diffraction, and surface charge measurement. The carbon black nanoparticles were also characterized with a reductive capacity assay and by x-ray photoelectron spectroscopy (XPS). Cellular uptake of nanoparticles was analyzed via transmission electron microscopy and fluorescence microscopy; cellular uptake of iron was quantified using inductively coupled plasma mass spectrometry (ICP-MS). Both the MTT assay and the ethidium homodimer and calcein AM live/dead assay were used to measure cellular proliferation and cytotoxicity, respectively. The dichlorofluorescein diacetate (DCFH-DA) assay was used to measure

* “Reproduced with permission from Berg JM, Ho S, Hwang W, Zebda R, Cummins K, Soriaga M, Taylor R, Guo B, and Sayes C.M. 2010. Internalization of carbon black and maghemite iron oxide nanoparticle mixtures leads to oxidant production. *Chemical Research in Toxicology* 23(12): 1874-1882. Copyright © [2010] American Chemical Society.”

intracellular generation of reactive oxygen species. Results show that both Fe_2O_3 and ECB (or Fe_2O_3 and ox-ECB) are co-internalized in intracellular vesicles. Additionally, after exposure to the mixture of nanoparticles, the amount of acidified lysosomes increases over time. Cellular uptake of Fe_2O_3 nanoparticles was unaffected by mixing with ECB. Significant oxidant production occurred in cells exposed to mixed Fe_2O_3 and ECB, but not in cells exposed to mixed Fe_2O_3 and ox-ECB, nor in cells exposed to Fe_2O_3 and ECB with ascorbic acid addition. Furthermore, exposure to mixed Fe_2O_3 and ECB exhibited a dose-dependent decrease in cellular proliferation (MTT assay) and a decrease in cellular viability (ethidium homodimer and calcein AM live/dead assay) that were not seen in the Fe_2O_3 and ox-ECB scenario. The results support the hypothesis that exposure to mixed Fe_2O_3 and ECB produces oxidants that are mediated by the surface reductive capability of ECB when both particle types are co-localized in acidic cellular compartments. This oxidant production mechanism may lead to oxidative stress, but it can be mitigated by an anti-oxidant such as ascorbic acid, or by surface treatment of the ECB to decrease its surface reductive capacity.

3.1 Introduction

Metal oxide nanomaterial systems are promising candidates for many industrial, consumer, and medical applications due to their unique physicochemical properties (i.e. high surface areas and extraordinary electronic properties) (Li et al. 2008a; Provenzale and Silva 2009; Choquet et al. 2008; Hexsel et al. 2008). Given the widespread applications and their commercialization, there is an increasing potential for humans to be exposed to a multitude of nanomaterials. While much work in nanotoxicology has

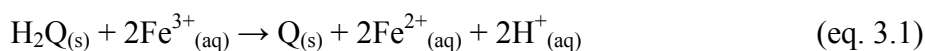
focused upon the etiology of specific nanoparticle effects, little attention has been given to the effects of mixtures, or combinations, of various nanoparticles on biological systems.

However, real-world exposure is very likely a mixture of multiple substances, such as airborne particulate matter. Previously, epidemiological data had suggested that airborne particulate matter (a mixture of many different substances) were more toxic than the sum of its parts. This was attributed to some sort of “synergistic” effect due to the mixture nature of airborne particulate matter (Valberg et al. 2006). In the nanotoxicology setting, human exposure to mixed nanomaterials is likely because multiple types of nanomaterials are often used simultaneously. For example, both metal oxide nanoparticles (e.g. Fe_2O_3) and graphitic carbon nanoparticles (e.g. carbon black) are likely to be used in various industrial applications (Alcantara et al. 2004; Bulushev et al. 2002; Martirosyan et al. 2007). Therefore, it is imperative to understand the toxicological effect of exposure to mixed nanomaterials. Recent publications have highlighted the importance of studying multiple nanoparticle exposure scenarios (Schulte et al. 2009; Sharma 2010). Additionally, while the nanoparticles used in this study (carbon black and iron oxide) are specific nanoparticle-types, they may be considered as representative elemental carbon or transition metal oxides found in the urban atmosphere (Cass et al. 2000).

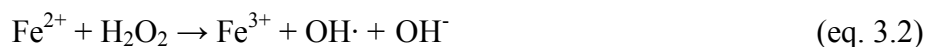
Previously, we have evaluated the oxidative stress of cells after simultaneous exposure to iron oxide (Fe_2O_3) and engineered carbon black (ECB) nanoparticles. This oxidative stress was measured by both protein and lipid oxidation (Guo et al. 2009).

Results indicated that exposure to both materials simultaneously, induced a synergistic oxidative stress effect to a human lung epithelial cell, even though exposure to either nanomaterial alone induced no significant oxidative stress. Our findings indicated that the ECB and Fe₂O₃ caused a synergistic effect greater than the sum of each particle tested individually.

We explained the synergism between engineered carbon black and iron oxide nanoparticles through an oxidative stress paradigm. This effect was largely attributed to the surface reductive capacity of the carbon black nanoparticles, which enabled redox cycling of the iron ions and hence caused significant oxidative stress in cells (Guo et al. 2009). Graphitic (non-diamond) carbon nanomaterials such as carbon black have chemically active sites (functional groups) on their surfaces that give rise to surface redox capabilities. In aqueous solutions, carbon black nanoparticles can reduce Fe³⁺ ions to Fe²⁺ (Guo et al. 2009). This may be schematically represented by the oxidation of the surface hydroquinone (H₂Q) groups by Fe³⁺ to surface quinones (Q) (Fu et al. 1993; Kung and McBride 1988):



where the subscript (s) represents surface moieties. Fe²⁺ is membrane permeable and has the ability to undergo further intracellular Fenton reactions in the cytosol (Hediger 1997; Rauen et al. 2004). Thus, Fe²⁺ can facilitate the generation of reactive oxygen species, for example, through the Fenton reaction:



It should be noted that nanoparticles could induce reactive oxygen species (ROS) production through abiotic and/or biotic pathways. For example, nanometer sized TiO_2 , in the anatase crystal form, is able to generate $\cdot\text{OH}$ radicals from water in the presence of UV light (Serpone et al. 2001), which may then elicit a biological response such as inflammation or oxidation of cellular substructures (Warheit et al. 2007a; Sayes et al. 2006). This type of ROS generation apparently has little dependence on the biological system, because TiO_2 nanoparticles are known to generate ROS in abiotic aqueous environments under UV irradiation. On the other hand, the ROS generation that was proposed in the previous study requires the dissolution of the Fe^{3+} from Fe_2O_3 nanoparticles, which would be pH-dependent and hence related to the locality within the biological system (Guo et al. 2009). Also, the synergism mechanism proposed above requires the Fe_2O_3 nanoparticles and the carbon black nanoparticles to be co-located in the same cellular compartments so that the dissolved Fe^{3+} ions would have access to the reductive sites on the surface of carbon black particles; this is evidently dependent on the interaction between the particles and the biological system.

With this study, we set out to elucidate the mechanism behind the synergistic toxicological effect of mixed Fe_2O_3 and carbon black. One objective of the study was to determine whether the two types of particles were indeed co-localized inside acidic cellular compartments. The second objective of this study was to determine whether there was a synergistic effect between Fe_2O_3 nanoparticles and surface-oxidized ECB (ox-ECB). Since the reductive capacity of engineered carbon black nanoparticles may be diminished by surface oxidation, we hypothesized that exposure to mixed Fe_2O_3 and ox-

ECB (with a decreased reductive capacity relative to ECB), would have a mitigated synergistic effect in comparison to the mixed Fe_2O_3 and ECB.

3.2 Experimental Procedures

3.2.1 Nanomaterial Preparation

Maghemite iron oxide (Fe_2O_3) nanoparticles were produced using a flame synthesis method that has been described in detail elsewhere (Guo and Kennedy 2007). Carbon black particles were produced in a hydrocarbon/air diffusion flame. Ethylene (C_2H_4) was used as a hydrocarbon fuel gas for the flame-engineered carbon black (ECB) nanoparticle synthesis. The burner features a fuel/oxidant co-flow structure described in Guo et al. (Guo and Kennedy 2007). Oxidized engineered carbon black (ox-ECB) was prepared by vigorous stirring in a neutral aqueous suspension under O_2 purge in continuous light for 2 weeks (Cheng et al. 2004). Fe_2O_3 , ECB, and ox-ECB nanoparticles were suspended in deionized water (Guo et al. 2009).

3.2.2 Chemical and Physical Characterization

Nanoparticle size was measured via transmission electron microscopy (TEM). Nanoparticle zeta potential was measured with a Malvern Nano-ZS (Malvern Inc, Worcestershire, UK) using dynamic light scattering (DLS) combined with phase analysis light scattering (PALS) (Berne and Pecora 1976). Samples for surface charge measurements were suspended in ultrapure water (18.2 M Ω) at a pH of 5.9 and bath sonicated for 30 minutes at 40 kHz. Nanoparticle specific surface area (SSA) was measured via the BET method under N_2 absorption (Brunauer et al. 1938). Size from SSA measurements was calculated. Discrepancies between TEM size and SSA size are

discussed elsewhere (Guo et al. 2009). Surface oxygen species for the ECB and ox-ECB samples were quantitated via X-ray photoelectron spectroscopy (XPS) following published procedures (Fairley et al. 2005; Briggs and Seah 1990; Xie and Sherwood 1991; Canas-Ventura et al. 2006; Popat et al. 1995; Estrade-Szwarckopf 2004; Szabó et al. 2006). Samples were dried onto a micro coverslip and analyzed on a Kratos Axis Ultra Imaging X-ray photoelectron spectrometer.

3.2.3 Reductive Capacity of Engineered Carbon Black and Oxidized Engineered Carbon Black Nanoparticles, Ex Vivo Analyses

The reductive capacities of the engineered carbon black and oxidized engineered carbon black particles were measured using a spectrophotometric method that was modified from a previous method (Guo et al. 2009; Guo and Kennedy 2007). Briefly, 30 mg of ECB (or ox-ECB) nanoparticles and 9 mg of $\text{Fe}_2(\text{SO}_4)_3$ was added to 75 ml of ultrapure water to obtain a suspension of carbon black nanoparticles in ferric sulfate solution. This suspension was incubated in a water bath at 37 °C for 16 hrs. Then the carbon black particles were filtered out to obtain a clear solution containing Fe^{3+} and Fe^{2+} ions. To this clear solution, 0.25 ml 20% sulfuric acid was added to adjust the pH; then the solution was diluted to 100 ml in a volumetric flask. The concentrations of Fe^{3+} and Fe^{2+} ions in the solution were determined using the spectrophotometric method at an absorbance wavelength of 512 nm, as described previously (Guo et al. 2009; Guo and Kennedy 2007).

3.2.4 Cell Culture Conditions

A549 Human lung epithelial cells (CCL-185, ATCC) were cultured using F-12K media supplemented with 10% fetal bovine serum and 1% penicillin, streptomycin, and amphotericin B (Sigma Aldrich, St. Louise, MO). Cells were seeded at 1.5×10^4 cells/well in 96 well-plates. This cell seeding concentration was predetermined to yield ~90% coverage of the cell plate surface at time of analysis. After allowing 24 hrs for attachment, cells were exposed to known concentrations of nanoparticle suspensions ranging from 0.01 $\mu\text{g/mL}$ to 100 $\mu\text{g/mL}$. Cells were co-exposed to differing ratios of $\text{Fe}_2\text{O}_3\text{:ECB}$ or $\text{Fe}_2\text{O}_3\text{:ox-ECB}$, including 0.01:4, 0.1:4, and 1.0:4 and 100:4 $\mu\text{g/mL}$. For exposure scenarios, a stock solution of Fe_2O_3 , ECB, or ox-ECB (1000 $\mu\text{g/mL}$) was prepared in ultrapure water and briefly sonicated (40 kHz) to break up nanoparticle agglomerates. Stock solutions were serially diluted in F-12K medium containing serum. Care was taken to preserve similar osmolarity between samples.

3.2.5 Intracellular Nanomaterial Localization Analyses

A549 cells were treated with 10 $\mu\text{g/mL}$ Fe_2O_3 nanoparticles and 4 $\mu\text{g/mL}$ ECB (or ox-ECB) nanoparticles for 25 hrs. The inoculated culture media was replaced with 3% (v/v) glutaraldehyde in 1X Hank's balanced salt solution (HBSS). After incubation, the cells and fixative were placed in a PELCO Biowave cold microwave (Ted Pella, Redding, CA) at 250 W for a 6 minute cycle. Following washing, post-fixation was performed with a 1% osmium tetroxide (wt/v) solution overnight. Samples were then washed with HBSS and dehydrated in increasing methanol steps. An epoxy formula was prepared using Quetol 651, Araldite, and DDSA (A:E ratio 1:1) with benzyldimethyl-

amine (BDMA) used as the accelerant. Following polymerization, the blocks were sectioned and mounted on grids. Post staining was performed using both 2% uranyl acetate (wt/v) and Reynolds lead citrate (Reynolds 1963). The grids were washed, dried, and examined using transmission electron microscopy (TEM). TEM analysis was performed using a Morgani Electron Microscope (FEI corp.) at 100 keV.

3.2.6 Intracellular Metal Analysis

Iron content within the cells was analyzed using inductively coupled plasma-mass spectroscopy (ICP-MS). A549 cells were seeded, exposed to 50 $\mu\text{g}/\text{mL}$ of Fe_2O_3 , or co-exposed to equal parts of 50 $\mu\text{g}/\text{mL}$ ECB and Fe_2O_3 nanoparticle suspensions. Following 25 hrs exposure time, the cell culture media was removed from cells and kept for analysis. Cells were washed with warm PBS repeatedly to remove residual nanoparticles on the surface of the cells. Following washing, exposed cells were detached from the culture dish with 1X Trypsin-EDTA and collected by centrifugation. All suspensions were digested under heat (60°C) and acid (5% HCl and 1% nitric acid, by volume), and analyzed for iron content via ICP-MS using an Elan DRC II, Perkin Elmer SCIEX (Waltham, MA).

3.2.7 Lysosomal Characterization

Visualization of lysosomal presence was performed using fluorescence microscopy techniques. Briefly, A549 cells were incubated with 10 $\mu\text{g}/\text{mL}$ Fe_2O_3 nanoparticles and 4 $\mu\text{g}/\text{mL}$ ECB (or ox-ECB) nanoparticles for 1 hrs, 3 hrs, or 24 hrs. Following nanoparticle incubation, LysoTracker™ (75 nM, Invitrogen Corp., Carlsbad, CA) was added to both control (unexposed) and nanoparticle exposed cells and

incubated for 1.5 hrs. Cells were fixed with paraformaldehyde and subsequently counterstained with DAPI (4',6-diamidino-2-phenylindole) (300 nm, Invitrogen Corp., Carlsbad, CA) . Following staining, cells were preserved with Slo-fade® (Invitrogen Corp, Carlsbad, CA) and imaged on an Olympus inverted fluorescent microscope.

3.2.8 Cellular Proliferation

The 1-(4,5-dimethylthiazol-2-yl)-3,5-diphenylformazan (MTT) assay (Sigma Aldrich, St. Louise, MO) is a spectrophotometric way to assess cellular proliferation via quantification of the enzyme mitochondrial dehydrogenase. Actively respiring mitochondria reduce the tetrazolium salt to a water insoluble purple formazan dye which is solubilized in MTT solubilization solution (10% Triton X-100 in 0.1 N HCl in anhydrous isopropanol). After solubilization in acidic isopropanol, the product was quantified by measuring absorbance at 570 nm. Briefly, cells were co-exposed to differing ratios of Fe₂O₃:ECB or Fe₂O₃:ox-ECB, including 0.01:4, 0.1:4, and 1.0:4 10:4 and 100:4 µg/mL. After 25 hrs, MTT (5 mg/mL) was added to each well and incubated for 4 hrs. Subsequent experiments were performed using the ECB and ox-ECB nanomaterials in cell-free conditions to verify the absence of *ex vivo* reduction of the salt by the particles themselves.

3.2.9 Cellular Viability

Cellular viability was assessed using the live/dead viability/cytotoxicity assay (Molecular Probes, Invitrogen Corp., Carlsbad, CA). This assay utilizes the fluorescent dyes ethidium homodimer and calcein AM. Ethidium homodimer (red) increases in fluorescence intensity upon binding to DNA. Calcein AM (green) is hydrolyzed by

intracellular hydrolases found in living cells and subsequently increases in fluorescence intensity. Therefore, in this assay, viable cells fluoresce green while non-viable cells fluoresce red. Briefly, cells were co-exposed to differing ratios of Fe₂O₃:ECB or Fe₂O₃:ox-ECB, including 0.01:4, 0.1:4, and 1.0:4 10:4 and 100:4 µg/mL. Following 25 hrs exposure, cells were washed and incubated with 2 µM ethidium homodimer and 1.5 µM calcein AM for 40 minutes. Positive control samples (nonviable cells) were incubated with 70% methanol in phosphate buffered saline for 0.5 hrs. Nanoparticle-only controls were incorporated to assure no interference with the assay. Following dye incubation, stained cells were viewed under an inverted fluorescence microscope. Multiple field images (~2500 cells) were collected and cell viability was assessed as follows:

$$\text{Percent Dead Cells (\%)} = \frac{\text{Number of dead cells}}{\text{Total cell count}} \times 100 \quad (\text{eq. 3.3})$$

3.2.10 Intracellular ROS Detection

DCFH-DA (2',7'-dichlorofluorescein diacetate) was used to measure the levels of intracellular reactive oxygen species (Sigma Aldrich, St. Louise, MO). Briefly, a 20 µM DCFH-DA solution in Hank's balanced salt solution (HBSS) was made without serum or other additives. A549 cells were cultured and exposed to nanoparticle suspensions as described above and incubated for 2.5 hrs or 25 hrs. After washing, cells were then incubated with the DCFH-DA working solution for 0.5 hrs. Fluorescence was measured at 485/520 nm (excitation/emission) using a fluorescence plate reader (Synergy MX, BioTek).

3.2.11 Antioxidant Addition

A 1 mM L-ascorbic acid (Sigma Aldrich, St. Louis, MO) solution in ultrapure water (18.2 M Ω) was prepared fresh each day. A549 cells were incubated in appropriate media and inoculated with Fe₂O₃:ECB, as described above. For the 2.5 hrs nanoparticle co-exposure, ascorbic acid was added at t=0 hrs. For the 25 hrs co-exposure, ascorbic acid was added 19 hrs post nanoparticle exposure. L-ascorbic acid was added to yield a concentration of 0.083 mM in total cell culture media volume. Intracellular reactive species were probed via DCFH-DA, as described above, after either 2.5 hrs or 25 hrs post-exposure.

3.3 Results

3.3.1 Physicochemical Characterization

Nanomaterial characterization was assessed with a variety of methods and reported in Table 3.1. The size of the Fe₂O₃ particles, assessed by transmission electron microscopy, was 41 \pm 17 nm, while that of ECB and ox-ECB (surface oxidized ECB) was 47 \pm 7 nm. Surface charge was assessed through measurement of the zeta potential. All three types of nanoparticles displayed highly negative zeta potentials when dispersed in ultrapure water. Iron oxide nanoparticles had a zeta potential of -44.2 \pm 5.9 mV. The zeta potentials of ECB and ox-ECB were -51 \pm 6.02 mV and -52 \pm 6.02 mV, respectively. The flame-synthesized iron oxide particles were of very high purity (>99.99%, mass ratio of Fe to total metal) based on ICP-MS elemental analysis (Guo and Kennedy 2007). The reductive capacity of ECB towards Fe³⁺ was measured to be 9.0 \times 10⁻³ g(Fe³⁺)/g(carbon). Following surface oxidation, the ability for ox-ECB to

reduce Fe^{3+} was decreased significantly to $2.4 \times 10^{-4} \text{ g}(\text{Fe}^{3+})/\text{g}(\text{carbon})$. This represents a 97.3% loss of ECB reductive capacity following surface oxidation. The XPS measurements showed that surface oxidation of the ECB resulted in a 15% increase in the ratio of oxidized to unoxidized C, from 0.113 in ECB to 0.130 in ox-ECB. Quantitation of the deconvoluted (Fairley et al. 2005; Briggs and Seah 1990; Xie and Sherwood 1991; Canas-Ventura et al. 2006; Popat et al. 1995; Estrade-Szwarckopf 2004; Szabó et al. 2006) C1s XPS peaks for ox-ECB further indicated a remarkable increase in the fraction of interfacial quinonoid moieties: the ratio $Q_{(s)}/H_2Q_{(s)}$ in ox-ECB was found to be *ca.* 5000 times greater than in ECB. Based upon a molecular model of the carbon nanoparticles, estimated from TEM experiments to be cubic with a 50-nm edge, in conjunction with the escape-depth properties of X-ray photoelectrons, at least 90% of the XPS carbon peaks may be presumed to emanate from edge-sites. This is important because surface redox activity is possible only on such edge-sites and not on the terrace (graphene) sheets and hence modification (oxidation) of these sites will alter the redox capacity. Whereas specific surface area (SSA) was found to be $49 \text{ m}^2/\text{g}$ for the iron oxide nanoparticles and $63 \text{ m}^2/\text{g}$ for the ECB nanoparticle sample, none was measured for the ox-ECB sample as it remained in aqueous suspension.

Table 3.1 Characterization of Fe₂O₃, ECB, and ox-ECB nanoparticles

Property	Fe₂O₃	ECB	ox-ECB
Size, nm	41 ± 17	47 ± 7	47 ± 7
Zeta Potential, mV	-44.2 ± 5.9	-51.2 ± 6.02	-52.4 ± 6.02
Crystalline Structure	Maghemite	Amorphous	Amorphous
Specific Surface Area, m ² /g	49	63	Not measured
SSA Calculated Size, nm	23.5	52.8	N/A
Reductive Capacity, g(Fe ³⁺)/g(carbon)	Not Measured	9.0 x 10 ⁻³	2.4 x 10 ⁻⁴
%C:%O (O/C Ratio)	Not measured	89.88:10.12 (0.1126)	88.53:11.47 (0.1295)

3.3.2 Intracellular Nanomaterial Localization Analyses

Figure 3.1 shows TEM images of ultrathin sections of A549 human lung epithelial cells following incubation with mixed Fe_2O_3 and ECB for 25 hrs. The TEM results indicate that both Fe_2O_3 and ECB were internalized into micron-sized vesicles within lung epithelial cells. These intracellular organelles most resemble endosomal-like and/or lysosomal-like structures (Li et al. 2008c; Sadauskas et al. 2009). Ultrathin, 2-D sections revealed the presence of either ECB (or ox-ECB) and Fe_2O_3 nanoparticles co-localized within the same intracellular vesicle. In exposures to both ECB and Fe_2O_3 (Figure 3.1A & 3.1B) and ox-ECB and Fe_2O_3 (Figure 3.1C), intracellular uptake and co-localization the two types of particles occurred. The presence of large agglomerates of both Fe_2O_3 and ECB or ox-ECB nanoparticles was observed. The ECB and the Fe_2O_3 particles were readily distinguishable in the electron micrographs due to their morphological differences; Fe_2O_3 particles exhibited multifaceted sides whereas ECB particles exhibited a more amorphous, rounded shape. Electron micrographs of particles under cell free conditions can be seen in Guo et al. (2009) (Guo et al. 2009).

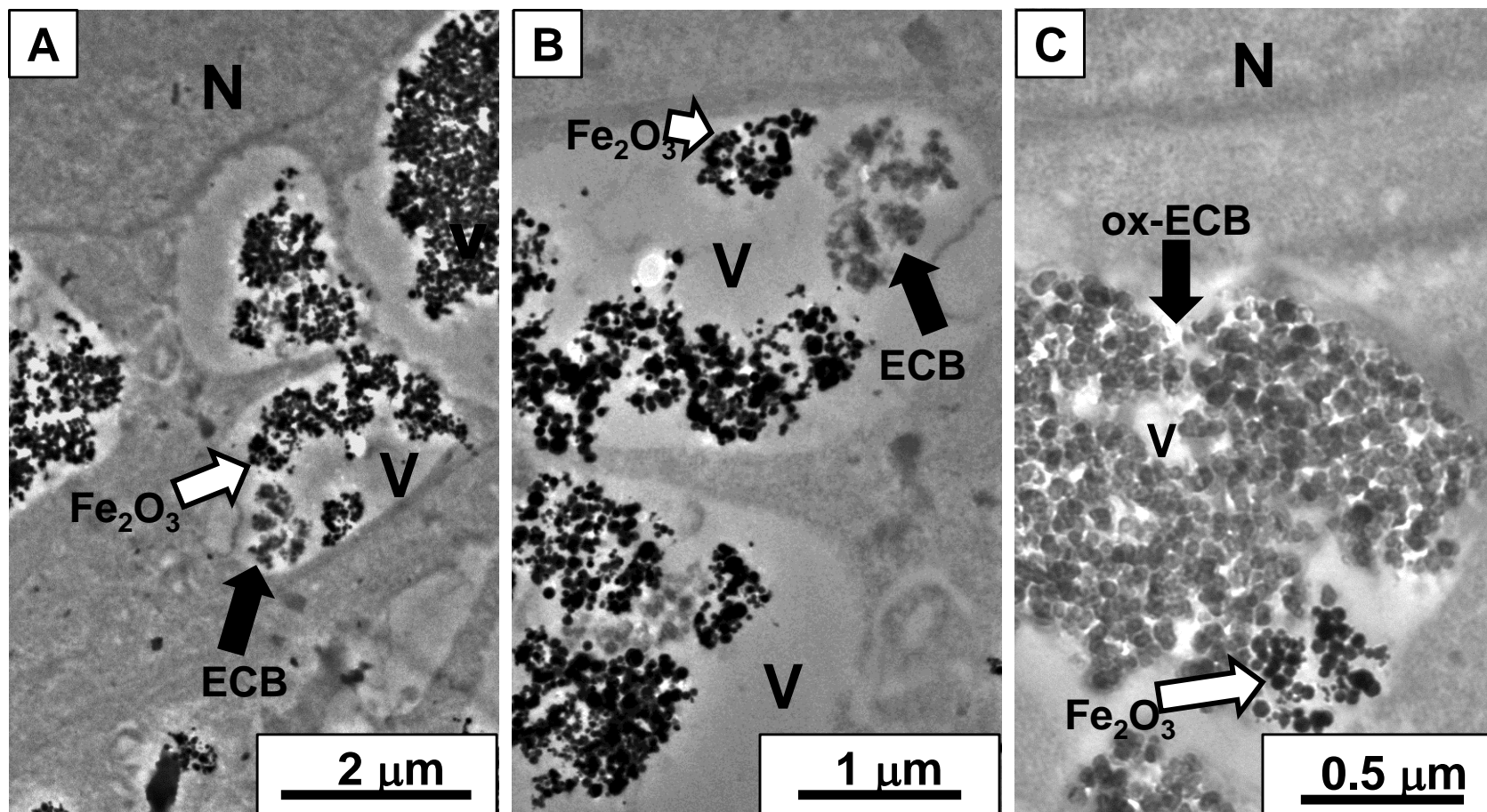


Figure 3.1 Intracellular nanomaterial localization analyses. (A) Internalization of both Fe_2O_3 and ECB agglomerates into A549 cells visualized through the use of electron microscopy. (B) Magnified image of vesicles in panel A. (C) Internalization of both Fe_2O_3 and ox-ECB agglomerates into A549 cell line. White arrows point to Fe_2O_3 nanoparticles, while black arrows point to ECB or ox-ECB nanoparticles. Nuclei (N) and vesicles (V) are labeled in each panel when present.

3.3.3 Additional Intracellular Metal Analysis

The presence of intracellular Fe_2O_3 was confirmed through inductively coupled plasma-mass spectroscopy (ICP-MS) (Figure 3.2). These measurements show the intracellular iron (cells), iron remaining in the culture medium (CCM), and total iron in the exposure medium (total). Results indicate similar Fe_2O_3 uptake in both the single and co-exposure scenarios (0.175 $\mu\text{g}/\text{mL}$ vs 0.177 $\mu\text{g}/\text{mL}$, respectively). Similarly, the iron content in the cell culture media removed from cell culture after Fe_2O_3 exposure was 0.017 $\mu\text{g}/\text{mL}$ while the iron content in the cell culture medium in a mixtures situation involving both ECB and Fe_2O_3 was 0.014 $\mu\text{g}/\text{mL}$. Identical Fe_2O_3 exposure in both the single exposure and mixture exposure was confirmed via measurement of the total iron present in the combination of cellular lysate and spent medium (0.193 $\mu\text{g}/\text{mL}$ vs 0.192 $\mu\text{g}/\text{mL}$). Furthermore, the sum of Fe_2O_3 in the spent cell culture medium (CCM) and total intracellular iron (cells) agrees with the exposure concentration (total).

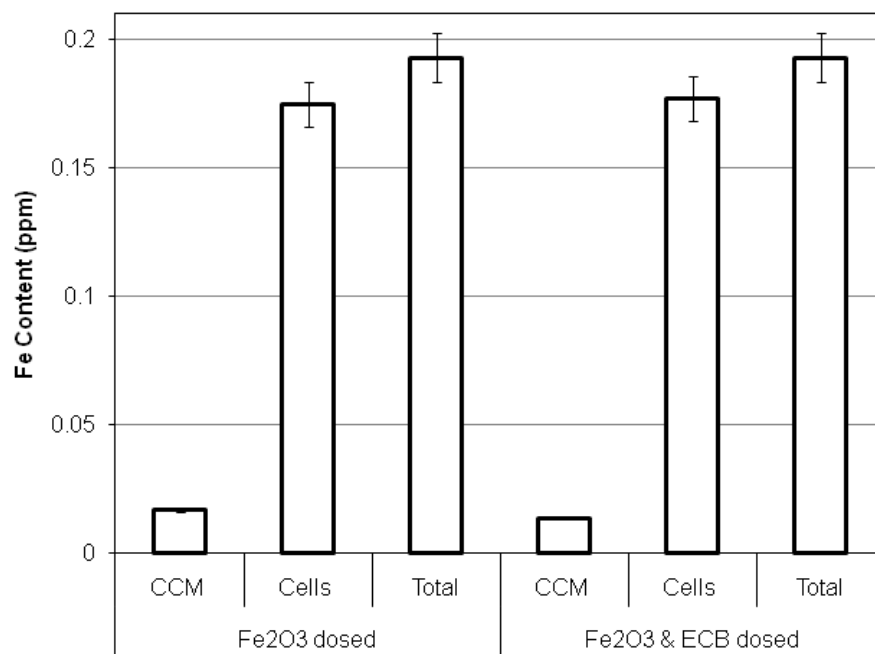


Figure 3.2 Intracellular metal analysis of lung epithelial cells. Cells were dosed with either Fe₂O₃ nanoparticles or ECB and Fe₂O₃ nanoparticles alone via inductively coupled plasma-mass spectroscopy. These measurements show the intracellular iron (cells), iron remaining in the culture medium (CCM), and total iron in the exposure medium (total).

3.3.4 Lysosomal Characterization

The increased presence of lysosomal compartments was confirmed through fluorescence microscopy with the use of LysoTracker™ red dye. LysoTracker™ dye consists of a fluorophore linked to a weak base that accumulates in cellular compartments with a low internal pH. Additionally, cell nuclei were counterstained with DAPI. Figure 3.3 indicates a low basal level of lysosomal presence in many control cells at 1 hr, 3 hrs, and 24 hrs. While a low basal level may be seen in the control cells, actively proliferating cells exhibited higher fluorescence intensity. Additionally, by visual inspection, the A549 control cells appeared to be increasing in number and confluency as the time points progressed. In cells exposed to 10 µg/mL Fe₂O₃ and 4 µg/mL ECB, an increase in fluorescence was observed at all time points. At 1 hr following exposure, a low basal level of lysosomal presence was observed similar to the control; however, some individual cells exhibited increased punctate fluorescence. At 3 hrs, this trend was exacerbated, coupled with a moderate degree of fluorescence. Following 24 hrs exposure, the A549 cells continued to proliferate, albeit with slightly different cell densities, with fluorescence intensity comparable to 3 hrs post-exposure time point. Similar trends were observed in the co-exposure consisting of 10 µg/mL Fe₂O₃ and 4 µg/mL ox-ECB.

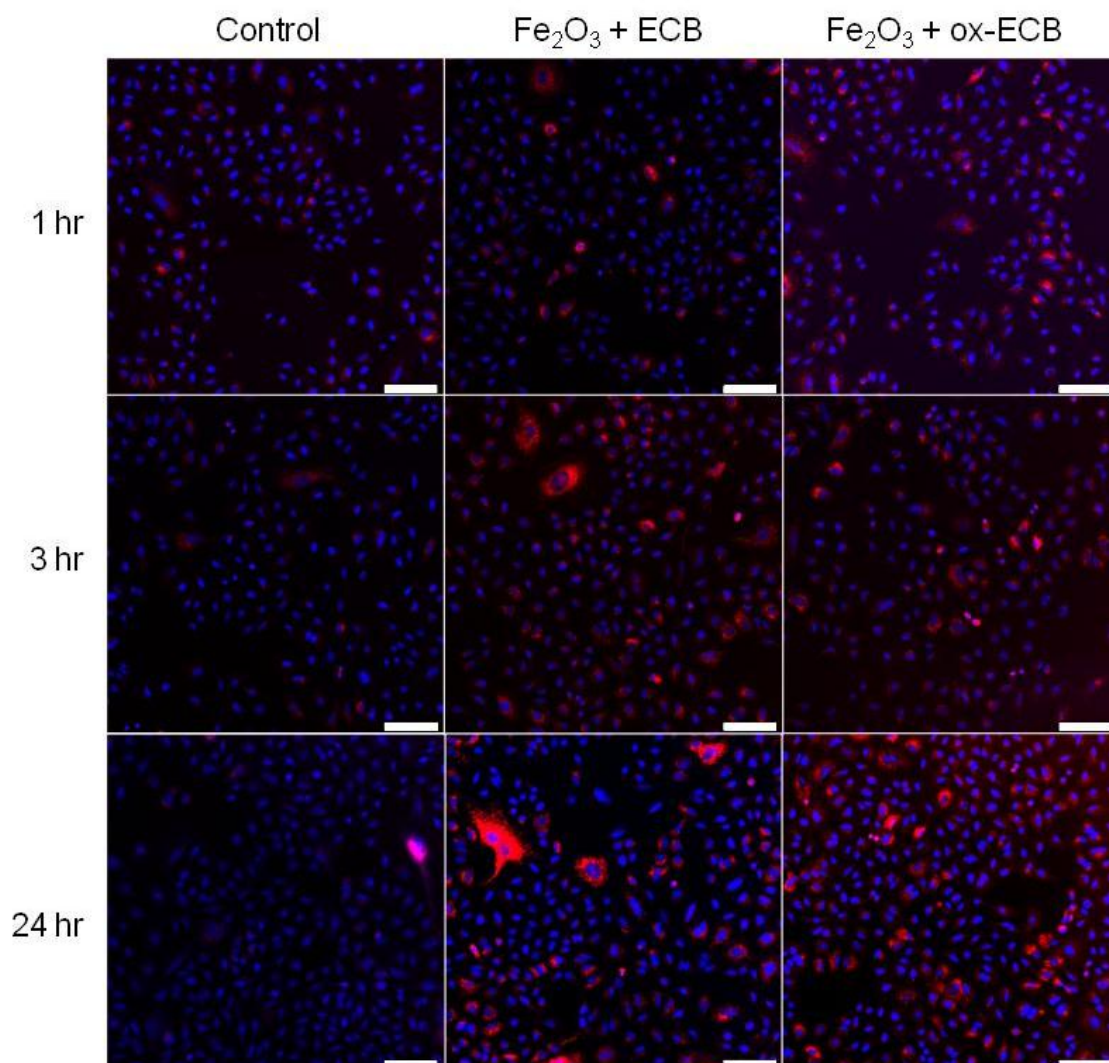


Figure 3.3 Lysosomal characterization. Lung epithelial cells were exposed to both Fe₂O₃ and ECB/ox-ECB nanoparticles for a variety of time points ranging from 1 hrs to 24 hrs and subsequently incubated with Lysotracker™ red dye. Low basal levels of lysosomes were found in control cells at all time points with an increase seen in actively dividing cells. Acidified lysosomes (pH<5.2) (red) are increasingly visualized in both Fe₂O₃ and ECB (or ox-ECB) co-exposed samples. Lysosome fluorescence is found to increase throughout both exposed cell populations as the time increases from 1 hrs to 24 hrs. This increase in acidified lysosomes yields conditions which may promote dissolution of the surface of the Fe₂O₃ nanoparticle. Cell nuclei were counterstained with DAPI (blue). Scale bar = 100 μm.

3.3.5 Oxidant Production

The DCFH-DA assay provides an estimate of instantaneous intracellular ROS (Figure 3.4). While relatively non-specific, the DCFH-DA is a cell based assay for measuring relative concentrations of oxidants (i.e. hydroxyl, peroxy, etc.) and has been suggested as a good measure of the oxidative status in cells in culture (Wang and Joseph 1999; Foucaud et al. 2007). Control cells exhibited little intracellular ROS. This is hypothesized to be a byproduct of normal cellular respiration. While the lower concentration of Fe₂O₃, at 2.5 hrs, did not generate significant or increasing amounts of oxidative species as determined by fluorescence spectroscopy (increase of 6.9% for 0.01 µg/mL and 5.4% for 0.1 µg/mL), Fe₂O₃ at a higher dose (100 µg/mL) showed a heightened response (increase of 28.1%) when compared to the control. At 25 hrs, the cells exposed to 100 µg/mL Fe₂O₃ still exhibited a heightened response, however the difference between the high (increase of 35%) and low doses (increase of 31.3% for 0.01 µg/mL and 24.0% for 0.1 µg/mL) is not as significant as was observed at 2.5 hrs. In addition, A549 cells were exposed to mixtures of both Fe₂O₃ and ECB simultaneously. This scenario produced a significant amount of ROS when compared to the control. Mixture scenarios at 25 hrs produced an increase of 103.6% for the 0.01 µg/mL Fe₂O₃:4 µg/mL ECB ratio, 51.9% for the 0.1 µg/mL Fe₂O₃:4 µg/mL ECB ratio, and 34.8% for 100 µg/mL Fe₂O₃:4 µg/mL ECB ratio. A similar pattern existed at 2.5 hrs. This response was proportionally related to the increasing ratios of ECB to Fe₂O₃. Confirmation that the generation of intracellular ROS was not, in fact, an artifact produced by the

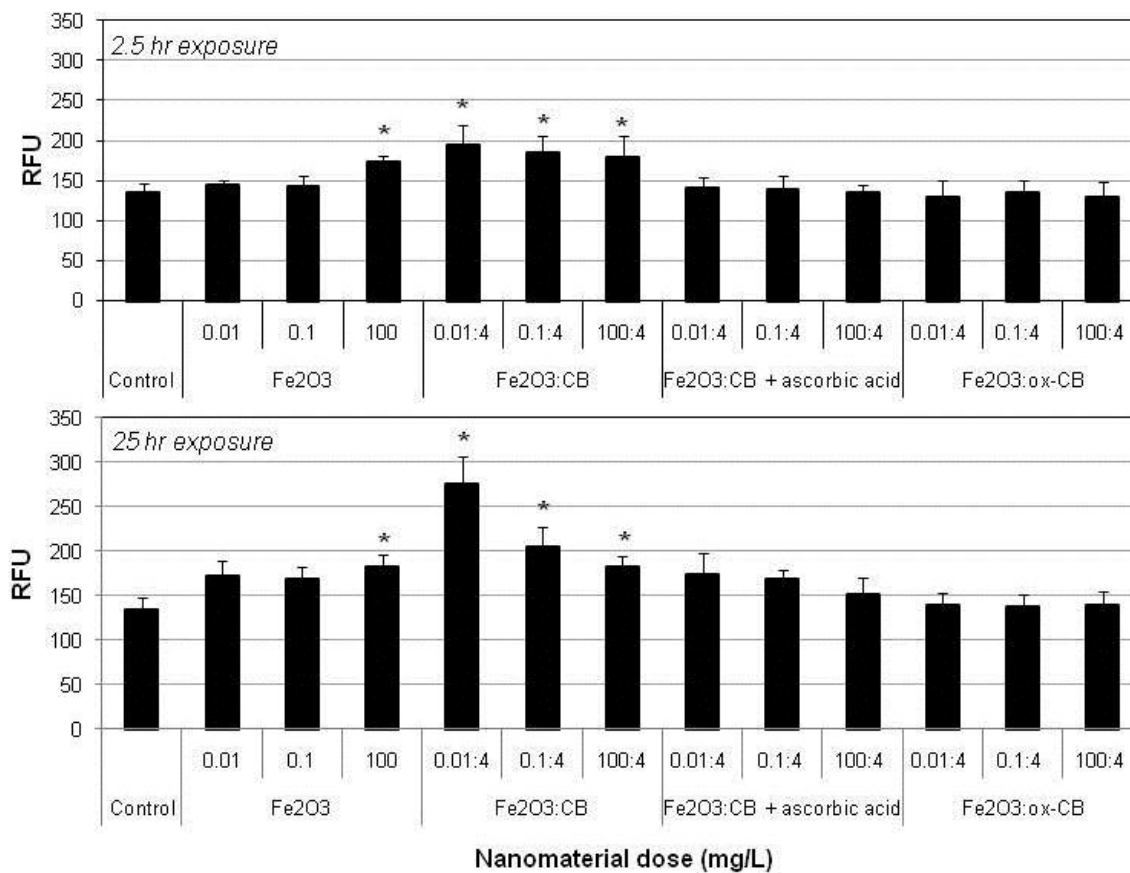


Figure 3.4 Intracellular oxidant production. Human lung epithelial cells were exposed to Fe_2O_3 only, Fe_2O_3 and ECB, a combination of Fe_2O_3 , ECB and L-ascorbic acid, or Fe_2O_3 and ox-ECB for both 2.5 hrs (top) and 25 hrs (bottom). Results indicate that co-exposure to Fe_2O_3 and ECB generate intracellular oxidant production that can be lessened by the addition of L-ascorbic acid or through surface oxidation of the ECB (ox-ECB). Values given are means \pm SD (* $p < 0.05$ relative to control cell population).

nanoparticles, was studied via the addition of L-ascorbic acid. L-ascorbic acid is a well characterized antioxidant that is able to function as an oxygen scavenger, thus limiting intracellular ROS. DCFH oxidation was diminished with the use of L-ascorbic acid.

Similarly, a secondary means of ameliorating the ROS generation via oxidation of the ECB to form ox-ECB was examined. Here, it was discovered that the oxidation of the surface of ECB resulted in oxidant production (as measured by DCF fluorescence) that was not significantly different from the control. Additionally, it was noted that for all co-exposure exposure values, at 25 hrs, ox-ECB produced less ROS than did the co-exposures incubated with L-ascorbic acid although these differences were not statistically significant.

3.3.6 Cellular Proliferation Assay

The MTT assay was used to compare the proliferative ability in both control samples as well as those exposed to mixed Fe₂O₃ and ECB (or ox-ECB) (Figure 3.5). Results indicate that there is a decrease in formazan formation at higher exposure limits in the Fe₂O₃ and ECB scenario, thus indicating a dose-response relationship. Throughout the dose-response curve, the Fe₂O₃ and ECB-exposed cells demonstrated a decrease in cell proliferation at 0.01 µg/mL Fe₂O₃ (4 µg/mL ECB) by 16.8% relative to control, at 0.1 µg/mL Fe₂O₃ (4 µg/mL ECB) by 16.9%, and at 1 µg/mL Fe₂O₃ (4 µg/mL ECB) by 16.8%; however at the higher doses of 10.0 µg/mL Fe₂O₃ (4 µg/mL ECB) and 100 µg/mL Fe₂O₃ (4 µg/mL ECB), the cells exhibited a significant decrease in cell proliferation by 24% and 29.6%, respectively. However, the cells exposed to both Fe₂O₃ and ox-ECB did not exhibit this dose-dependent response. The highest exposure scenario

(100 $\mu\text{g/mL}$ Fe_2O_3 and 4 $\mu\text{g/mL}$ ox-ECB) did not exhibit a significant difference when compared to the control. Background absorbance values, due to nanoparticles, were subtracted out of final absorbance value. As a number of reports suggest reduction of the tetrazolium salt to formazan by exogenous sources, *ex vivo* (cell free) incubations of ECB and ox-ECB nanoparticles incubated with MTT showed no interference (data not shown) (York et al. 1998; Wang et al. 2010; Maioli et al. 2009; Babior 1984).

3.3.7 Cellular Viability

A live/dead cytotoxicity assay was employed to determine the absolute percentage of dead cells following co-exposures to the aforementioned nanoparticles (Figure 3.5). Results indicate a slight dose-dependent decrease in cellular viability following co-exposure to 0.01 $\mu\text{g/mL}$ Fe_2O_3 combined with 4 $\mu\text{g/mL}$ ECB to 10 $\mu\text{g/mL}$ Fe_2O_3 and 4 $\mu\text{g/mL}$ ECB. This decrease ranged from 0.69% dead to 7.62% dead. At an exposure of 100 $\mu\text{g/mL}$ Fe_2O_3 and 4 $\mu\text{g/mL}$ ECB, a decrease in the amount of death was noted (3.48% dead).

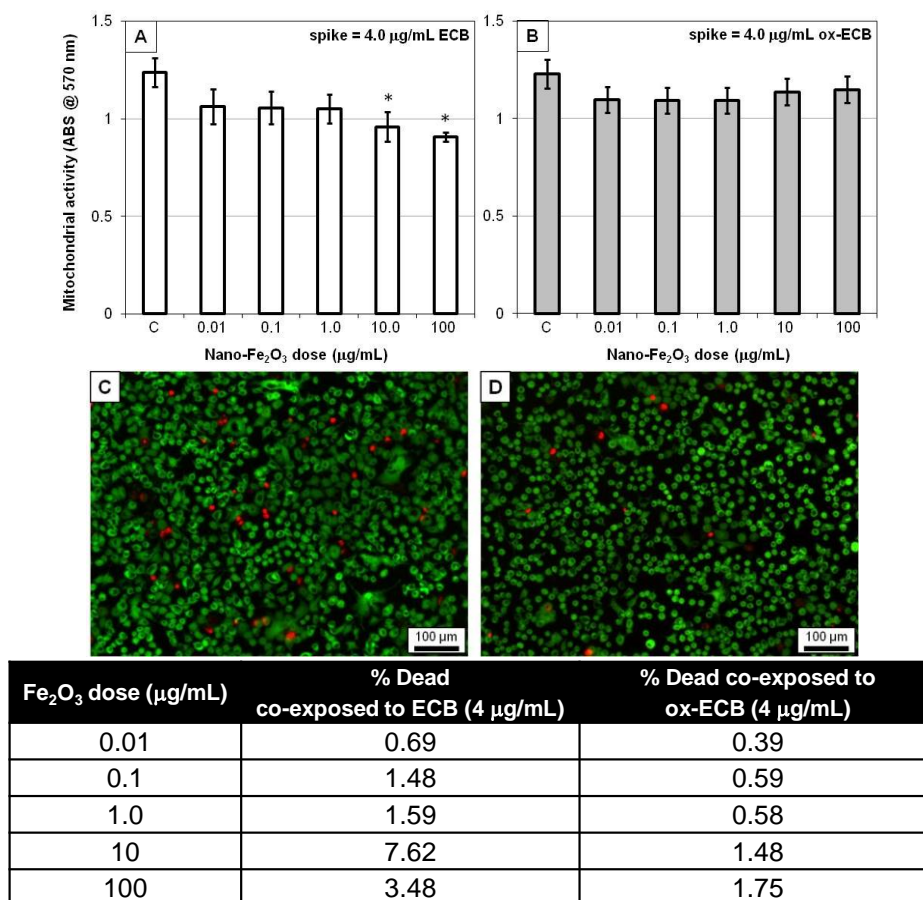


Figure 3.5 Cellular proliferation and viability. Human lung epithelial cells were exposed to both Fe₂O₃ nanoparticles and ECB nanoparticles or Fe₂O₃ nanoparticles and oxidized ECB nanoparticles at varying degrees of particle concentrations. (A) Cellular proliferation, as measured by mitochondrial dehydrogenase activity, of cells exposed to Fe₂O₃ (concentration noted on x-axis) spiked with 4.0 µg/mL ECB measured after 25 hrs exposure. (B) Cellular proliferation of cells exposed to Fe₂O₃ (concentration noted on x-axis) spiked with 4.0 µg/mL oxidized ECB measured after 25 hrs exposure. (C) Live/dead cytotoxicity assay of cells exposed to 10 µg/mL Fe₂O₃ and 4 µg/mL ECB. Live cells cytoplasm fluoresce green, while dead cell nuclei fluoresce red. (D) Live/Dead cytotoxicity assay of cells exposed to 10 µg/mL Fe₂O₃ and 4 µg/mL ox-ECB. (E) Analysis of multiple field shots (comprising ~2500 cells) with the absolute percentage of cell death. A slight decrease is noted in the co-exposure with ECB, which is not noted, to a similar extent, with ox-ECB. * p<0.05 as compared to the control.

This decrease in cellular viability was not noted in the co-exposed samples dosed with Fe₂O₃ and ox-ECB. In the ox-ECB co-exposure results indicate a slight dose-dependent decrease in cellular viability following co-exposure to 0.01 µg/mL Fe₂O₃ combined with 4 µg/mL ECB (0.39% dead) to 10 µg/mL Fe₂O₃ and 4 µg/mL ECB (1.75% dead). These results indicate that while a slight decrease in cellular viability exists in a co-exposure scenario (max. 7.62% dead, 10 µg/mL Fe₂O₃ and 4 µg/mL ECB) at 24 hrs; this decrease may be eliminated by surface oxidation of the ECB nanoparticle.

3.4 Discussion

Over the course of this examination, we aimed to continue to investigate the cellular response to exposure to a synergistic mixture of Fe₂O₃ and ECB nanoparticles in an *in vitro* model. While the A549 lung epithelial cell line is not a phagocytic cell line, it is routinely used to assess uptake of inhaled particulate in situations where the capacity of the alveolar macrophage to mitigate particle clearance has been exceeded. The human lung epithelial cell line A549 has been previously shown to be of utility for alveolar epithelial cell interaction with micro-sized particles and dusts (Stringer et al. 1996; Guo et al. 2009). Previously, Guo et al. (2009) suggested that mixtures of Fe₂O₃ and ECB nanoparticles induced cellular toxicity through an oxidative stress mechanism because the ECB nanoparticles were able to reduce Fe³⁺ to Fe²⁺ through surface functional groups. This paper expands upon this toxicity paradigm by not only confirming previous results, but elucidating a mechanism through which these nanoparticles elicit their effect.

3.4.1 Intracellular Localization and Lysosomal Analysis

All three nanoparticle-types were seen to be internalized into the cell in co-exposure scenarios. This study confirms the ability of both Fe₂O₃ and ECB and/or ox-ECB nanoparticles to enter the intracellular environment in a time-dependent fashion. Interestingly, the nanoparticles were localized in vesicles (i.e. endosomes and/or lysosomes) as either a single species (i.e. either Fe₂O₃ *or* ECB) or as a mixture of species (Fe₂O₃ *and* ECB). This leads to the possibility that each type of nanoparticle enters the cell through independent events, either through a type of receptor-mediated endocytosis or non-specific fluid phase uptake. Recent work has demonstrated the ability for nanoparticles to bind biological molecules including proteins in the physiological environment (Lundqvist et al. 2008). This protein adherence may lead to differences in the mechanism responsible for each specific endocytic event. Furthermore, many studies have demonstrated that nanoparticles enter a cellular system through a variety of mechanisms including clathrin-mediated endocytosis, macropinocytosis, phagocytosis, as well as simple passive diffusion (Dausend et al. 2008; Chithrani et al. 2006; Davada and Labhasetwar 2002; Qaddoumi et al. 2003; Harush-Frenkel et al. 2008). Intracellular trafficking normally directs endocytosed macromolecules into endosomal or lysosomal compartments. It is in these locations that the decrease in pH is responsible for not only the hydrolysis of ligands from their receptors, but additionally the degradation of macromolecules. Examinations by TEM and fluorescence microscopy confirm a similar fate (lysosomal incorporation) for both the carbonaceous and metal oxide nanoparticles studied here.

Zhang et al. (2009) demonstrated similar results with quantum dot nanoparticles. They examined an increase in lysosomal accumulation at 24 hrs as verified by fluorescence co-localization of quantum dot and CD63/Lamp-1 in an HEK cell line (Zhang and Monteiro-Riviere 2009). Nanoparticle accumulation in lysosomal compartments after 24 hrs provides the correct conditions (acidic pH) to begin the intracellular release of Fe^{3+} ions from the surface of the Fe_2O_3 nanoparticle.

3.4.2 The Production of Oxidants

The oxidative stress paradigm has thus far had a major impact in the nanotoxicology literature. The data here indicates that this particular particle-cell interaction is no different. While Fe_2O_3 at the highest dose exhibits a significant amount of oxidant production, Fe_2O_3 alone at lower concentrations (0.1 $\mu\text{g}/\text{mL}$ and 0.01 $\mu\text{g}/\text{mL}$) does not produce oxidant species at the time points reported in this study. At 2.5 hrs post-exposure, oxidation of DCFH is seen at similar levels throughout all the co-exposed ratios, however at 25 hrs this is not the case. The lowest ratio (0.01 $\text{mg}/\mu\text{L}$ Fe_2O_3 :4.0 $\mu\text{g}/\text{mL}$ ECB) of nanoparticles exhibited the highest oxidative stress of all the co-exposure scenarios. This effect may be due to the decrease in cellular proliferation and slight decrease in cellular viability occurring at the higher nanoparticle ratios as evidenced by the MTT assay.

Co-exposures to Fe_2O_3 and ECB demonstrated significant oxidative stress in previous cell culture studies, while exposures to Fe_2O_3 or ox-ECB alone did not induce significant oxidative stress (Guo et al. 2009). In this study, we have shown that after cell culture inoculation to mixed Fe_2O_3 and ECB and/or ox-ECB, both materials are

endocytosed within the same vesicular structure. Additionally, after exposure to the mixture of nanoparticles, the amount of acidified lysosomes increases over time. Furthermore, intracellular reactive oxygen species were found. However, the oxidant production of Fe₂O₃ and ECB was mitigated when the surface of the carbon black was oxidized before co-exposure or prevented after addition of L-ascorbic acid to the culture medium as an antioxidant.

3.4.3 Cellular Proliferation and Viability

Cellular proliferation was measured via the MTT assay. The MTT assay is very widely accepted in the literature as a measure of cell proliferation, mitochondrial activity, and/or cytotoxicity (Mosmann 1983). However, in this manuscript, we conclude that while the MTT assay shows a decrease in cellular proliferation, a similar degree of cell death was not observed using the live/dead assay. Therefore, it remains possible that exposure to ECB and Fe₂O₃ causes inhibition of cellular proliferation without appreciable cell death occurring. Similar results have been shown by Stone et al. (1998) (Stone et al. 1998). In the manuscript by Stone et al., the MTT assay was used to study the relative inhibitory effects of particles. Furthermore, it is indicated that the A549 cell line shows inhibition of proliferative effects following exposure to fine-sized carbon black, which may be recovered at later time points. Similarly, a decrease in proliferation rate, combined with no reduction in cellular viability was shown in A549 cells grown under hyperoxic conditions (McGrath-Morrow and Stahl 2002). As only slight cell death was noted at 24 hrs, it may be possible that the cells utilized for this experiment yield a different cytotoxic response at a later time point.

Previously, we asked if this oxidative stress was particle generated or if the oxidative stress had basis within a cellular mediated event. We concluded that this mechanism demonstrates qualities of both. In Figure 3.1, we have shown that both Fe_2O_3 and ECB (or Fe_2O_3 and ox-ECB) are internalized within cells. Also, Figure 3.3 shows that after exposure to these nanoparticles, the amount of acidified lysosomes increases over time. Based on these two conclusions, we ascertain that these acidified lysosomes contain both Fe_2O_3 and ECB (or Fe_2O_3 and ox-ECB). From *ex vivo* analysis, we have previously shown that under acidic conditions (i.e. lysosome), Fe^{3+} is released from the surface of the Fe_2O_3 nanoparticles. Interactions between nanoparticles in close proximity allow ECB to reduce the Fe^{3+} to the soluble Fe^{2+} . These Fe^{2+} ions are then thought to proceed through well documented intracellular redox cycling reactions, such as the Fenton Reaction, in which ROS are generated. Furthermore, we have shown that this reaction can be mitigated by prior oxidation of the ECB to ox-ECB before exposure. Oxidation of the ECB surface (from ECB to ox-ECB) was shown to drastically increase the fraction of interfacial quinoid moieties as the ratio $Q_{(s)}/H_2Q_{(s)}$ in ox-ECB was found to be *ca.* 5000 times greater than in ECB. This remarkable increase in $Q_{(s)}/H_2Q_{(s)}$ ratio may be responsible for the alterations in reductive capacity towards Fe^{3+} in solution (Kung and McBride 1988). Furthermore, our data indicates that decreased conversion of Fe^{3+} to Fe^{2+} (by ECB) is associated with intracellular oxidant production and changes in cellular proliferation and viability that is not statistically different from the control.

Toxicity data sets collected from cellular systems exposed to a nanomaterial or a mixture of nanomaterials can aid in the material design process and risk assessment.

Nanoparticle-specific modes/mechanisms of toxicity are, in some cases, complex. This is especially true when combining the enormous range of nanoparticle-types, morphologies, and redox capacities with the uncertainty of both occupational exposures and subsequent consumer use of nanoparticle-enabled products. Particle toxicology in this emerging area must provide a basis for predicting how the biological behavior after a nanomaterial exposure relates to the nanomaterial physicochemical properties, including chemical composition and reduction capacity.

Our aim is that this work will establish a new direction for future efforts to characterize the environmental and health impacts of nanoparticle mixtures. This proactive approach is necessary to safeguard the nanomaterial design and regulatory environment.

4. CELLULAR RESPONSE IS ASSOCIATED WITH ANTIOXIDANT ABILITY: A COMPARISON BETWEEN HUMAN PULMONARY EPITHELIAL AND MESOTHELIAL CELLS EXPOSED TO SiO₂ NANOPARTICLES

As the literature on nanoparticle toxicity continues to expand, there is an emergent need to examine and understand the differences among cell-types utilized in nanotoxicological studies. Here, we analyze the antioxidant capacity of both human pulmonary epithelial (A549) and human mesothelial (MeT-5A) cell lines as models for detecting nanoparticle-induced oxidative damage. The nanoparticle utilized in these studies was colloidal 33 nm SiO₂. Mutations in NRF2-KEAP1 antioxidant response system, previously reported in the A549 cell line, were expected to yield increased antioxidant activity and decreased sensitivity towards oxidative stress. Basal expression of superoxide dismutase (Mn & Cu/Zn) was found to be higher in MeT-5A cells, while catalase expression and activity, along with glutathione content, were higher in A549 cells. Cellular proliferation in response to hydrogen peroxide (H₂O₂) and silica nanoparticles (SiO₂) was measured using an absorbance-based MTT assay. MeT-5A cells were significantly more sensitive to both peroxide and SiO₂ than A549 cells. However, in both cell lines, significant oxidant production was detected, as measured by the DCFH-DA assay, and was associated with decreased glutathione. Furthermore, stabilization of the NRF2 transcription factor coupled with subsequent induction of catalase activity was observed. This study suggests that MeT-5A cells are a more sensitive model for nanoparticle toxicity and that markers of oxidative stress are differentially expressed with cell type variation. The identification of susceptible cell-

types or tissues is a critical step in the development of comprehensive nanomaterial risk assessments.

4.1 Introduction

The inclusion of nanomaterials into consumer-based products is increasing at an exponential rate. These nanomaterials, which include colloids, metal oxides, and carbonaceous particles, are at the forefront of basic and applied research, product development, and environmental health and safety assessments. The nanotechnology sector, when combined with the biotechnology sector, is expected to generate revenue upwards of \$2.6 trillion by the year 2014 (Dai 2010). Nanomaterials hold the potential to generate added value to consumer products through the addition of novel properties such as increased scratch resistance, insulating capacity, or antibacterial abilities (Richardson 2010). One of the most widely studied nanomaterials to be used in a variety of consumer goods are silica (SiO_2) nanoparticles. SiO_2 on the nano-size scale is often used to increase strength of polymers, improve UV resistance, and increase insulating ability. However, the incorporation of nanomaterials into consumer products elicits the need to develop risk-mitigating methods associated with potential increased exposure.

Traditionally, silica describes a group of minerals containing particulates ranging from ultrafine (<100 nm) to micrometer (> 5 μm) in size. These particulates are formed (naturally or synthetically) as either amorphous or crystalline materials. Data on silica exposure is gathered primarily in occupational settings with the inhalation route of exposure being the primary focus in research. Throughout epidemiological efforts, differences in toxicological responses between amorphous and crystalline SiO_2 are

attributed to differences in physicochemical properties relating to factors such as biopersistence and solubility. The toxicity of crystalline SiO₂ (namely, quartz) is widely established and has a well-developed epidemiological basis in severe respiratory diseases including both silicosis and fibrosis. Crystalline silica is classified by the International Agency for Research on Cancer (IARC) as a probable carcinogen, and is often used as a positive control in particulate toxicological studies (Donaldson and Borm 1998; Schottenfeld and Beebe-Dimmer 2006; IARC 1997; Fubini and Hubbard 2003; Shi et al. 1998). The differences in pathogenicity between crystalline and amorphous SiO₂ have been previously well defined. For example, Pratt (1983) determined that crystalline SiO₂, while cleared more effectively from the guinea pig pulmonary system, produces greater cellular damage than amorphous silica (Pratt 1983). Additionally, Johnston et al. (2000) observed greater respiratory cell damage after exposure to crystalline SiO₂ when compared to amorphous SiO₂ (Johnston et al. 2000). *In vitro* studies suggest that reactive oxygen species derived from crystalline surface parameters (i.e. freshly fractured crystal planes) are a potential progenitor able to increase production and release of proinflammatory cytokines and chemokines both *in vitro* and *in vivo* (Vallyathan et al. 1988; Vallyathan et al. 1995; Ovreik et al. 2006; Barrett et al. 1999). Hubbard et al. (2002) observed activation of the NF-κB pathway in pulmonary epithelial cells and macrophages following exposure to crystalline silica (Hubbard et al. 2002). Contrary to crystalline silica, amorphous silica is known to elicit either minimal or no fibrogenicity following exposure and, in inhalational studies, adverse effects seen were partially or completely regressed after short periods of time (Ruezel et al. 1991;

Johnston et al. 2000). Similarly, epidemiological studies by McLaughlin et al. (1997) suggest no evidence of silicosis or carcinogenicity from amorphous SiO₂ exposure (McLaughlin et al. 1997). Due to the low toxicity of amorphous SiO₂, it is an established additive in many consumer applications including medicinal diagnostics, cosmetics, and plastics (Wang et al. 2006; Barbe et al. 2004; Tago et al. 2003).

As nanometer sized amorphous SiO₂ particles find their way into consumer products and applications, it may be necessary to reevaluate the risks associated with the use of this material of identical chemical composition to micron-sized SiO₂ but on a different size scale. Numerous studies have determined that ultrafine particles have the ability to elicit greater pulmonary effects than their fine-sized counterparts of identical composition (Brown et al. 2000; Zhang et al. 2003). Amorphous silica literature has reported similar conclusions (Kaewamatawong et al. 2005). For example, reports of ROS production and cytotoxicity stemming from amorphous nanosilica exposure have become pronounced in *in vitro* studies (Lin et al. 2006; Chang et al. 2007; Yu et al. 2009). These cytotoxicological findings have been attributed to the physicochemical characteristics of nanoparticles. For example, Donaldson (2001) has suggested that the higher surface area of ultrafine particles can play a role as carriers for co-pollutants such as organics or transition metals (Donaldson and MacNee 2003). As the use of nanometer sized amorphous SiO₂ increases in the consumer setting, it is meaningful to elucidate the safety measures for precautionary reasoning. Therefore, we have utilized two cell lines with differing antioxidant capacities to determine if ROS generation plays

a critical role in amorphous silica toxicity *in vitro*. In addition, elaboration on the antioxidant differences between the two cell types tested will be given.

To our knowledge, this is the first work in the nanotoxicology literature deciphering the difference in cellular response following SiO₂ nanoparticle exposure between the cancerous lung epithelial cell line A549, and the mesothelial cell line MeT-5A. The A549 cell line is often utilized throughout particle toxicology literature as a model epithelial cell type; however simple genetic modifications, such as mutations in the NRF2 repressor protein, KEAP1, enable increased basal levels of a variety of phase II enzymes and low molecular weight antioxidants (Singh et al. 2006; Wang et al. 2008; Kensler and Wakabayashi 2010). A549 cells have been shown previously to exhibit relatively high levels of intracellular antioxidant mechanisms (i.e. low molecular weight antioxidants and enzymes) (Jarvinen et al. 2000). On the other hand, mesothelial cells (MeT-5A), derived from the pleural mesothelium, are more susceptible to foreign materials which drive the production of intracellular oxidants. Human studies suggest that pleural mesothelium exhibits much less γ -GCS expression (rate-limiting enzyme in glutathione synthesis) than the bronchial epithelium (Puhakka et al. 2002). It is hypothesized that the A549 cell line will be less susceptible to damage by toxicants which are presumed to proceed through an oxidative stress mechanism (i.e. SiO₂ nanoparticles), when compared to cell types with low antioxidant capacity, such as mesothelial cells. Exposure to nanoparticles is likely to occur through multiple pathways. Common among most exposure pathways is the potential of nanoparticles to translocate to different cells, tissues, and organs (Kreyling et al. 2002; Oberdorster et al.

2004; Oberdorster et al. 2002). Similarly, nanometer sized particles have also been shown to decrease the macrophage uptake efficacy, thus increasing the possibility that these particles will interact with both local and distant targets (Renwick et al. 2001). Due to the distinct ability of nanoparticles to migrate from their primary site of exposure, this study highlights the importance of testing multiple cell lines at a variety of nanoparticle doses between “overload” (100 $\mu\text{g}/\text{mL}$) and “non-overload” (0.01 $\mu\text{g}/\text{mL}$) concentrations.

The purpose of this manuscript is two-fold. First, we performed a comparative *in vitro* toxicological study of a more highly susceptible versus a less susceptible sub-population of cells which are predisposed to damage by ROS. By comparing the basal, and induced levels of antioxidant capabilities of A549 and MeT-5A cells, we distinguish differences in antioxidant defenses. Second, we utilized these characterized cell models to measure oxidant production, as well as subsequent cellular enzymatic and genetic responses following exposure to SiO_2 nanoparticles. These particles not only represent the shape and size of the most commonly studied particle-types, but are also expected to be mass-produced and incorporated into a variety of consumer products.

4.2 Experimental Procedures

4.2.1 Nanoparticle Preparation

SiO_2 nanoparticles were purchased from NanoAmor (Houston, TX). Particles were characterized for size using both transmission electron and scanning electron microscopy. Zeta potential measurements of the nanoparticle were performed as discussed elsewhere (Berg et al. 2009). Particle density was assessed using a

pycnometer (Micromeritics, Norcross, GA) via helium gas absorption. Surface area was assessed using the BET method under N₂ adsorption (Brunauer et al. 1938). Nanoparticles were suspended in ultrapure water and briefly bath sonicated (40 kHz) prior to dilution in serum-containing cell culture media for *in vitro* experiments.

4.2.2 Cell Culture

A549 human lung epithelial cells (CCL-185, ATCC Manassas, VA) were cultured using F-12K cell culture medium (ATCC) supplemented with 10% fetal bovine serum and 1% penicillin, streptomycin, and amphotercin B. MeT-5A mesothelium derived epithelial cells (CRL-9444, ATCC) were cultured using Medium 199 (Invitrogen Corp., Carlsbad, CA) as a base medium. Complete medium for the MeT-5A cell line contained 10% fetal bovine serum, 3.3 nM epidermal growth factor, 400 nM hydrocortisone, 870 nM insulin, 20 mM HEPES, trace elements B and 1% penicillin, streptomycin, and amphotercin B. Both A549 and MeT-5A cells were cultured at 37°C in a humidified incubator with 5% CO₂.

4.2.3 Western Blotting

Western immunoblotting was utilized in an effort to compare the basal expression of catalase, Cu/Zn SOD, and Mn SOD enzymes as well as the NRF2 induction following SiO₂ exposure. Proteins were isolated from the respective cell lines using a high salt lysis buffer with protease inhibitor cocktail. Following protein determination, equal amounts of protein was loaded into a 10 % Mini-PROTEAN® TGX gel (BioRad, Hercules, CA). Subsequent to electrophoretic separation, proteins were transferred to a PVDF membrane and incubated with primary antibody. Rabbit

anti-catalase primary (ab16731) antibody was purchased from Abcam (Cambridge, MA). Rabbit anti-Mn-SOD (ADI-SOD-110) and Rabbit anti-Cu/Zn-SOD (ADI-SOD-100) were purchased from Assay Designs (Plymouth Meeting, PA). Goat anti-rabbit IgG secondary antibodies (sc-2004; Santa Cruz Biotechnology, Santa Cruz, CA) provided chemiluminescent detection. Throughout the study, b-actin (p-8340; Sigma Aldrich) and GAPDH (#AM4300, Ambion) were utilized as loading controls. In experiments involving cell line comparison, preliminary data revealed differential expression of β -actin between the A549 and MeT-5A cell types. Therefore, in studies involving a comparison among the cell types GAPDH was utilized as a loading control.

4.2.4 Real-Time Polymerase Chain Reaction

Nrf2 mRNA in the MeT-5a cell line was analyzed using real-time polymerase chain reaction (RT-PCR). Briefly, mRNA was harvested using a RNeasy® mini kit (Qiagen, Valencia, CA) followed by subsequent generation of corresponding cDNA using the First Strand cDNA Synthesis Kit (Roche, Indianapolis, IN). Primers from Sigma Aldrich included both NRF2 and GAPDH and were received as follows. *Nrf2* forward (5'-3') ACCCAACCAGTTGACAGTGA and *nrf2* reverse (5'-3') CTCAGCTATGAAAGCAGAATAAAATTCA. *Gapdh* forward (5'-3') CCTCCCGCTTCGCTCTCT and *gapdh* reverse (5'-3') GCTGGCGACGCAAAGA. RT-PCR was performed on an Applied Biosystems 7500 Fast Real Time PCR machine using a FastStart Universal Sybr Green master mix (Roche). *Nrf2* expression was normalized to *gapdh* expression.

4.2.5 Total Glutathione Measurement

Total intracellular glutathione was measured using a GSH-Glo™ assay (Promega Corp, Madison, WI). Briefly, 10,000 cells were isolated, washed and suspended in phosphate buffered saline (PBS). This cell suspension was deposited into a white-walled 96-well plate in an effort to eliminate well crosstalk and decrease light absorbance. GSH-Glo™ reagent consisting of luciferin-NT, glutathione s-transferase, and GSH-Glo™ reaction buffer was added to each well and incubated for 30 minutes. Subsequently, luciferin detection reagent was added to each well and, following a 15 minute incubation, luminescence intensity was acquired. To measure total glutathione (GSH and GSSG), tris(2-carboxyethyl)phosphine (500 μM) was added to the sample lysate to reduce any oxidized GSSG present to measurable GSH. Luminescence readings were then compared to a provided GSH standard.

4.2.6 MTT Assay

The 1-(4,5-dimethylthiazol-2-yl)-3,5-diphenylformazin (MTT) assay (Sigma Aldrich, St. Louis, MO) is a spectrophotometric technique to assess cellular proliferation via quantification of the enzyme mitochondrial dehydrogenase. Actively respiring mitochondria reduce the tetrazolium salt to a water insoluble purple formazan dye which is then solubilized in MTT solubilization solution (10% Triton X-100 in 0.1 N HCl in anhydrous isopropanol. After solubilization in acidic isopropanol, the suspension is quantified by measuring the absorbance at 570 nm. A549 cells were seeded at a concentration of 5×10^3 cells/well, while MeT-5A cells were seeded at 1×10^4 cells/well. Differences in cell seeding were due to differing cellular proliferation rates.

4.2.7 Reduced Glutathione (GSH) Analysis

GSH response following SiO₂ nanoparticle exposure was measured using the GSH-GLOTM assay as described above, with few modifications. A549 cells were seeded in a 96-well plate with white walls at 5 x 10³ cells/well. MeT-5A cells were seeded at 1 x 10⁴ cells/well. Differences in cell seeding densities were due to differing cellular proliferation rates. Following 24 hrs of SiO₂ nanoparticle exposure, cells were lysed in the plate using the provided lysis buffer and GSH concentrations were measured via luminescence as discussed previously.

4.2.8 Catalase Activity Assay

Catalase activity was measured using an Amplex Red® Catalase Activity Assay (A22180, Invitrogen Corp.). Briefly, a saturating amount of H₂O₂ is supplied to the sample of interest. After an allotted time, unreacted H₂O₂ is quenched with the Amplex Red® reagent providing colorimetric (or fluorometric) detection. The change in H₂O₂ concentration was compared to a catalase-free control. Results are reported as a change in fluorescent units (Δ) when comparing within the same cell line. When making comparisons between cell lines, measured catalase activity was normalized to total protein content.

4.2.9 DCFH-DA Assay

A 20 μ M 2', 7' - dichlorofluorescein diacetate (DCFH-DA) solution (Sigma Aldrich, St. Louise, MO) in Dulbecco's phosphate buffered saline (DPBS) was prepared without other additives. Both cell types were incubated with DCFH-DA for 15 minutes. After washing once with D-PBS, cells were then exposed to SiO₂ nanoparticle

suspensions at concentrations of 0.01 – 100 $\mu\text{g/mL}$. Cells were then incubated for 24 hrs, washed briefly, and fluorescence was measured at 485/520 nm (excitation/emission) using a fluorescence plate reader (Synergy MX, Biotek).

4.2.10 NRF2 Immunofluorescence

Localization of the transcription factor NRF2 was assessed through immunofluorescence techniques. Viable A549 and MeT-5A cells were cultured on sterile glass coverslips prior to exposure to SiO_2 nanoparticle or tBHQ (positive control). Following 24 hrs incubation with SiO_2 or tBHQ, cells were washed and fixed with a 4% paraformaldehyde solution. Membranes were permeabilized with 0.25% (vol/vol) Triton X-100 in PBS. A 1% bovine serum albumin solution (0.3 M glycine) was used as a blocking agent. Cells were incubated with rabbit anti-NRF2 (Ab62352, Abcam) primary antibody followed by an Alexa Fluor 488-conjugated goat anti-rabbit IgG secondary (A11008, Invitrogen Corp.). Fluorescence detection was achieved using an Olympus IX-71 inverted fluorescence microscope. Micrograph exposure conditions remained identical within each cell type.

4.3 Results

4.3.1 Cellular Antioxidant Characterization

In an effort to examine the basal intracellular antioxidant levels, a variety of enzymatic proteins as well as intracellular glutathione levels were examined using both western blot and fluorescence-based techniques. Catalase is responsible for the degradation of moderately reactive cellular peroxides to water and oxygen. Western blot analysis revealed increased basal catalase expression in the A549 cell line over the MeT-5A cell line (Figure 4.1, top), which, when approximated with semi-quantitative densitometric analysis, was estimated at an increase of 39%. A fluorescence-based assay was also utilized to examine catalase activity. Confirming western blot expression, the basal catalase activity in the A549 cell line exhibited a statistically significant increase when compared to the MeT-5A cell line (34.35 ± 0.20 vs. 31.63 ± 0.01 mU/mL protein solution/mg total proteins, respectively). Similar techniques were employed to assess both Cu/Zn SOD and Mn SOD levels. Cu/Zn SOD (SOD1), highly conserved among eukaryotes, is located in the cytosol. Mn SOD (SOD2) confined to the mitochondria. Both forms of SOD are responsible for the degradation of the superoxide anion ($O_2^{\cdot -}$) to peroxide and water. Results indicate that both Cu/Zn SOD and Mn SOD, basal expression was greater in the MeT-5A cells (increases of 48% and 105%, respectively) than in the A549 cells. Expression was compared using the loading control glyceraldehyde 3-phosphate dehydrogenase (GAPDH).

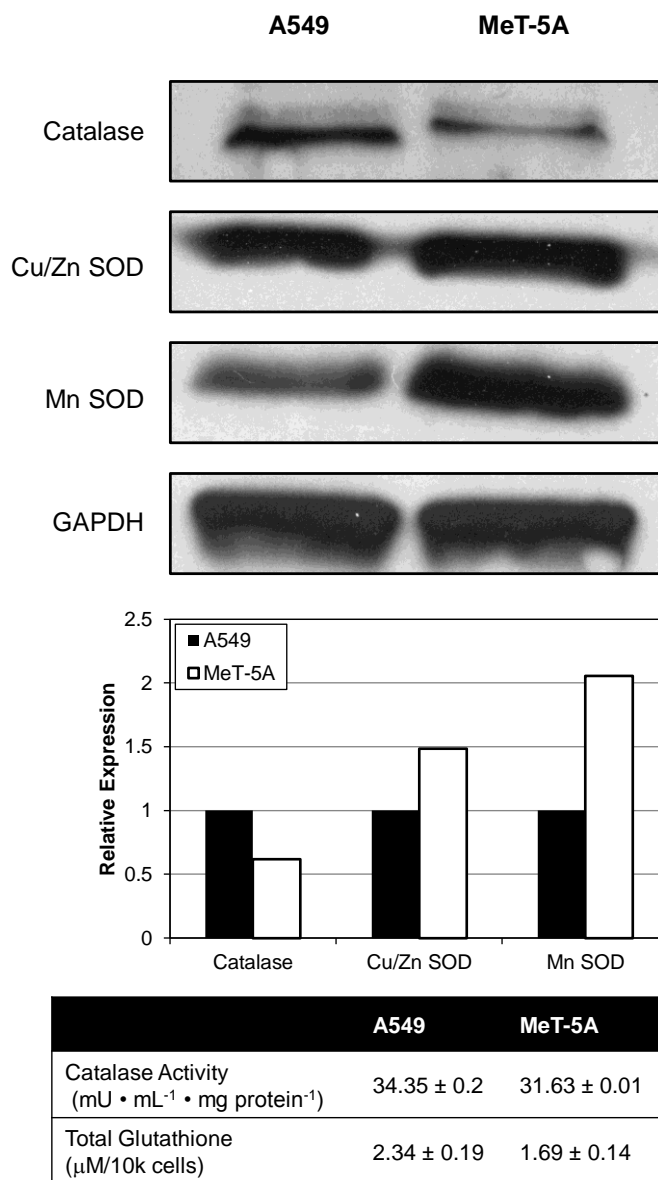


Figure 4.1 Cellular antioxidant characterization. Constitutive levels of catalase, Mn SOD, and Cu/Zn SOD in human lung (A549) and human mesothelial (MeT-5A) cell lines were measured using western blot analysis (top) combined with densitometric analysis (middle). While greater expression of both SOD isoforms was noted in the MeT-5A cell line, catalase expression was significantly higher A549 cells than MeT-5A cells. Catalase activity measurement (bottom) confirmed the results of the western blot. Furthermore, total glutathione was found to be significantly higher in A549 cells when compared to MeT-5A cells.

Following enzymatic analysis, total basal intracellular glutathione was measured via a luminescence-based assay (Figure 4.1, bottom). Glutathione content was assessed in 10,000 cells each of both cell lines. The A549 cells exhibited a 38% higher GSH level when compared to the MeT-5A cells (2.34 ± 0.19 vs. 1.69 ± 0.14 $\mu\text{M}/10,000$ cells, respectively).

Following characterization of intracellular antioxidants, both A549 and MeT-5A cells were exposed to a range of H_2O_2 concentrations (50 μM -2mM) for a period of 24 hrs (Figure 4.2). At doses ranging from 50 to 800 μM , A549 cells exhibited little to no change in growth as evidenced by the metabolized tetrazolium salt. Significant decreases in metabolized tetrazolium salt were evidenced at doses of 1500 μM to 2000 μM . The MeT-5A cell line was far more susceptible to peroxide damage with statistically significant cell viability decreases beginning at 100 μM peroxide (66.28% of control). Furthermore, at doses above 100 μM (up to 2000 μM), MeT-5A cells exhibited total cell death, as evidenced by little MTT conversion (<10 % of control). This data indicates that the MeT-5A cell line is significantly more susceptible to damage from H_2O_2 exposure than the A549 cell line. These results were confirmed by a live/dead cell viability assay (data not shown).

4.3.2 Nanoparticle Characterization

SiO_2 nanoparticles were characterized in-house. TEM analysis revealed a size of 33.5 ± 7.73 nm (Figure 4.3A and Appendix A.1). Furthermore, size results were confirmed through measurement with SEM (Appendix A.1). It is important to note that these nanoparticles in their powder form agglomerate to the micron scale (Figure 4.3B).

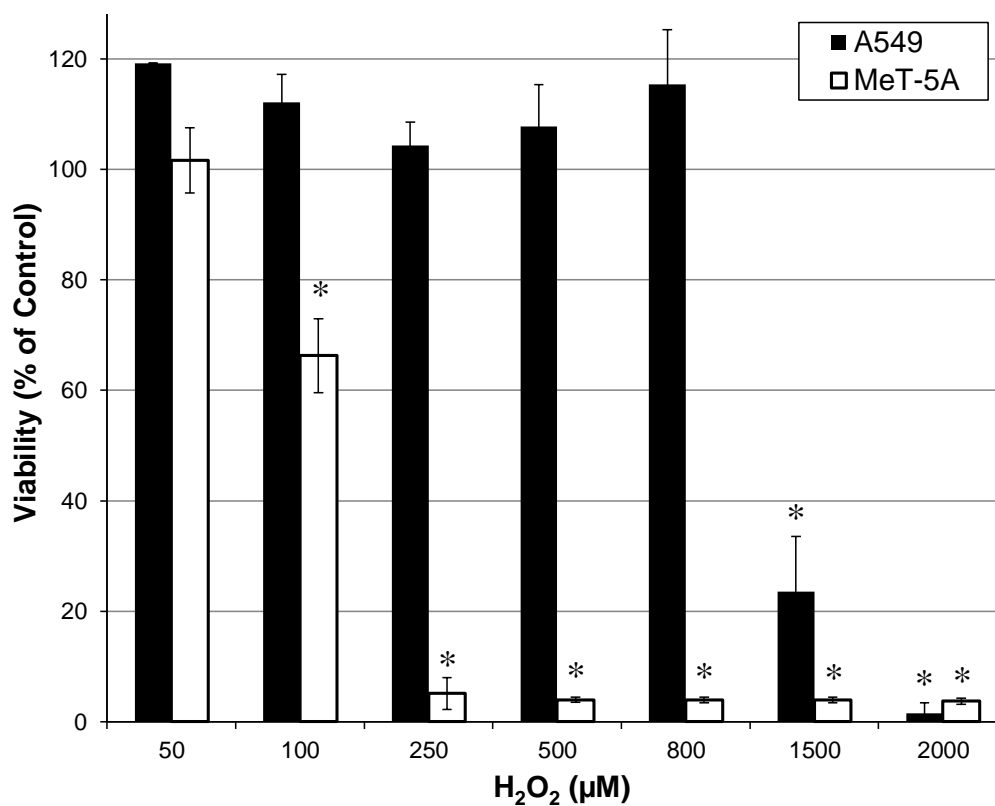


Figure 4.2 Dose-response relationships to hydrogen peroxide. A549 and MeT-5A cells were incubated with increasing concentrations of hydrogen peroxide for 24 hrs. Following incubation, cellular proliferation was measured via the MTT assay. MeT-5A cells were more susceptible to peroxide-induced damage. * $p < 0.05$ when compared to the unexposed (negative control) A549 and MeT-5A cells.

Elemental composition was confirmed with energy dispersive x-ray spectroscopy (EDS). The spectral peak at 0.52 KeV represents oxygen while the peak at 1.74 KeV represents silicon (Figure 4.3C). Surface area analysis was measured at 576.23 m²/g.

4.3.3 Intracellular Oxidant Production

Intracellular ROS was determined using the DCFH-DA assay (Figure 4.4, top). Within this assay, the non-fluorescent DCFH molecule is converted to fluorescent DCF upon reaction with intracellular oxidants. Both the A549 and MeT-5A cells were incubated with various doses (0.01 – 100 µg/mL) of SiO₂ particles for 24 hrs. In both cell lines exposed to particle concentrations greater than 1 µg/mL, statistically significant increases in fluorescence were noted, with maximum oxidant production at 75 µg/mL. At this particular concentration, A549 cells attained an increase in fluorescence greater than 166% of the control while the MeT-5A cells elicited an increase of 187% over the control. At a concentration of 100 µg/mL, both cell lines exhibited a decrease in fluorescence when compared to the 75 µg/mL exposure. This decrease may be associated with increasing particle agglomeration and decreasing particle uptake at a higher dose of 100 µg/mL. DCFH oxidation was more prevalent in the MeT-5A cells than in the A549 cells, with an increase in fluorescence values in 5 of the 8 points measured. Throughout the DCFH-DA assay, controls experiments were performed to ensure that SiO₂ particles did not interfere with DCF fluorescence (Appendix A.2).

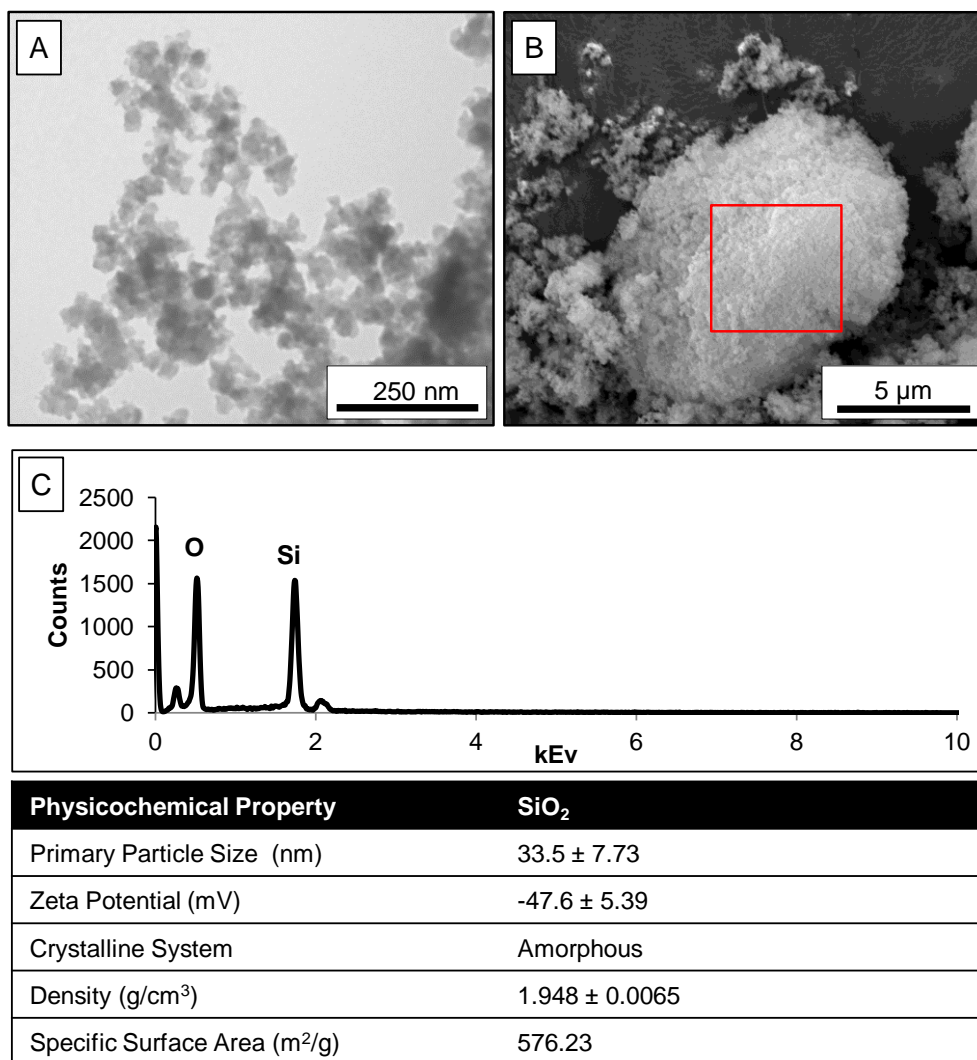


Figure 4.3 Characterization of SiO₂ nanoparticles. SiO₂ nanoparticles were thoroughly characterized prior to experimentation utilizing a variety of techniques. Although primary particle definition is evident under TEM (A), micron-sized agglomerates predominate in powder form, as examined by SEM (B). Furthermore, the elemental composition of silica was confirmed as silicon and oxygen via energy dispersive x-ray spectroscopy on box in panel B (C). Additional physicochemical properties are included in the table.

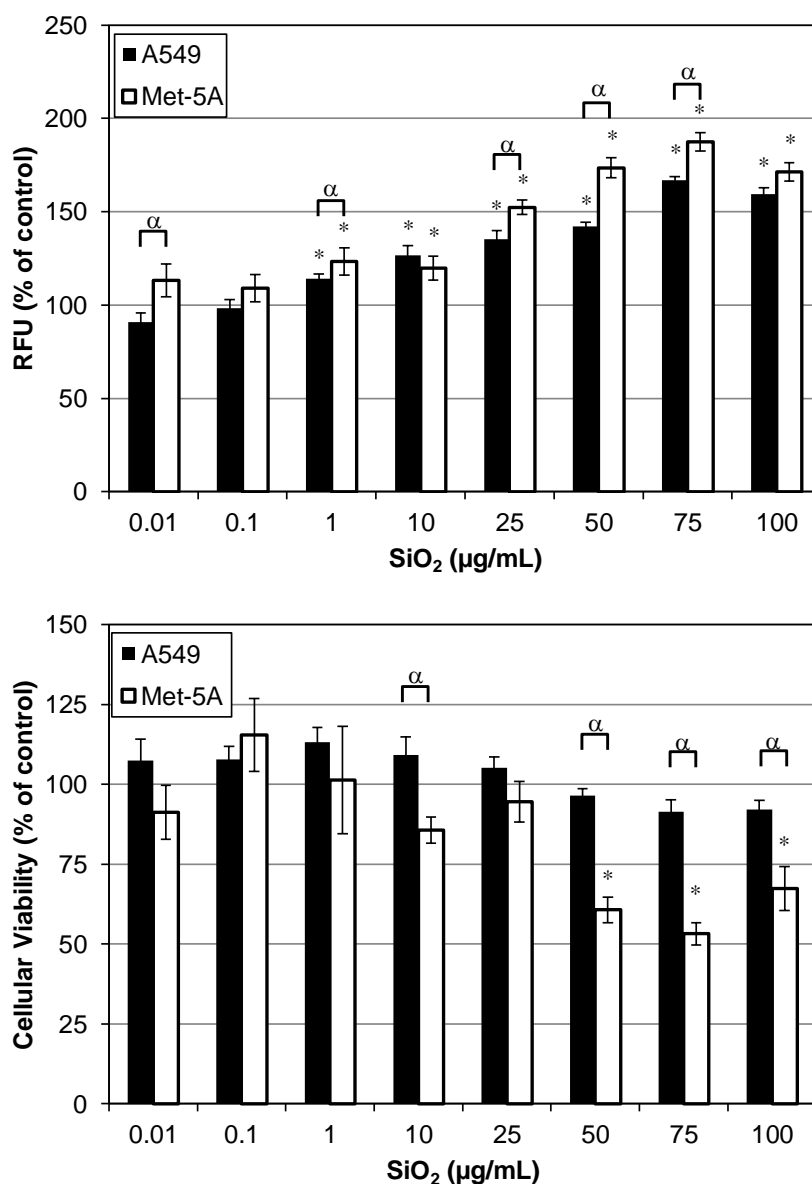


Figure 4.4 Intracellular oxidant production and dose-response relationship. Following incubation with SiO₂ nanoparticles for 24 hrs, differences in intracellular oxidant production were observed. MeT-5A cells revealed increased DCFH oxidation when compared to A549 cells. The highest intracellular oxidant production measured in either cell line (75 μg/mL; 24 hrs) was associated with the largest decrease in cellular proliferation in the Met-5A cell line. Similarly, differences in cellular proliferation between cell lines were evident following exposure to SiO₂ nanoparticles. A549 cells displayed high tolerance to SiO₂ nanoparticle exposure (93% viable at highest dose), while the Met-5A exhibited more susceptibility (67% viability at highest dose). * p<0.05 compared to A459 and Met-5A unexposed (control) cells, respectively; α p<0.05 when comparing both A549 and Met-5A cells at same exposure values.

4.3.4 Cellular Proliferation

Cellular proliferation was assessed using the absorbance based MTT assay (Figure 4.4, bottom). This assay measures the conversion of a tetrazolium salt to a formazan dye. Both A549 and MeT-5A cells were exposed to various concentrations (0.01 – 100 $\mu\text{g}/\text{mL}$) of SiO_2 particles for 24 hrs and, subsequently, cellular proliferation was measured. The A549 cell line exhibited a slight decrease in cellular proliferation at the higher concentrations (minimum 91.4% of control; 75 $\mu\text{g}/\text{mL}$). Similarly, the MeT-5A cell line experienced decreases in cellular proliferation at the higher doses, albeit a more significant decrease was observed at 50 $\mu\text{g}/\text{mL}$ (decrease 60.7% of control). Exposed MeT-5A cells exhibited a minimum viability at 75 $\mu\text{g}/\text{mL}$ (53.3% of control). Statistically significant differences in MeT-5A cellular proliferation were seen at the highest three concentrations tested in this study (50, 75, 100 $\mu\text{g}/\text{mL}$). As with the DCFH-DA assay, controls were incorporated to ensure SiO_2 nanoparticles did not interfere with the absorbance based readings (Appendix A.3).

4.3.5 Glutathione Measurements

Glutathione (GSH in its reduced form, only) was measured following 24 hrs exposure to SiO_2 nanoparticles (Figure 4.5). GSH levels in the A549 cells slightly decreased GSH levels after 24 hrs exposure to SiO_2 particles. Conversely, all exposure concentrations (0.01 – 100 mg/mL) decreased GSH levels in the MeT-5A cells. Interestingly, only a slight dose-response relationship was noted throughout the range (Figure 4.5).

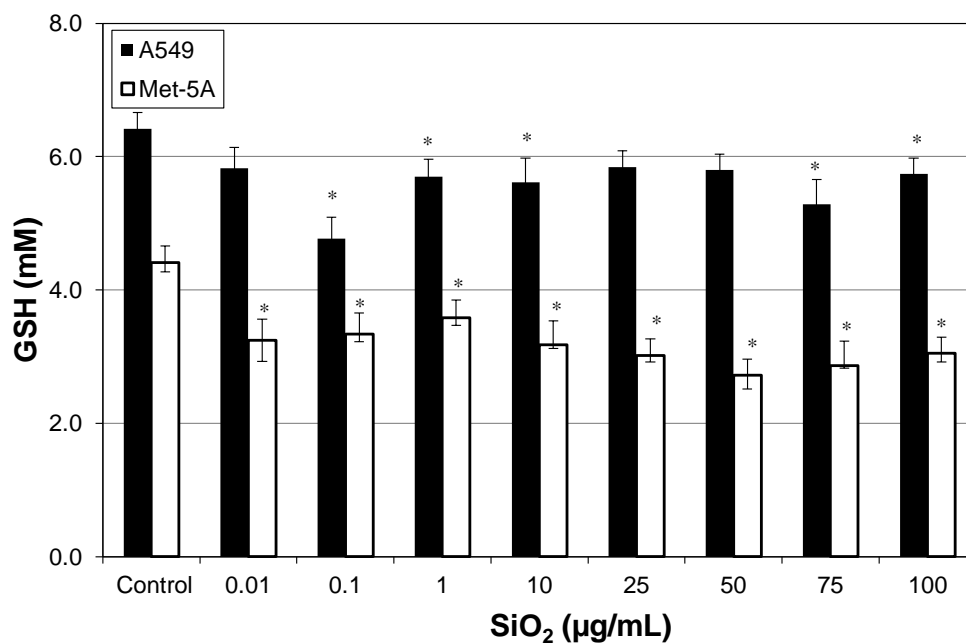


Figure 4.5 Glutathione depletion following exposure to SiO₂ nanoparticles. Cellular glutathione (GSH) concentration was measured following exposure to SiO₂ nanoparticle for 24 hrs. In both the A549 and Met-5A cell lines a decrease in GSH level was noted at all doses used in this study. However, statistically significant decreases were evident to a higher extent in the Met-5A at every concentration tested. * $p < 0.05$ compared to A549 and Met-5A unexposed (control) cells, respectively.

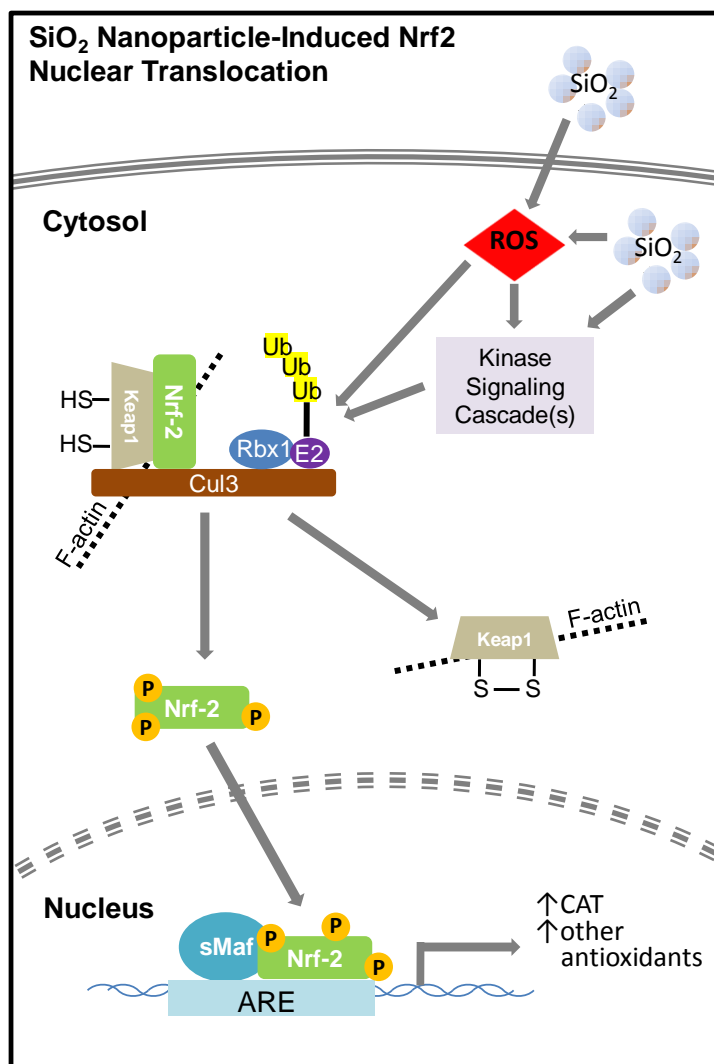


Figure 4.6 NRF2 translocation schematic. NRF2 cytosolic stabilization and nuclear translocation stems from the release of NRF2 from KEAP-1 in the cytosol. This release inhibits proteolytic degradation which persists under normal redox circumstances. Nuclear translocation of NRF2 can lead to the induction of a variety of phase II metabolizing enzymes.

4.3.6 NRF2 Stabilization

The KEAP1-NRF2 transcription factor provides an excellent sensor for oxidative stress (Figure 4.6). Therefore, in a more concerted effort to examine the oxidative stress response, we analyzed the cytoplasmic stabilization and nuclear translocation of the NRF2 transcription factor. Whole cell NRF2 protein expression in both cell lines was examined with western blotting techniques. NRF2 expression exhibited a time-dependent increase with a maximum peak at 8 hrs following SiO₂ exposure, although all time points were enhanced over the loading control in both cell lines (Figure 4.7). Using immunofluorescence techniques, it was possible to assess the levels and location of NRF2 following 24 hrs exposure to 75 µg/mL SiO₂ particles (Figure 4.8). In subsequent experiments, 75 µg/mL was chosen as the exposure dose due to its highest oxidant production combined with the minimum cell proliferation in both cell lines. NRF2 was detected using a green fluorophore (AlexaFluor 488). Cell nuclei were counterstained with DAPI. Both cell lines exhibited cytoplasmic stabilization and nuclear translocation of NRF2, as evidenced by increasing nucleic and cytoplasmic fluorescence when compared to the control. Similarly, both cell lines displayed overlapping fluorophores in the nuclear region, which is characteristic of NRF2 nuclear translocation. Tert-Butylhydroquinone (tBHQ) (50 µM; 24 hrs) was incorporated as a positive control. Single channel micrographs indicated minimal cellular autofluorescence or non-specific antibody binding (Appendix A.4 & A.5).

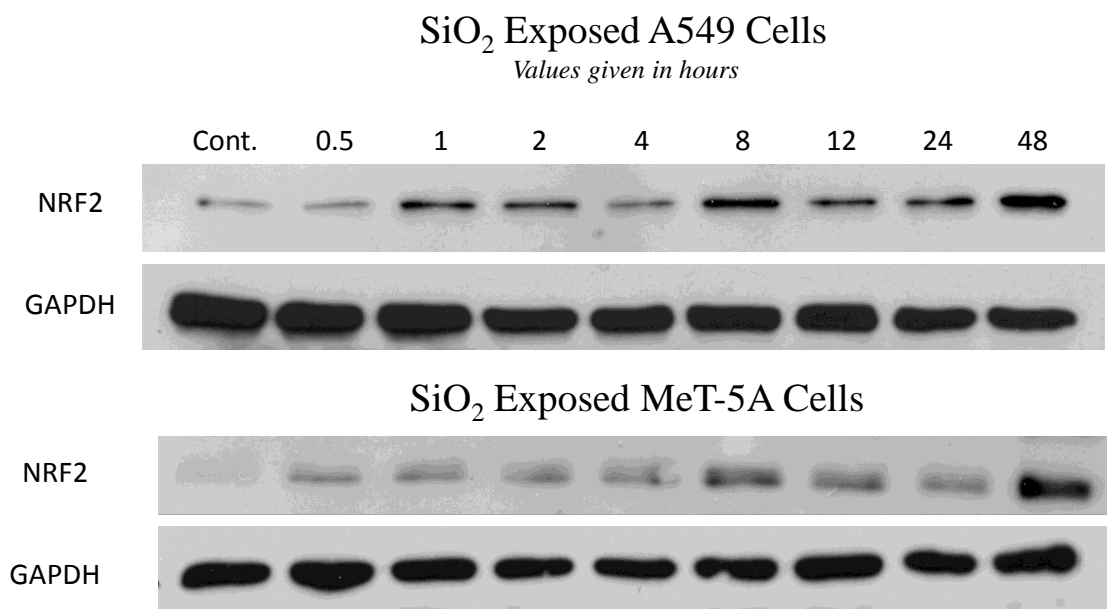


Figure 4.7 Time-dependent NRF2 protein expression. A549 and MeT-5A cells were exposed to SiO₂ nanoparticles for up to 48 hrs. NRF2 protein increases in quantity as either a direct or indirect response to oxidative stress. In both cell lines, NRF2 expression exhibits a maximum intensity at 8 hrs and 48 hrs.

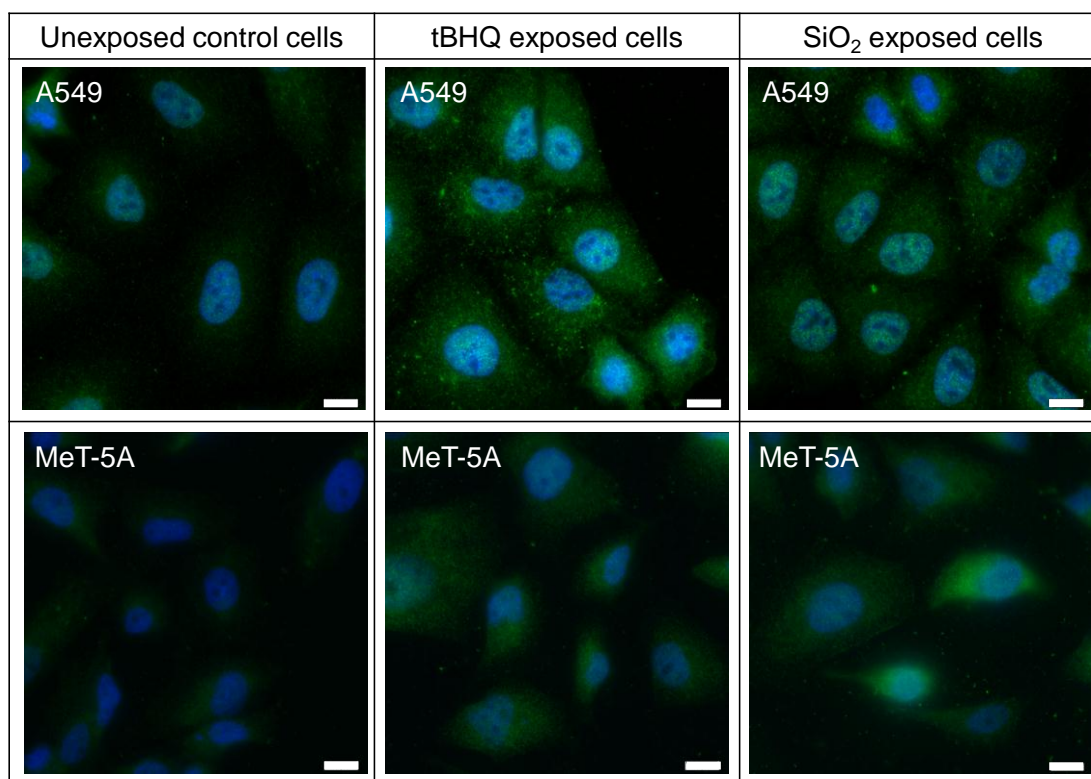


Figure 4.8 Stabilization of NRF2 transcription factor. Cytoplasmic stabilization and nuclear translocation of NRF2 (green) is shown following treatment with tBHQ (50 μ M; positive control) or SiO₂ nanoparticles (75 μ g/mL) for 24 hrs in both cell lines. Stabilization of NRF2 is evidenced by the increase in green signal fluorescence located in both the cytosol and nucleus. Nuclear translocation is indicated by the overlay of green (NRF-2) and blue (DAPI) fluorescence. Scale bar = 10 μ m.

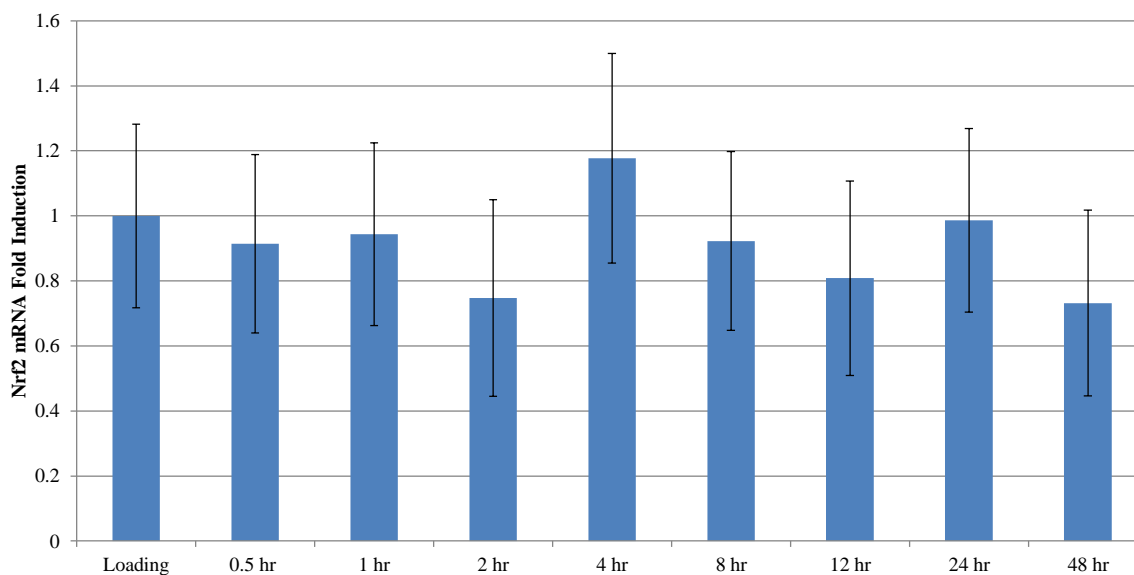


Figure 4.9 mRNA levels of *nrf2* transcript. The mRNA levels of the *nrf2* transcript in the MeT-5A cell line were analyzed in an effort to ensure that the NRF2 protein was posttranscriptionally regulated. No significant differences were observed in the *nrf2* mRNA level over the time course studied.

In an effort to ensure increased NRF2 protein was posttranscriptionally regulated, *nrf2* mRNA expression was analyzed in the MeT-5A cell line (Figure 4.9). No significant increases in *nrf2* mRNA expression were observed over the time course studied (0.5 hrs to 48 hrs).

4.3.7 Catalase Induction

In an effort to further characterize the downstream response to intracellular oxidant production induced after SiO₂ exposures, we examined the induction of the antioxidant gene catalase activity in both cell lines following exposure to 75 µg/mL SiO₂ nanoparticles (Figure 4.10). Catalase activity measurements were taken 48 hrs post-exposure and compared with an unexposed control. In both cell lines, statistically significant differences were noted pertaining to increased catalase activity. Catalase activity (measured as a change in fluorescence units) in the A549 cell line was significantly greater after 48 hrs (Δ fluorescent units 34,350 vs. 38,020, respectively). Similar confirmation was seen in the MeT-5A cell line with a significant increase following 48 hrs exposure (Δ fluorescent units 31,620 vs. 34,680, respectively).

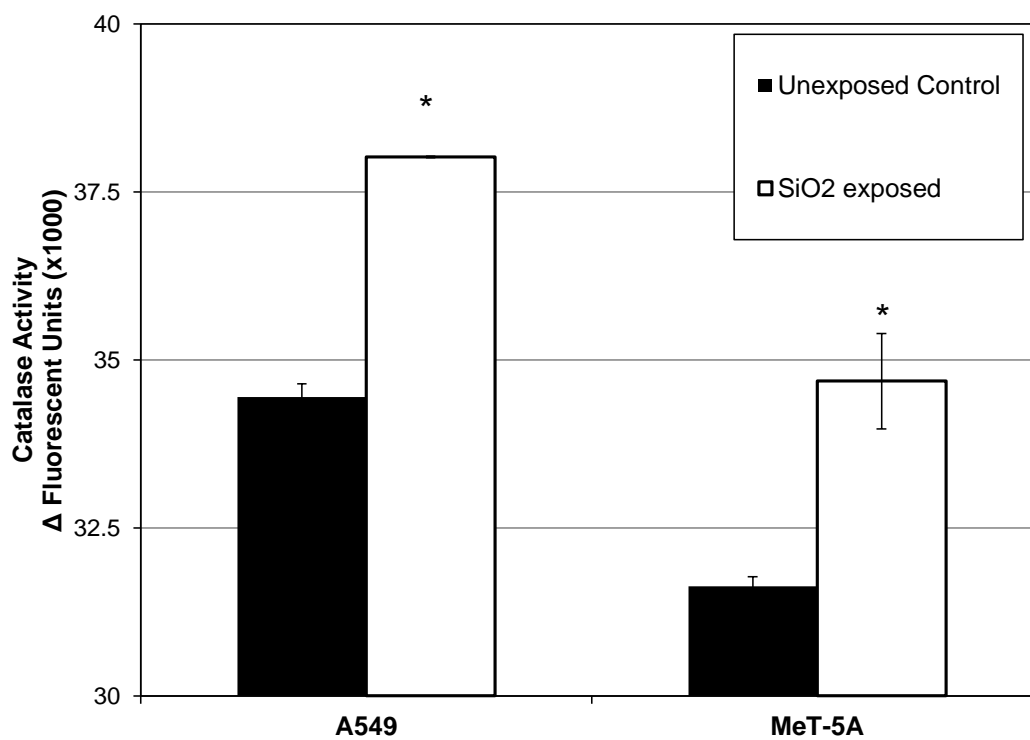


Figure 4.10 Cell line and time dependent induction of catalase. In both cell lines, catalase activity was significantly higher after 48 hrs exposure to SiO₂ than when compared to an unexposed (negative) control. * $p < 0.01$ when compared to respective cell line control.

4.4 Discussion

Expression of enzymes and low molecular weight antioxidants present in the intracellular environment remains a critical aspect of toxicology when dealing with compounds that act through an oxidative stress mechanism. While the eukaryotic cell lines tested here are generally exposed to ROS through their aerobic environment as well as from byproducts of normal cellular metabolism, an increase in intracellular oxidants may lead to damage of protein, lipids, and DNA. Results indicate that the A549 cell line contains higher basal levels of both catalase and glutathione than the MeT-5A cell line. Higher levels of these antioxidants may be associated with their location in relation to the external environment (i.e. lung airway vs. plural space). The difference in basal catalase expression agrees strongly with the dose-response curve generated using H_2O_2 .

As with catalase, glutathione may play a role in the metabolism of H_2O_2 by acting through the enzyme glutathione peroxidase. Glutathione peroxidase catalyzes the oxidation of GSSG to GSH and water (Heffner and Repine 1989). Studies have shown that differences in glutathione levels may be due to differences in the rate of GSH synthesis. For example, Jarvin and others (2000) have shown that expression of γ -GCS, the rate limiting enzyme in glutathione synthesis, has been shown to be higher in A549 cells than M14K cells (Jarvinen et al. 2000). Similarly, *in vivo* experiments dictate that normal bronchial epithelium contains increased γ -GCS over normal mesothelium (Puhakka et al. 2002). Our observations demonstrating differences in glutathione levels between two cell types from adjacent locations complement these results.

Additionally, we found that both superoxide dismutase (SOD) isoforms assessed were present in lower amounts in the A549 cell line when compared to the MeT-5A cell line. Similar results have been noted in a variety of tumor cell lines (Oberley and Buettner 1979). It has been suggested that Mn-SOD may act as a tumor suppressor gene, thus cancerous cell lines which exhibit this decreased SOD level may be more susceptible to damage by superoxide generating nanoparticles (Li et al. 1995). Elevated Cu/Zn SOD in the Met-5A cell line may be due to either decreased Cu/Zn SOD found in tumor cells (Oberley et al. 1978) or elevated SOD levels after SV40 transformation (Yamanaka and Deamer 1974). While basal catalase and GSH levels in A549 cells were well-correlated with the pattern observed in the dose-response curve to SiO₂ nanoparticles used in this study, SOD isoforms were not. Therefore, we conclude that SOD is not a primary enzyme involved in metabolism of oxidants produced by cell-SiO₂ interaction.

Although the SOD expression is an unlikely participant in the metabolism of oxidants produced by SiO₂ nanoparticles, we hypothesized that both catalase and GSH may play a protective role in SiO₂ nanoparticle exposure. Both cell lines were exposed to SiO₂ nanoparticles over a wide dose range (0.01 – 100 µg/mL). Following exposure to these nanoparticles, we assessed an array of toxicological endpoints including oxidant production, cell proliferation, GSH depletion, NRF2 stabilization and translocation, and downstream catalase activity induction. To examine oxidant production, the DCFH-DA assay was utilized to provide an estimate of intracellular ROS. While the DCFH-DA is non-specific (i.e. it reacts with multiple oxidants), DCFH-DA has been suggested as an

excellent tool for measuring the status of oxidative stress of cells in culture (Foucaud et al. 2007; Wang and Joseph 1999). Both cell lines exhibited a classic dose-response relationship at doses up to 75 $\mu\text{g}/\text{mL}$. Significant increases in DCFH oxidation were noted at all doses above 1 $\mu\text{g}/\text{mL}$. A similar relationship was observed by Lin et al. (2006); however our data suggests that this oxidant production occurs at least 24 hrs prior to the results reported in their work (Lin et al. 2006). On the contrary, Yu et al. (2009) suggests that while both 30 nm and 48 nm amorphous silica increased cellular membrane damage and decreased cellular viability, they did not observe any difference in ROS production or GSH decrease with the exception of the highest concentration tested (200 $\mu\text{g}/\text{mL}$) (Yu et al. 2009). Work by Limbach et al. (2007) suggests that pure SiO_2 at 30 $\mu\text{g}/\text{ml}$ did not induce ROS production but upon the intercalation of FeO within the SiO_2 nanoparticle, increases in ROS were evident (Limbach et al. 2007). At most exposures, the MeT-5A cell line exhibited heightened DCFH oxidation over the A549 cells. This could be due to direct competition between DCFH and GSH, which is higher in A549 cells.

The MTT assay revealed an inverse relationship between DCFH oxidation and cellular proliferation. The proliferation of A549 cells, while trending downward, did not exhibit any significant decreases when compared to the undosed control. Similar results have been elucidated in other cell lines including MSTO and 3T3 cells at doses of up to 15 $\mu\text{g}/\text{mL}$ (Brunner et al. 2006). Alternatively, the Met-5A cell line exhibited significant decreases in cellular proliferation at doses at or above 50 $\mu\text{g}/\text{mL}$. This decrease in proliferation may be related, in part, to the decreased ability to detoxify ROS measured

throughout the duration of the DCFH assay. However, when examining the levels of GSH in both cell lines following 24 hrs exposure to SiO₂ particles, neither cell line exhibited a dose-dependent response. Rather, a general decrease in GSH levels was evident following inoculation with SiO₂ particles. Tirumalai *et. al.* (2002) examined GSH levels following exposure to acrolein and found significant decreases in GSH at time points as early as 30 minutes. However, at 24 hrs GSH concentrations had almost fully recovered to that of the control cell population (Tirumalai et al. 2002). Therefore, in our study, it may be possible that at any time point prior to 24 hrs, GSH levels could have exhibited a more significant decrease than what is evidenced here. Due to significantly decreased levels following 24 hrs of exposure, it is possible that SiO₂ particle-induced generation of ROS may be an insult that is more continuous in nature than instantaneous with subsequent rapid oxidant metabolism.

Treatment of cells with electrophilic xenobiotics often invokes the transcriptional activation of genes involved in both detoxification and metabolism. This reaction, often known as the electrophile counterattack response, is, in part, mediated by the binding of sensitive transcription factors to the antioxidant response element located in the promoter regions of genes involved in ROS detoxification (Ishii et al. 2000; Prester et al. 1993). Central to this response is the NRF2-KEAP1 transcription factor. NRF2, a cap 'n' collar basic leucine zipper transcription factor, remains bound to KEAP1 in the cytosol under normal redox conditions. In this state, forced proteosomal degradation of NRF2 limits intracellular accumulation. However, under conditions of oxidative stress, the NRF2-KEAP1 bond is cleaved resulting in increased overall NRF2 levels and

subsequent nuclear translocation. Recent literature suggests that a variety of lung cancer cell lines, including A549, H460, H838, and H1435 harbor loss of function mutations in KEAP1, which increase basal stabilization and translocation of NRF2 (Singh et al. 2006). NRF2 has been reported play a role in the regulation of both catalase and glutathione synthesis, however; NRF2-null cells demonstrate no change in SOD activity (Zhu et al. 2005). Our results demonstrating the differences in antioxidant capability between cell lines are consistent with these findings. While Singh et al. (2009) suggests that regulation of NRF2 is decreased in the A549 cell line, several studies indicate that this signaling pathway in the A549 cell line may still be activated (Tirumalai et al. 2002; Kode et al. 2008). Such increases in NRF2 activation have been thoroughly characterized using tert-Butylhydroquinone, a positive control utilized in our experimental design (Yueh and Tukey 2007; Li et al. 2009; Rao et al. 2010).

In both cell lines, an increase in overall NRF2 protein expression and nuclear translocation, combined with no significant increases in mRNA *nrf2* levels, occurred after treatment with SiO₂ nanoparticles. Similar results have been obtained for CeO₂ nanoparticles (Eom and Choi 2009). While NRF2 stabilization and nuclear translocation were documented, confirmation of a protein with a gene that lies downstream of the NRF2 consensus binding sequence was needed. Catalase, for which the basal expression was earlier assessed, has previously been reported to be regulated by NRF2 and was thus identified as an ideal candidate (Zhu et al. 2005). In both cell lines, catalase was induced after 48 hrs, as reported through a catalase activity assay. While the induction of catalase was examined here, increased expression of various antioxidant phase II genes

may also play an important role in the response to oxidative stress driven by nanoparticles.

As the field of nanotoxicology increases its breadth and depth in human and environmental health research, the utilization of *in vitro* toxicological tests will play a central role in the identification of potential targets (e.g. mesothelial-like cells). The goal of these findings is to supplement the current particle toxicology literature and serve as a basis for future *in vivo* hypothesis-driven research. Additionally, the use of multiple cell types in a mechanistic toxicity study could further strengthen hazard identification and exposure evaluations, thereby contributing to future comprehensive nanomaterial risk assessments.

5. CONCLUSIONS

The science of nanotechnology is growing rapidly. With the exponential increase in the number of consumer products utilizing nanomaterials, there is a need to determine if the potential for negative human health effects exists. This “precautionary principle” approach is necessary because it remains possible that the same physicochemical properties which make nanomaterials, including nanoparticles, beneficial, *may* also yield negative toxicological consequences. These negative conditions may occur if nanoparticles are present in the right dose at the right place and for long enough duration to elicit a biological response. Even though there is currently a broad array of nanoparticles synthesized, this number is increasing daily. Because of this, it may not be feasible to examine the toxicological profiles of each particle individually, and thus, identifying a structure-activity relationship based each nanoparticle’s physicochemical parameters is a necessary development (Sayes and Ivanov 2010).

Numerous exclamations in the nanotoxicology community link the physicochemical properties of nanomaterials to an oxidative stress, inflammatory, or cytotoxic response. While a variety of factors have been implicated in playing a role in nanoparticle toxicity (e.g. size, crystallinity, surface functionalization), the work here demonstrates that the nanoparticle surface charge, or zeta potential, may be a physical parameter worthy of consideration. As previously discussed, the nanoparticle zeta potential often influences the agglomeration state of particles in suspension. These

measurements are often very dynamic and influenced by the suspension medium parameters such as pH and ionic strength.

While the zeta potential is often impacted by the nanoparticle's environmental conditions, it may also be influential in determining a potential biological response. For example, it was observed that nanoparticles which exhibited a charged surface at physiological pH (TiO_2 and Fe_2O_3) lead to decreases in cell viability, while those with near neutral charges did not. However, this decrease in cell viability may not be due to the nanoparticle zeta potential alone, as charged particles often exhibit an increased tendency to bind biological macromolecules and enter the cellular environment. Therefore, careful characterization of each nanoparticle is necessary prior to experimentation.

While the identification of physicochemical parameters is often useful in an exposure involving one particle type, it becomes more complicated upon the exposure to a mixture of nanoparticles that is more representative of the real world. As visualized in Table 1.1, occupational studies measuring nanoparticles released from workplace activities often result in the conclusion that background particles from other external sources (e.g. combustion derived ultrafine particles) were present along with the chosen nanoparticle of interest. In an effort to examine the potential toxicological implications of nanoparticles mixtures, an *in vitro* experiment was developed using Fe_2O_3 (a transition metal oxide) nanoparticles co-exposed with flame synthesized carbon black. Not surprisingly, the mixtures of nanoparticles exhibited greater toxicity (as measured by decreases in cellular proliferation). This phenomenon was believed to be due to the

nanoparticles tendency to proceed through an oxidative stress mechanism. Additionally, we confirmed and expanded upon a previously published paper by identifying a more specific mechanism through which this oxidative stress occurs (Guo et al. 2009).

The unique combination of transition metals and carbonaceous nanometer sized particles are present in large amounts in diesel exhaust. Previous reports have concluded that there is possibly a reducing agent present in such particulate mixtures which may act to yield increased oxidative stress (Donaldson et al. 1997). However, beyond this conclusion, little research involving the mechanism behind this effect is available. In an effort to increase the knowledge in the fields of both nanotoxicology and ultrafine particle toxicology, we set out to identify the potential mechanism behind this synergistic reaction. Our studies indicate that both transition metal oxides (Fe_2O_3) and carbonaceous nanoparticles (ECB) were incorporated into the endosomal or lysosomal environment following cellular internalization. This acidic environment may release Fe^{3+} from the nanoparticle surface where it may be reduced to Fe^{2+} by hydroquinone moieties bound to the surface of the combustion-derived ECB. This reduction in Fe, coupled with intracellular responses such as the Fenton and Haber-Weiss reactions, may lead to increased oxidant production through redox cycling which, if proceeds uninhibited, may lead to cellular oxidative stress.

Oxidative stress is defined as the cellular response to reactive oxygen species which are present in high enough concentrations to strain the cellular antioxidant defense system. This imbalance in oxidation status of the cell has been implicated in many biological diseases ranging from atherosclerosis to Alzheimer's. Therefore, any

toxicological process which retains the ability to generate reactive oxygen species may pose a threat to human health. In this respect, many materials which are traditionally inert at the micron scale have been shown to exhibit greater oxidative effects at the nanometer size scale. In the last section of this work, a model *in vitro* system utilizing a previously reported KEAP1 genetically mutated cancer-derived lung epithelial cell (A549), in comparison with a transformed mesothelial cell line (MeT-5A), was characterized for use in nanotoxicology studies (Singh et al. 2006). Furthermore, this model was utilized to identify the oxidant production and subsequent cellular antioxidant response (e.g. NRF2 stabilization, GSH depletion) stemming from exposure to silica nanomaterials. SiO₂ nanoparticles were observed to induce oxidant production and antioxidant responses in both cell lines, however, only a significant decrease in cell proliferation were observed for the MeT-5A cell line.

Understanding the cellular response of multiple cell types *in vitro* could help to strengthen the hazard identification of the risk assessment process. Currently, comprehensive risk assessments in the arena of nanotoxicology remain implausible due to the vagueness of hazard identification and exposure values. For example, the hazard identification process may be complicated by the presence of multiple background particles or organics bound to the nanoparticle surface. Alternatively, it remains to be answered if actual exposures to engineered nanoparticles are at a level high enough to lead to adverse health effects. This has been highlighted by Beckett et al. (2005) who suggests that human exposure to zinc oxide nanoparticles at a concentration of 500 µg/m³ for 2 hrs did not yield any significant increases in leukocyte surface markers,

hemostasis, or cardiac electrophysiology (Beckett et al. 2005). While no markers of acute systemic effects were witnessed in this previously reported study, it has yet to be determined the disease endpoints that are appropriate for nanoparticle toxicology. In this respect, may we rely on previously determined endpoints from classical particulate toxicology, or will a novel biological response be observed?

As with broad classes of organic compounds, one nanoparticle cannot generally be expected to behave like another particle even within the same composition. This has been highlighted by the numerous studies showing that slight alteration in nanoparticle size or charge will lead to a different cellular response (Jiang et al. 2008b; Dausend et al. 2008). Similarly differences in particle solubility may require alternate methods in toxicological testing as their effects may be more chronic than those of soluble particles. With the large increase in the amount and diversity of nanomaterials currently being synthesized, proper characterization of both material and biological systems prior to toxicology testing will help to further define and illustrate the nanoparticle characteristics relevant to toxicology.

REFERENCES

- Aitken R, Creely K, Tran C. 2004. Nanoparticles: An occupational hygiene review. Accessed May 2011 from the website: <http://www.hse.gov.uk/research/rrpdf/rr274.pdf>.
- Al-Jamal WT, Al-Jamal KT, Bomans PH, Frederik PM, Kostarelos K. 2008. Functionalized-quantum-dot-liposome hybrids as multimodal nanoparticle for cancer. *Small* 4: 1406-1435.
- Alcantara R, Lavela P, Ortiz GF, Tirado JL, Stoyanova R, Zhecheva E, Mateos J. 2004. Modification of petroleum coke for lithium-ion batteries by heat-treatment with iron oxide. *J Electrochem So* 151: A2113-A2119.
- Anderson RGW. 1998. The caveolae membrane system. *Ann Rev Biochem* 67: 199-225.
- Aoyama Y, Kanamori T, Nakai T, Sasaki T, Horiuchi S, Sando S, Niidome T. 2003. Artificial viruses and their application to gene delivery. Size-controlled gene coating with glycocluster nanoparticles. *J Am Chem So* 125: 3455-3457.
- Auffan M, Rose J, Bottero J, Lowry G, Jolivet J, Wiesner M. 2009. Towards a definition of inorganic nanoparticles from an environmental, health and safety perspective. *Nature Nanotech* 4: 634-641.
- Babior BM. 1984. Oxidants from phagocytes - Agents of defense and destruction. *Blood* 64: 959-966.
- Barbe C, Bartlet J, Kong L, Finnie K, Lin H, Larkin M, Callega S, Bush A, Calleja G. 2004. Silica particles: A novel drug delivery system. *Advan Mater* 16: 1959-1966.
- Barnes CA, Elsaesser A, Arkusz J, Smok A, Palus J, Lesniak A, Salvati A, Hanrahan JP, Jong WH, Dziubaltowska E, Stepnik M, Rydzynski K, Mckerr G, Lynch I, Dawson KA, Howard CV. 2008. Reproducible comet assay of amorphous silica nanoparticles detects no genotoxicity. *Nano Lett* 8: 3069-74.
- Barrett EG, Johnston C, Oberdorster G, Finkelstein JN. 1999. Silica-induced chemokine expression in alveolar type II cells is mediated by TNF-alpha-induced oxidant stress. *Am J Physiol* 276: L979-88.
- Beak DG, Basta NT, Scheckel KG, Traina SJ. 2006. Bioaccessibility of arsenic(V) bound to ferrihydrite using a simulated gastrointestinal system. *Environ Sci Technol* 40: 1364-70.

- Beckett WS, Chalupa DF, Pauly-Brown A, Speers DM, Stewart JC, Frampton MW, Utell MJ, Huang LS, Cox C, Zareba W, Oberdorster G. 2005. Comparing inhaled ultrafine versus fine zinc oxide particles in healthy adults: A human inhalation study. *Am J Respir Crit Care Med* 171: 1129-35.
- Bello D, Hart AJ, Ahn K, Hallock M, Yamamoto N, Garcia E, Ellenbecker M, Wardle B. 2008. Particle exposure levels during CVD growth and subsequent handling of vertically-aligned carbon nanotube films. *Carbon* 46: 974-981.
- Berg JM, Ho S, Hwang W, Zebda R, Cummins K, Soriaga M, Taylor R, Guo B, Sayes C. 2010. Internalization of carbon black and maghemite iron oxide nanoparticle mixtures leads to oxidant production. *Chem Res Toxicol* 23: 1874-1992.
- Berg JM, Romoser AR, Banerjee N, Zebda R, Sayes C. 2009. The relationship between pH and zeta potential of ~30 nm metal oxide nanoparticle suspensions relevant to *in vitro* toxicological evaluations. *Nanotoxicology* 3: 276-283.
- Berne BJ, Pecora R. 1976. *Dynamic light scattering*. New York, NY: Wiley & Sons, Inc.
- Bhattacharya K, Davoren M, Boertz J, Schins RP, Hoffmann E, Dopp E. 2009. Titanium dioxide nanoparticles induce oxidative stress and DNA-adduct formation but not DNA-breakage in human lung cells. *Part Fibre Toxicol* 6: 17.
- Bihari P, Vippola M, Schultes S, Praetner M, Khandoga A, Reichel C, Coester C, Toumi T, Rehberg M, Krombach F. 2008. Optimized dispersion of nanoparticles for biological *in vitro* and *in vivo* studies. *Part Fibre Toxicol* 5: 14.
- Boylan AM, Sanan DA, Sheppard D, Broaddus VC. 1995. Vitronectin enhances internalization of crocidolite asbestos by rabbit pleural mesothelial cells via the integrin alpha-v-beta-5. *J Clin Invest* 96: 1987-2001.
- Braydich-Stolle LK, Schaeublin NM, Murdock RC, Jiang J, Biswas P, Schlager JJ, Hussain SM. 2009. Crystal structure mediates mode of cell death in TiO₂ nanotoxicity. *J Nanoparticle Res* 11: 1361-1374.
- Brigger I, Dubernet C, Couvreur P. 2002. Nanoparticles in cancer therapy and diagnosis. *Adv Drug Deliv Rev* 54: 631-651.
- Briggs D, Seah MP 1990. *Practical surface analysis*. Vol. 1, Auger and X-ray photoelectron spectroscopy. Chichester, UK: Wiley & Sons, Inc.
- Bronikowski MJ, Willis P, Colber D, Smith K, Smalley RE. 2001. Gas-phase production of carbon single-walled nanotubes from carbon monoxide via the HiPco process: A parametric study. *J Vac Sci Technol A* 19: 1800-1805.

- Brouwer D, Duuren-Sturman V, Berges M, Jankowska E, Bard D, Mark D. 2009. From workplace air measurement results toward estimates of exposure? Development of a strategy to assess exposure to manufactured nano-objects. *J Nanopart Res* 11: 1867-1881.
- Brown D, Stone V, Findlay P. 1999. Increased inflammation and intracellular calcium caused by ultrafine carbon black is independent of transition metals or other soluble components. *Occup Environ Med* 57: 85-91.
- Brown DM, Stone V, Findlay P, Macnee W, Donaldson K. 2000. Increased inflammation and intracellular calcium caused by ultrafine carbon black is independent of transition metals or other soluble components. *Occup Environ Med* 57: 685-91.
- Brown DM, Wilson MR, Macnee W, Stone V, Donaldson K. 2001. Size-dependent proinflammatory effects of ultrafine polystyrene particles: A role for surface area and oxidative stress in the enhanced activity of ultrafines. *Toxicol Appl Pharm* 175: 191-199.
- Brunauer S, Emmett PH, Teller E. 1938. Adsorption of gases in multimolecular layers. *J Am Chem Soc* 60: 309-319.
- Brunner T, Wick P, Manser P, Spohn P, Grass RN, Limbach LK, Bruinink A, Stark WJ. 2006. *In vitro* cytotoxicity of oxide nanoparticles: Comparison to asbestos, silica, and the effects of particle solubility. *Environ Sci Tech* 40: 3474-4381.
- Bulushev DA, Kiwi-Minsker L, Yuranov I, Suvorova EI, Buffat PA, Renken A. 2002. Structured Au/FeOX/C catalysts for low-temperature CO oxidation. *Catalysis* 210: 149-159.
- Cael V, Van Der Heyden A, Champmartin D, Barzyk W, Rubini P, Rogalska E. 2003. Interfacial approach to aluminum toxicity: Interactions of Al(III) and Pr(III) with model phospholipid bilayer and monolayer membranes. *Langmuir* 19: 8697-8708.
- Canas-Ventura ME, Klappenberger F, Clair S, Pons S, Kern K, Brune H, Strunskus T, Woll C, Fasel R, Barth JV. 2006. Coexistence of one- and two-dimensional supramolecular assemblies of terephthalic acid on Pd(111) due to self-limiting deprotonation. *J Chem Phys* 125: 184710-8.
- Carp O, Huisman C, Reller A. 2004. Photoinduced reactivity of titanium dioxide. *Prog Solid State Chem* 32: 33-177.

- Cass GR, Hughes LA, Bhawe P, Kleeman MJ, Allen JO, Salmon LG. 2000. The chemical composition of atmospheric ultrafine particles. *Philos Trans Roy Soc Lond Ser A-Math Phys Engin Sci* 358: 2581-2592.
- Chang JS, Chang KLB, Hwang DF, Kong ZL. 2007. *In vitro* cytotoxicity of silica nanoparticles at high concentrations strongly depends on the metabolic activity type of the cell line. *Environ Sci Tech* 41: 2064-2068.
- Chen C, Daniel MC, Quinkert ZT, De M, Stein B, Bowman VD, Chipman PR, Rotello VM, Kao CC, Dragnea B. 2006. Nanoparticle-templated assembly of viral protein cages. *Nano Lett* 6: 611-615.
- Chen C, Kwak ES, Stein B, Kao CC, Dragnea B. 2005. Packaging of gold particles in viral capsids. *J Nanosci Nanotech* 5: 2029-2033.
- Cheng XM, Kan AT, Tompson MB. 2004. Naphthalene adsorption and desorption from aqueous C₆₀ fullerene. *J Chem Eng Data* 49: 675-683.
- Chithrani BD, Ghazani AA, Chan WCW. 2006. Determining the size and shape dependence of gold nanoparticle uptake into mammalian cells. *Nano Lett* 6: 662-668.
- Choquenot B, Couteau C, Papisaris E, Coiffard L. 2008. Quercetin and rutin as potential sunscreen agents: Determination of efficacy by an *in vitro* model. *J Nat Prod* 71: 1117-1118.
- Dadosh T. 2009. Synthesis of uniform silver nanoparticles with a controllable size. *Mater Lett* 63: 2236-2238.
- Dai R. 2010. IBISWorld Industry Report 54171 Scientific Research & Development in the US. Santa Monica, CA: IBISWorld Inc.
- Damke H, Baba T, Warnock DE, Schmid SL. 1994. Induction of mutant dynamin specifically blocks endocytic coated vesicle formation. *J Cell Biol* 127: 915-934.
- Dausend J, Musyanovych A, Dass M, Walther P, Schrezenmeier H, Landfester K, Mailander V. 2008. Uptake mechanism of oppositely charged fluorescent nanoparticles in HeLa cells. *Macromol Biosci* 8: 1135-43.
- Davada J, Labhasetwar V. 2002. Characterization of nanoparticle uptake by endothelial cells. *Internat J Pharm* 233: 51-59.
- Demou E, Peter P, Hellweg S. 2008. Exposure to manufactured nanostructured particles in an industrial pilot plant. *Ann Occup Hyg* 52: 695-706.

- Demou E, Stark W, Hellweg S. 2009. Particle emission and exposure during nanoparticle synthesis in research laboratories. *Ann Occup Hyg* 52: 829-838.
- Diaz-Griffero F, Hoschander SA, Brojatsch J. 2002. Endocytosis is a critical step in entry of subgroup B avian leukosis viruses. *J Virol* 76: 12866-76.
- Dockery DW, Pope CA, 3rd, Xu X, Spengler JD, Ware JH, Fay ME, Ferris BG, Jr., Speizer FE. 1993. An association between air pollution and mortality in six U.S. cities. *N Engl J Med* 329: 1753-9.
- Donaldson K, Borm PJA. 1998. The quartz hazard: A variable entity. *Ann Occup Hyg* 42: 287-294.
- Donaldson K, Brown D, Clouter A, Duffin R, Macnee W, Renwick L, Tran L, Stone V. 2002. The pulmonary toxicology of ultrafine particles. *J Aerosol Med* 15: 213-20.
- Donaldson K, Brown DM, Mitchell C, Dineva M, Beswick PH, Gilmour P, Macnee W. 1997. Free radical activity of PM10: Iron-mediated generation of hydroxyl radicals. *Environ Health Perspect* 105: 1285-1289.
- Donaldson K, Macnee W. 2003. Potential mechanisms of adverse pulmonary and cardiovascular effects of particulate air pollution (PM10). *Internat J Hyg Environmen Health* 203: 377-495.
- Donaldson K, Stone V, Clouter A, Renwick L, Macnee W. 2001. Ultrafine particles. *Occup Environ Med* 58: 211-216.
- Dreher KL, Jaskot RH, Lehmann JR, Richards JH, Mcgee JK, Ghio AJ, Costa DL. 1997. Soluble transition metals mediate residual oil fly ash induced acute lung injury. *J Toxicol Environ Health* 50: 285-305.
- Driscoll KE, Carter JM, Howard BW, Hassenbein D, Janssen YM, Mossman BT. 2002. Crocidolite activated NF-kB and MIP-2 gene expression in rat alveolar epithelial cells: Role of mitochondrial derived oxidants. *Environ Health Perspect* 106: 1171-1174.
- Eom HJ, Choi J. 2009. Oxidative stress of CeO₂ nanoparticles via p38-Nrf-2 signaling pathway in human bronchial epithelial cell, Beas-2B. *Toxicol Lett* 187: 77-83.
- Estrade-Szwarckopf H. 2004. XPS photoemission in carbonaceous materials: A "defect" peak beside the graphitic asymmetric peak. *Carbon* 42: 1713-1721.
- Fairley N, Carrick A, Fairly N 2005. *The Casa cookbook : Pt. 1: Recipes for XPS data processing*. Knutsford, UK: Acolyte Science.

- Farber JL. 1994. Mechanisms of cell injury by activated oxygen species. *Environ Health Perspect* 102: 17-24.
- Fenart L, Casanova A, Dehouck B, Duhem C, Slupek S, Cecchelli R, Betbeder D. 1999. Evaluation of effect of charge and lipid coating on ability of 60-nm nanoparticles to cross an *in vitro* model of the blood-brain barrier. *J Pharm Exper Ther* 291: 1017-1022.
- Fenion HJ. 1894. Oxidation of tartaric acid in the presence of iron. *J. Chem. So.* 65: 899-910.
- Feron VJ, Arts JH, Kuper CF, Slootweg PJ, Woutersen RA. 2001. Health risks associated with inhaled nasal toxicants. *Crit Rev Toxicol* 31: 313-47.
- Ferrari M. 2008. Nanogeometry: Beyond drug delivery. *Nat Nanotechnol* 3: 131-2.
- Feynman. 1992. There's plenty of room at the bottom. *J Microelectromech Sys* 1: 60-66.
- Fichthorn KA, Qin Y. 2008. Molecular dynamics simulation of the forces between colloidal nanoparticles in Lennard-Jones and n-decane solvent. *Gran Matt* 10: 105-111.
- Foley S, Crowley C, Smaih M, Bonfils C, Erlanger BF, Seta P, Larroque C. 2002. Cellular localisation of a water-soluble fullerene derivative. *Biochem Biophys Res Comm* 294: 116-119.
- Foucaud L, Wilson MR, Brown DM, Stone V. 2007. Measurement of reactive species production by nanoparticles prepared in biologically relevant media. *Toxicol Lett* 174: 1-9.
- Franklin NM, Rogers NJ, Apte SC, Batley GE, Gadd GE, Casey PS. 2007. Comparative toxicity of nanoparticulate ZnO, bulk ZnO, and ZnCl to a freshwater microalga (*Pseudokirchneriella subcapitata*): The importance of particle solubility. *Environ Sci Techn* 41: 8484-8490.
- Fu RW, Zeng HM, Lu Y. 1993. The reduction property of activated carbon-fibers. *Carbon* 31: 1089-1094.
- Fubini B, Giamello E, Volante M, Bolis V. 1990. Chemical functionalities at the silica surface determinint its reactivity when inhaled. Formation and reactivity of surface radicals. *Toxicol Ind Health* 6: 571-598.
- Fubini B, Hubbard A. 2003. Reactive oxygen species (ROS) and reactive nitrogen species (RNS) generation by silica in inflammation and fibrosis. *Free Rad Biol Med* 34: 1507-1516.

- Fujitani Y, Kobayashi T, Arashidani K, Kunugita N, Suemura K. 2008. Measurement of the physical properties of aerosols in a fullerene factory for inhalation exposure assessment. *J Occup Environ Hyg* 5: 380-9.
- Gao H, Shi W, Freund LB. 2005. Mechanics of receptor-mediated endocytosis. *Proc Natl Acad Sci U S A* 102: 9469-74.
- Gatti AM, Tossini D, Gambarelli A, Montanari S, Capitani F. 2009. Investigation of the presence of inorganic micro- and nanosized contaminants in bread and biscuits by environmental scanning electron microscopy. *Crit Rev Food Sci Nutr* 49: 275-82.
- Geiser M, Rothen-Rutishauser B, Kapp N, Schurch S, Kreyling W, Schulz H, Semmler M, Hof VI, Heyder J, Gehr P. 2005. Ultrafine particles cross cellular membranes by nonphagocytic mechanisms in lungs and in cultured cells. *Environ Health Perspect* 113: 1555-1560.
- Gomes A, Fernandes E, Lima JLFC. 2005. Fluorescence probes used for detection of reactive oxygen species. *J Biochem Biophys Meth* 65: 45-80.
- Gould GW, Lippincott-Schwartz J. 2009. New roles for endosomes: From vesicular carriers to multi-purpose platforms. *Nat Rev Mol Cell Bio* 10: 287-292.
- Griffiths SM, Singh N, Jenkins GJS, Williams PM, Orbaek AW, Barron AR, Wright CJ, Doak SH. 2011. Dextran coated ultrafine superparamagnetic iron oxide nanoparticles: Compatibility with common fluorometric and colorimetric dyes. *Anal Chem* 83: 3778-3785.
- Guo B, Kennedy IM. 2007. Gas-phase flame synthesis and characterization of iron oxide nanoparticles for use in a health effects study. *Aerosol Sci Tech* 41: 944-951.
- Guo B, Zebda R, Drake SJ, Sayes CM. 2009. Synergistic effect of co-exposure to carbon black and Fe₂O₃ nanoparticles on oxidative stress in cultured lung epithelial cells. *Part Fibre Toxicol* 6: 4.
- Hakim LF, Blackson JH, Weimer AW. 2007. Modification of interparticle forces for nanoparticles using atomic layer deposition. *Chem Eng Sci* 62: 6199-6211.
- Han JH, Lee EJ, Lee JH, So KP, Lee YH, Bae GN, Lee SB, Ji JH, Cho MH, Yu IJ. 2008. Monitoring multiwalled carbon nanotube exposure in carbon nanotube research facility. *Inhal Toxicol* 20: 741-9.
- Handy RD, Owen R, Valsami-Jones E. 2008. The ecotoxicology of nanoparticles and nanomaterials: Current status, knowledge gaps, challenges, and future needs. *Ecotoxicology* 17: 315-325.

- Harush-Frenkel O, Rozentur E, Benita S, Altschuler Y. 2008. Surface charge of nanoparticles determines their endocytic and transcytotic pathway in polarized MDCK cells. *Biomacromolecules* 9: 435-43.
- Hediger MA. 1997. Membrane permeability. The diversity of transmembrane transport processes. *Curr Opin Cell Biol* 9: 543-6.
- Heffner JE, Repine JE. 1989. Pulmonary strategies of antioxidant defense. *Am Rev Respir Dis* 140: 531-554.
- Hens SC, Cunningham G, Tyler T, Moseenkov S, Kuznetsov V, Shenderova O. 2008. Nanodiamond bioconjugate probes and their collection by electrophoresis. *Dia Rel Mater* 17: 1858-1866.
- Hexsel CL, Bangert SD, Herbert AA, Lim HW. 2008. Current sunscreen issues: 2007 Food and Drug Administration sunscreen labelling recommendations and combination sunscreen/insect repellent products. *J Am Acad Dermatol* 59: 316-323.
- Ho CM, Yau SKW, Lok CN, So MH, Che CM. 2010. Oxidative dissolution of silver nanoparticles by biologically relevant oxidants: A kinetic and mechanistic study. *Chem Asian J* 5: 285-293.
- Huang XL, Bronstein LM, Retrum J, Dufort C, Tsvetkova I, Aniagyei S, Stein B, Stucky G, Mckenna B, Remmes N, Baxter D, Kao CC, Dragnea B. 2007. Self-assembled virus-like particles with magnetic cores. *Nano Lett* 7: 2407-2416.
- Hubbard AK, Timblin CR, Shukla A, Rincon M, Mossman BT. 2002. Activation of NF-kappaB-dependent gene expression by silica in lungs of luciferase reporter mice. *Am J Physiol Lung Cell Mol Physiol* 282: L968-75.
- Hwang Y, Lee JK, Lee JK, Jeong YM, Cheong SI, Ahn YC, Kim SH. 2008. Production and dispersion stability of nanoparticles in nanofluids. *Powder Tech* 186: 145-153.
- IARC. 1997. IARC Working Group on the Evaluation of Carcinogenic Risks to Humans: Silica, some silicates, coal dusts and paraaramid fibrils. *IAEC Monogr Eval Carcinog Risks Hum* 68: 1-202.
- Inoue K, Takano H, Yanagisawa R, Hirano S, Sakurai M, Shimada A, Yoshikawa T. 2006. Effects of airway exposure to nanoparticles on lung inflammation induced by bacterial endotoxin in mice. *Environ Health Perspect* 114: 1325-30.

- Ishii T, Itoh K, Takahashi S, Sato H, Yanagawa T, Katoh Y, Bannai S, Yamamoto M. 2000. Transcription factor Nrf2 coordinately regulates a group of oxidative stress-inducible genes in macrophages. *J Biol Chem* 275: 16023-16029.
- Itoh K, Chiba T, Takahashi S, Ishii T, Igarashi K, Katoh Y, Oyake T, Hayashi N, Satoh K, Hatayama I, Yamamoto M, Nabeshima Y. 1997. An Nrf2 small Maf heterodimer mediates the induction of phase II detoxifying enzyme genes through antioxidant response elements. *Biochem Biophys Res Com* 236: 313-322.
- Itoh K, Wakabayashi N, Katoh Y, Ishii T, Igarashi K, Engel JD, Yamamoto M. 1999. Keap1 represses nuclear activation of antioxidant responsive elements by Nrf2 through binding to the amino-terminal Neh2 domain. *Genes Develop* 13: 76-86.
- Jaiswal AK. 2004. Nrf2 signaling in coordinated activation of antioxidant gene expression. *Free Rad Biol Med* 36: 1199-1207.
- Jarvinen K, Pietarinen-Runtti P, Linnainmaa K, Raivia K, Krejsa C, Kavanagh T, Kinnula V. 2000. Antioxidant defense mechanisms of human mesothelioma and lung adenocarcinoma cells. *Am J Physiol Lung Cell Mol Physiol* L696-L702.
- Jiang J, Oberdorster G, Elder A, Gelein R, Mercer P, Biswas P. 2008a. Does nanoparticle activity depend upon size and crystal phase? *Nanotoxicology* 2: 33-42.
- Jiang W, Kim BY, Rutka JT, Chan WC. 2008b. Nanoparticle-mediated cellular response is size-dependent. *Nat Nanotechnol* 3: 145-50.
- Johnston CJ, Driscoll KE, Finkelstein JN, Baggs R, O'reilly MA, Carter J, Gelein R, Oberdorster G. 2000. Pulmonary chemokine and mutagenic responses in rats after subchronic inhalation of amorphous and crystalline silica. *Toxicol Sci* 56: 405-13.
- Kaewamatawong T, Kawamura N, Okajima M, Sawada M, Morita T, Shimada A. 2005. Acute pulmonary toxicity caused by exposure to colloidal silica: Particle size dependent pathological changes in mice. *Toxicol Path* 33: 745-751.
- Kanaras AG, Kamounah FS, Schaumburg K, Kiely CJ, Brust M. 2002. Thioalkylated tetraethylene glycol: A new ligand for water soluble monolayer protected gold clusters. *Chem Commun* 20: 2294-5.
- Karakoti AS, Hench LL, Seal S. 2006. The potential toxicity of nanomaterials - The role of surfaces. *J Med* 58: 77-82.

- Kemp SJ, Thorley AJ, Gorelik J, Seckl MJ, O'hare MJ, Arcaro A, Korchev Y, Goldstraw P, Tetley TD. 2008. Immortalization of human alveolar epithelial cells to investigate nanoparticle uptake. *Am J Resp Cell and Mole Biol* 39: 591-597.
- Kensler TW, Wakabayashi N. 2010. Nrf2: Friend or foe for chemoprevention? *Carcinogenesis* 31: 90-99.
- Kim JS, Yoon TJ, Yu KN, Noh MS, Woo M, Kim BG, Lee KH, Sohn BH, Park SB, Lee JK, Cho MH. 2006. Cellular uptake of magnetic nanoparticle is mediated through energy-dependent endocytosis in A549 cells. *J Vet Sci* 7: 321-6.
- Klaassen C, Watkins J. 2003. Casarett & Doull's essentials of toxicology. New York, NY: The McGraw-Hill Companies, Inc.
- Kode A, Rajendrasozhan S, Caito S, Yang SR, Megson IL, Rahman I. 2008. Resveratrol induces glutathione synthesis by activation of Nrf2 and protects against cigarette smoke-mediated oxidative stress in human lung epithelial cells. *Am J Physiol Lung Cell Mol Physiol* 294: L478-88.
- Kreyling WG, Semmler M, Erbe F, Mayer P, Takenaka S, Schulz H, Oberdorster G, Ziesenis A. 2002. Translocation of ultrafine insoluble iridium particles from lung epithelium to extrapulmonary organs is size dependent but very low. *J Toxicol Environ Health A* 65: 1513-1530.
- Kuhlbusch T, Neumann S, Fissan H. 2010. Number size distribution, mass concentration, and particule composition of PM1, PM2.5, and PM10 in bag filling areas of carbon black production. *J Occup Environ Hyg* 1: 660-671.
- Kuhlbusch TA, Fissan H. 2006. Particle characteristics in the reactor and pelletizing areas of carbon black production. *J Occup Environ Hyg* 3: 558-67.
- Kung KH, McBride MB. 1988. Electron transfer processes between hydroquinone and iron oxides. *Clays Clay Miner* 36: 303-309.
- Lamb FS, Moreland JG, Miller FJ. 2009. Electrophysiology of reactive oxygen production in signaling endosomes. *Antioxid Redox Sig* 11: 1335-1347.
- Lee PC, Meisel D. 1982. Adsorption and surface-enhanced raman of dyes on silver and gold sols. *J Phy Chem* 86: 3391-3395.
- Levy R, Thanh NTK, Doty RC, Hussain I, Nichols RJ, Schiffrin DJ, Brust M, Fernig DG. 2004. Rational and combinatorial design of peptide capping ligands for gold nanoparticles. *J Am Chem So* 126: 10076-10084.

- Li CQ, Kim MY, Godoy LC, Thiantanawat A, Trudel LJ, Wogan GN. 2009. Nitric oxide activation of Keap1/Nrf2 signaling in human colon carcinoma cells. *Proc Natl Acad Sci U S A* 106: 14547-14551.
- Li JJ, Oberley LW, Stclair DK, Ridnour LA, Oberley TD. 1995. Phenotypic changes induced in human breast-cancer cells by overexpression of manganese-containing superoxide-dismutase. *Oncogene* 10: 1989-2000.
- Li M, Hong Z, Fang Y, Huang F. 2008a. Synergistic effect of two surface complexes in enhancing visible-light photocatalytic activity of titanium dioxide. *Mat Res Bull* 43: 2179-2186.
- Li N, Alam J, Venkatesan M, Eiguren-Fernandez A, Schmitz D, Stefano E, Miguel A, Cho A, Sioutas C, Nel A. 2004. Nrf2 is a key transcription factor that regulated antioxidant defense in macrophages and epithelial cells: Protecting against the proinflammatory and oxidizing effects of diesel exhaust chemicals. *J Immunol* 173: 3467-3481.
- Li N, Sioutas C, Cho A, Schmitz D, Misra C, Sempf J, Wang M, Oberley T, Froines J, Nel A. 2003. Ultrafine particulate pollutants induce oxidative stress and mitochondrial damage. *Environ Health Perspect* 111: 455-460.
- Li S, Zhu R, Xue M, Sun X, Yao S, Wang S. 2008b. Nanotoxicity of TiO₂ nanoparticles to erythrocyte *in vitro*. *Food Chem Toxicol* 46: 3525-3531.
- Li W, Chen CY, Ye C, Wei TT, Zhao YL, Lao F, Chen Z, Meng H, Gao YX, Yuan H, Xing GM, Zhao F, Chai ZF, Zhang XJ, Yang FY, Han D, Tang XH, Zhang YG. 2008c. The translocation of fullerene nanoparticles into lysosome via the pathway of clathrin-mediated endocytosis. *Nanotechnology* 19:0957-4484. doi. 10.1088/0957-4484/19/14/145102.
- Li XY, Brown D, Smith S, Macnee W, Donaldson K. 1999. Short-term inflammatory responses following intratracheal instillation of fine and ultrafine carbon black in rats. *Inhal Toxicol* 11: 709-731.
- Li XY, Gilmour PS, Donaldson K, Macnee W. 1996. Free radical activity and pro-inflammatory effects of particulate air pollution (PM(10)) *in vivo* and *in vitro*. *Thorax* 51: 1216-1222.
- Limbach LK, Wick P, Manser P, Grass RN, Bruinink A, Stark WJ. 2007. Exposure of engineered nanoparticles to human lung epithelial cells: Influence of chemical composition and catalytic activity on oxidative stress. *Environ Sci Tech* 41: 4158-4163.

- Lin W, Huang Y, Zhou X, Ma Y. 2006. *In vitro* toxicity of silica nanoparticles in human lung cancer cells. *Toxicol App Pharm* 217: 252-259.
- Lockman PR, Koziara JM, Mumper RJ, Allen D. 2004. Nanoparticle surface charges alter blood-brain barrier integrity and permeability. *J Drug Target* 12: 635-641.
- Long TC, Saleh N, Tilton RD, Lowry GV, Veronesi B. 2006. Titanium dioxide (P25) produces reactive oxygen species in immortalized brain microglia (BV2): implications for nanoparticle neurotoxicity. *Environ Sci Technol* 40: 4346-52.
- Lundqvist M, Stigler J, Elia G, Lynch I, Cedervall T, Dawson KA. 2008. Nanoparticle size and surface properties determine the protein corona with possible implications for biological impacts. *Proc Natl Acad Sci U S A* 105: 14265-70.
- Maioli E, Torricelli C, Carlucci F, Tommassini V, Pacine A. 2009. Critical appraisal of the MTT assay in the presence of rottlerin and uncouplers. *Biol Proced Online* 11: 227-240.
- Malvern Instruments. 2008. Electrophoretic light scattering overview. Worchestershire, UK. Malvern Instruments Technical Support Library
- Manna SK, Sarkar S, Barr J, Wise K, Barrera EV, Jejelowo O, Rice-Ficht AC, Ramesh GT. 2005. Single-walled carbon nanotube induces oxidative stress and activates nuclear transcription factor-kappa B in human keratinocytes. *Nano Letters* 5: 1676-1684.
- Martindale JL, Holbrook NJ. 2002. Cellular response to oxidative stress: Signaling for suicide and survival. *J Cell Phys* 192: 1-15.
- Martirosyan KS, Chang L, Rantschler J, Khizroev S, Luss D, Litvinov D. 2007. Carbon combustion synthesis and magnetic properties of cobalt ferrite nanoparticles. *Ieee Trans Magnet* 43: 3118-3120.
- Mayer A, Vadon M, Rinner B, Novak A, Wintersteiger R, Frohlich E. 2009. The role of nanoparticle size in hemocompatibility. *Toxicology* 258: 139-147.
- Maynard AD, Baron PA, Foley M, Shvedova AA, Kisin ER, Castranova V. 2004. Exposure to carbon nanotube material: Aerosol release during the handling of unrefined single-walled carbon nanotube material. *J Toxicol Environ Health A* 67: 87-107.
- Maynard AD, Zimmer AT. 2002. Evaluation of grinding aerosols in terms of alveolar dose: the significance of using mass, surface area and number metrics. *Ann Occup Hyg* 46: 315-319.

- McClure MO, Sommerfelt MA, Marsh M, Weiss RA. 1990. The pH independence of mammalian retrovirus infection. *J Gen Virol* 71 (Pt 4): 767-73.
- Mcgrath-Morrow SA, Stahl J. 2002. Inhibition of glutamine synthetase in A549 cells during hyperoxia. *Am J Respir Cell Mol Biol* 27: 99-106.
- Mclaughlin JK, Chow WH, Levy LS. 1997. Amorphous silica: A review of health effects from inhalation exposure with particular reference to cancer. *J Toxicol Environ Health* 50: 553-66.
- McMahon M, Itoh K, Yamamoto M, Hayes JD. 2003. Keap1-dependent proteasomal degradation of transcription factor Nrf2 contributes to the negative regulation of antioxidant response element-driven gene expression. *J Biol Chem* 278: 21592-21600.
- Mceil S. 2005. Nanotechnology for the biologist. *J Leuko Biol* 78: 585-594.
- Methner M, Hodson L, Dames A, Geraci C. 2010a. Nanoparticle Emission Assessment Technique (NEAT) for the identification and measurement of potential inhalation exposure to engineered nanomaterials--Part B: Results from 12 field studies. *J Occup Environ Hyg* 7: 163-76.
- Methner M, Hodson L, Geraci C. 2010b. Nanoparticle emission assessment technique (NEAT) for the identification and measurement of potential inhalation exposure to engineered nanomaterials--Part A. *J Occup Environ Hyg* 7: 127-32.
- Miller FJ, Filali M, Huss GJ, Stanic B, Chamseddine A, Barna TJ, Lamb FS. 2007. Cytokine activation of nuclear factor kappa B in vascular smooth muscle cells requires signaling endosomes containing Nox1 and CIC-3. *Circulation Res* 101: 663-671.
- Min YJ, Akbulut M, Kristiansen K, Golan Y, Israelachvili J. 2008. The role of interparticle and external forces in nanoparticle assembly. *Nat Mater* 7: 527-538.
- Mosmann T. 1983. Rapid colorimetric assay for cellular growth and survival: Application to proliferation and cytotoxicity assays. *J Immunol Methods* 65: 55-63.
- Murdock RC, Braydich-Stolle L, Schrand AM, Schlager JJ, Hussain SM. 2008. Characterization of nanomaterial dispersion in solution prior to *in vitro* exposure using dynamic light scattering technique. *Toxicol Sci* 101: 239-253.
- Murray AR, Kisin E, Leonard SS, Young SH, Kommineni C, Kagan VE, Castranova V, Shvedova AA. 2009. Oxidative stress and inflammatory response in dermal toxicity of single-walled carbon nanotubes. *Toxicology* 257: 161-71.

- Nabiev I, Mitchell S, Davies A, Williams Y, Kelleher D, Moore R, Gun'ko Y, Bryne S, Rakovich Y, Donegan J, Sukhanova A, Conroy J, Cottell D, Gaponik N, Rogach A, Volkov Y. 2007. Nonfunctionalized nanocrystals can exploit a cell's active transport machinery delivering them to specific nuclear and cytoplasmic compartments. *Nano Lett* 7: 3452-3461.
- Nakai T, Kanamori T, Sando S, Aoyama Y. 2003. Remarkably size-regulated cell invasion by artificial viruses. Saccharide-dependent self-aggregation of glycoviruses and its consequences in glycoviral gene delivery. *J Am Chem Soc* 125: 8465-75.
- Nan A, Bai X, Son SJ, Lee SB, Ghandehari H. 2008. Cellular uptake and cytotoxicity of silica nanotubes. *Nano Lett* 8: 2150-4.
- Nanotechproject. 2011. The project on emerging nanotechnologies. Accessed May 2011 from the website: <http://www.nanotechproject.org/inventories/consumer/>.
- Nativo P, Prior IA, Brust M. 2008. Uptake and intracellular fate of surface-modified gold nanoparticles. *Am Chem So Nano* 2: 1639-1644.
- Nel A, Xia T, Madler L, Li N. 2006. Toxic potential of materials at the nanolevel. *Science* 311: 622-627.
- Nemmar A, Hoylaerts MF, Hoet PHM, Vermeylen J, Nemery B. 2003. Size effect of intratracheally instilled particles on pulmonary inflammation and vascular thrombosis. *Toxicol App Pharm* 186: 38-45.
- Niu J, Azfer A, Rogers LM, Wang X, Kolattukudy PE. 2007. Cardioprotective effects of cerium oxide nanoparticles in a transgenic murine model of cardiomyopathy. *Cardiovasc Res* 73: 549-59.
- National Science and Technology Council. 2011. National nanotechnology initiative strateic plan. Accessed May 2011 from the website: http://www.nano.gov/sites/default/files/pub_resource/2011_strategic_plan.pdf
- Oberdorster E. 2004. Manufactured nanomaterials (fullerenes, C60) induce oxidative stress in the brain of juvenile largemouth bass. *Environ Health Perspect* 112: 1058-62.
- Oberdorster G. 1995. Lung particle overload - implications for occupational exposures to particles. *Regul Toxicol Pharm* 21: 123-135.
- Oberdorster G. 2001. Pulmonary effects of inhaled ultrafine particles. *Int Arch Occup Environ Health* 74: 1-8.

- Oberdorster G. 2007. Nanoparticles and the brain: Cause for concern? *Amino Acids* 33: 28.
- Oberdorster G, Oberdorster E, Oberdorster J. 2005. Nanotoxicology: An emerging discipline evolving from studies of ultrafine particles. *Environ Health Perspect* 113: 823-839.
- Oberdorster G, Sharp Z, Atudorei V, Elder A, Gelein R, Kreyling W, Cox C. 2004. Translocation of inhaled ultrafine particles to the brain. *Inhal Toxicol* 16: 437-445.
- Oberdorster G, Sharp Z, Atudorei V, Elder A, Gelein R, Lunts A, Kreyling W, Cox C. 2002. Extrapulmonary translocation of ultrafine carbon particles following whole-body inhalation exposure of rats. *J Toxicol Environ Health A* 65: 1531-1543.
- Oberley LW, Bize IB, Sahu SK, Chanleuthauser SWH, Gruber HE. 1978. Superoxide-dismutase activity of normal murine liver, regenerating liver, and H6-hepatoma. *J Nat Cancer Ins* 61: 375-379.
- Oberley LW, Buettner GR. 1979. Role of superoxide-dismutase in cancer - Review. *Cancer Res* 39: 1141-1149.
- Osaki F, Kanamori T, Sando S, Sera T, Aoyama Y. 2004. A quantum dot conjugated sugar ball and its cellular uptake. On the size effects of endocytosis in the subviral region. *J Am Chem Soc* 126: 6520-1.
- Ovrevik J, Refsnes M, Namork E, Becher R, Sandnes D, Schwarze PE, Lag M. 2006. Mechanisms of silica-induced IL-8 release from A549 cells: Initial kinase-activation does not require EGFR activation or particle uptake. *Toxicology* 227: 105-16.
- Panessa-Warren BJ, Warren JB, Maye MM, Van Der Lelie D, Gang O, Wong SS, Ghebrehiwet B, Tortora GT, Misewich JA. 2008. Human epithelial cell processing of carbon and gold nanoparticles. *Internat J Nanotech* 5: 55-91.
- Park EJ, Park K. 2009. Oxidative stress and pro-inflammatory responses induced by silica nanoparticles *in vivo* and *in vitro*. *Toxicol Lett* 184: 18-25.
- Park J, Kwak B, Bae E, Lee J, Kim Y, Choi K, Yi J. 2009. Characterization of exposure to silver nanoparticles in a manufacturing facility. *J Nanopart Res* 11: 1705-1712.
- Pauluhn J. 2009. Pulmonary toxicity and fate of agglomerated 10 and 40 nm aluminum oxyhydroxides following 4-week inhalation exposure of rats: Toxic effects are determined by agglomerated, not primary particle size. *Toxicol Sci* 109: 152-167.

- Peters TM, Elzey S, Johnson R, Park H, Grassian VH, Maher T, O'shaughnessy P. 2009. Airborne monitoring to distinguish engineered nanomaterials from incidental particles for environmental health and safety. *J Occup Environ Hyg* 6: 73-81.
- Popat RP, Sutherland I, Sheng E-S. 1995. Vapour-phase chemical derivatisation for the determination of surface functional groups by X-ray photoelectron spectroscopy. *J Materials Chem* 5: 713-717.
- Porter D, Sriram K, Wolfarth M, Jefferson A, Schwegler-Berry D, Andrew M, Castranova V. 2008. A biocompatible medium for nanoparticle dispersion. *Nanotoxicology* 2: 144-154.
- Pratt PC. 1983. Lung dust content and response in guinea-pigs inhaling 3 forms of silica. *Arch Environ Health* 38: 197-204.
- Prester T, Zhang YS, Spencer SR, Wilczak CA, Talalay P. 1993. The electrophile counterattack response - Protection against neoplasia and toxicity. *Adv Enzyme Regul* 33: 281-296.
- Provenzale JM, Silva GA. 2009. Uses of nanoparticles for central nervous system imaging and therapy. *Am J Neuroradiol* 30: 1293-301.
- Puhakka A, Ollikainen T, Soini Y, Kahlos K, Saily M, Koistinen P, Paakko P, Linnainmaa K, Kinnula VL. 2002. Modulation of DNA single-strand breaks by intracellular glutathione in human lung cells exposed to asbestos fibers. *Mutat Res-Genetic Toxicol Environ Mutagen* 514: 7-17.
- Qaddoumi MG, Gukasyan HJ, Davda J, Labhasetwar V, Kim KJ, Lee VH. 2003. Clathrin and caveolin-1 expression in primary pigmented rabbit conjunctival epithelial cells: role in PLGA nanoparticle endocytosis. *Mol Vis* 9: 559-68.
- Qaddoumi MG, Ueda H, Yang J, Davda J, Labhasetwar V, Lee VHL. 2004. The characteristics and mechanisms of uptake of PLGA nanoparticles in rabbit conjunctival epithelial cell layers. *Pharm Res* 21: 641-648.
- Quinlan TR, Marsh JP, Janssen YM, Borm PJA, Mossman BT. 1994. Oxygen radicals and asbestos-mediated disease. *Environ Health Perspect* 102: 107-110.
- Rajh T, Nedeljkovic JM, Chen LX, Poluktov O, Thurnauer MC. 1999. Improving optical and charge separation properties of nanocrystalline TiO₂ by surface modification with vitamin C. *J Phy Chem B* 103: 3515-3519.
- Rancan F, Rosan S, Boehm F, Cantrell A, Brellreich M, Schoenberger H, Hirsch A, Moussa F. 2002. Cytotoxicity and photocytotoxicity of a dendritic C-60 mono-

- adduct and a malonic acid C-60 tris-adduct on Jurkat cells. *J Photochem Photobiol B-Biol* 67: 157-162.
- Rao VA, Klein SR, Bonar SJ, Zielonka J, Mizuno N, Dickey JS, Keller PW, Joseph J, Kalyanaraman B, Shacter E. 2010. The antioxidant transcription factor Nrf2 negatively regulates autophagy and growth arrest induced by the anticancer redox agent mitomycin. *J Biol Chem* 285: 34447-34459.
- Rauen U, Petrat F, Sustmann R, De Groot H. 2004. Iron-induced mitochondrial permeability transition in cultured hepatocytes. *J Hepatol* 40: 607-15.
- Reeves JF, Davies SJ, Dodd NJ, Jha AN. 2008. Hydroxyl radicals (*OH) are associated with titanium dioxide (TiO₂) nanoparticle-induced cytotoxicity and oxidative DNA damage in fish cells. *Mutat Res* 640: 113-22.
- Renwick LC, Donaldson K, Clouter A. 2001. Impairment of alveolar macrophage phagocytosis by ultrafine particles. *Toxicol App Pharm* 172: 119-127.
- Reynolds ES. 1963. The use of lead citrate at high pH as an electron-opaque stain in electron microscopy. *J Cell Bio* 17: 208-212.
- Richardson A. 2010. IBISWorld Industry Report 42295 Paint Wholesaling in the US. Santa Monica, CA: IBISWorld Inc.
- Rodal SK, Skretting G, Garred O, Vilhardt F, Van Deurs B, Sandvig K. 1999. Extraction of cholesterol with methyl-beta-cyclodextrin perturbs formation of clathrin-coated endocytic vesicles. *Mol Biol Cell* 10: 961-974.
- Rodriguez R, Basta N, Casteel S, Pace L. 1999. An *in vitro* gastrointestinal method to estimate bioavailable arsenic in contaminated soils and solid media. *Environ Sci Technol*: 642-649.
- Romoser AR, Chen PL, Berg JM, Seabury C, Ivanov I, Criscitello MF, Sayes CM. 2011. Quantum dots trigger immunomodulation of the NFκB pathway in human skin cells. *Mol Immunol* 48: 1349-1359.
- Rothen-Rutishauser B, Muhlfeld C, Blank F, Musso C, Gehr P. 2007. Translocation of particles and inflammatory responses after exposure to fine particles and nanoparticles in an epithelial airway model. *Part Fibre Toxicol* 4: 9.
- Rothen-Rutishauser BM, Schurch S, Haenni B, Kapp N, Gehr P. 2006. Interaction of fine particles and nanoparticles with red blood cells visualized with advanced microscopic techniques. *Environ Sci Tech* 40: 4353-4359.

- Ruezel P, Bruijntjes J, Feron V, Woutersen R. 1991. Subchronic inhalation toxicity of amorphous silicas and quartz dust in rats. *Fund Chem Toxicol* 29: 341-352.
- Sadauskas E, Jacobsen NR, Danscher G, Stoltenberg M, Vogel U, Larsen A, Kreyling W, Wallin H. 2009. Biodistribution of gold nanoparticles in mouse lung following intratracheal instillation. *Chem Central J* 3: 16.
- Sager T, Porter D, Robinson V, Lindsley W, Schwegler-Berry D, Castranova V. 2007. Improved method to disperse nanoparticles for *in vitro* and *in vivo* investigation of toxicity. *Nanotoxicology* 1: 118-129.
- Santhanam P, Wagner JG, Elder A, Gelein R, Carter JM, Driscoll KE, Oberdorster G, Harkema JR. 2008. Effects of subchronic inhalation exposure to carbon black nanoparticles in the nasal airways of laboratory rats. *Internat J Nanotech* 5: 30-54.
- Savic R, Luo L, Eisenberg A, Maysinger D. 2003. Micellar nanocontainers distribute to defined cytoplasmic organelles. *Science* 615: 615-618.
- Sayes C, Ivanov I. 2010. Comparative study of predictive computational models for nanoparticle-induced cytotoxicity. *Risk Anal* 30: 1723-1734.
- Sayes CM, Fortner JD, Guo W, Lyon D, Boyd AM, Ausman KD, Tao YJ, Sitharaman B, Wilson LJ, Hughes JB, West JL, Colvin VL. 2004. The differential cytotoxicity of water-soluble fullerenes. *Nano Lett* 4: 1881-1887.
- Sayes CM, Gobin AM, Ausman KD, Mendez J, West JL, Colvin VL. 2005. Nano-C-60 cytotoxicity is due to lipid peroxidation. *Biomater* 26: 7587-7595.
- Sayes CM, Wahi R, Kurian PA, Liu YP, West JL, Ausman KD, Warheit DB, Colvin VL. 2006. Correlating nanoscale titania structure with toxicity: A cytotoxicity and inflammatory response study with human dermal fibroblasts and human lung epithelial cells. *Toxicol Sci* 92: 174-185.
- Sayes CM, Warheit DB. 2009. Characterization of nanomaterials for toxicity assessment. *Nanomed Nanobiotech* 1: 660-670.
- Schellenberger E, Schnorr J, Reutelingsperger C, Ungethum L, Meyer W, Taupitz M, Hamm B. 2008. Linking proteins with anionic nanoparticles via protamine: Ultrasmall protein-coupled probes for magnetic resonance imaging of apoptosis. *Small* 4: 225-230.
- Schins RPF. 2002. Mechanisms of genotoxicity of particles and fibers. *Inhal Toxicol* 14: 57-78.

- Schmidt CW. 2009. Nanotechnology-related environment, health, and safety research: Examining the national strategy. *Environ Health Perspect* 117: A158-61.
- Schoepf U, Marecos EM, Melder RJ, Jain RK, Weissleder R. 1998. Intracellular magnetic labeling of lymphocytes for in vivo trafficking studies. *Biotechniques* 24: 642-651.
- Schottenfeld D, Beebe-Dimmer J. 2006. Chronic inflammation: A common and important factor in the pathogenesis of neoplasia. *CA: Cancer J Clin* 56: 69-83.
- Schulte PA, Schubauer-Berigan MK, Mayweather C, Geraci CL, Zumwalde R, Mckernan JL. 2009. Issues in the development of epidemiologic studies of workers exposed to engineered nanoparticles. *J Occupat Environ Med* 51: 323-35.
- Semmler-Behnke M, Takenaka S, Fertsch S, Wenk A, Seitz J, Mayer P, Oberdorster G, Kreyling WG. 2007. Efficient elimination of inhaled nanoparticles from the alveolar region: Evidence for interstitial uptake and subsequent reentrainment onto airway epithelium. *Environ Health Perspect* 115: 728-733.
- Serpone N, Salinaro A, Emeline AV. 2001. Deleterious effects of sunscreen titanium dioxide nanoparticles on DNA. Efforts to limit DNA damage by particle surface modification. *Proceed SPIE* 4258: 86-98.
- Sharma M. 2010. Understanding the mechanism of toxicity of carbon nanoparticles in humans in the new millennium: A systemic review. *Indian J Occupat Environ Med* 14: 3-5.
- Shen B, Scaiano JC, English AC. 2006. Zeolite encapsulation decreases TiO₂-sensitized ROS generation in cultured skin fibroblasts. *Photochem Photobiol* 82: 5-12.
- Shi XL, Castranova V, Halliwell B, Vallyathan V. 1998. Reactive oxygen species and silica-induced carcinogenesis. *J Toxicol Environ Health B-Crit Rev* 1: 181-197.
- Shukla A, Timblin C, Berube K, Gordon T, Mckinney W, Driscoll K, Vacek P, Mossman BT. 2000. Inhaled particulate matter causes expression of nuclear factor (NF)-kappaB-related genes and oxidant-dependent NF-kappaB activation *in vitro*. *Am J Respir Cell Mol Biol* 23: 182-7.
- Singh A, Misra V, R.K. T, Lee H, Ames S, Hoque M, Herman J, Sb B, Sidransky D, Gabrielson E. 2006. Dysfunctional KEAP1-NRF2 interaction in non-small-cell lung cancer. *PLoS One* 3: e420.
- Soh N. 2006. Recent advances in fluorescent probes for the detection of reactive oxygen species. *Anal Bioanal Chem* 386: 532-543.

- Song Y, Li X, Du X. 2009. Exposure to nanoparticles is related to pleural effusion, pulmonary fibrosis and granuloma. *Eur Respir J* 34: 559-67.
- Stoeger T, Takenaka S, Frankenberger B, Ritter B, Karg E, Maier K, Schultz H, Schmid O. 2009. Deducing *in vivo* toxicity of combustion-derived nanoparticles from a cell-free oxidative potency assay and metabolic activation of organic compounds. *Environ Health Perspect* 1: 54-60.
- Stone V, Shaw J, Brown DM, Macnee W, Faux SP, Donaldson K. 1998. The role of oxidative stress in the prolonged inhibitory effect of ultrafine carbon black on epithelial cell function. *Toxicol In Vitro* 12: 649-59.
- Stringer B, Imrich A, Kobzik L. 1996. Lung epithelial cell (A549) interaction with unopsonized environmental particulates: Quantitation of particle-specific binding and IL-8 production. *Exp Lung Res* 22: 495-508.
- Swanson JA, Watts C. 1995. Macropinocytosis. *Trends Cell Biol* 5: 424-428.
- Szabó T, Berkesi O, Forgó P, Josepovits K, Sanakis Y, Petridis D, Déckány I. 2006. Evolution of surface functional groups in a series of progressively oxidized graphite oxides. *Chem Mater* 18: 2740-2749.
- Tago T, Tashiro S, Hashimoto Y, Wakabayashi K, Kishida M. 2003. Synthesis and optical properties of SiO₂-coated CeO₂ nanoparticles. *J Nanopart Res* 5: 55-60.
- Tedesco S, Doyle H, Redmond G, Sheehan D. 2008. Gold nanoparticles and oxidative stress in *Mytilus edulis*. *Mar Environ Res* 66: 131-3.
- Thomassen LCJ, Aerts A, Rabolli V, Lison D, Gonzalez L, Kirsch-Volders M, Napierska D, Hoet PHM, Kirschhock C, Martens J. 2009. Synthesis and characterization of stable monodisperse silica nanoparticle sols for *in vitro* cytotoxicity testing. *Langmuir* 26: 328-335.
- Tirumalai R, Kumar T, Mai K, Biswal S. 2002. Acrolein causes transcriptional induction of phase II genes by activation of Nrf-2 in human lung type II epithelial (A549) cells. *Toxicol Lett*: 27-36.
- Tiyaboonchai W, Limpeanchob N. 2007. Formulation and characterization of amphotericin B-chitosan-dextran sulfate nanoparticles. *Internat J Pharm* 329: 142-149.
- Trouiller B, Reliene R, Westbrook A, Solaimani P, Schiestl RH. 2009. Titanium dioxide nanoparticles induce DNA damage and genetic instability *in vivo* in mice. *Cancer Res* 69: 8784-9.

- The Royal Society. 2004. Nanoscience and nanotechnologies: opportunities and uncertainties. Accessed May 2011 from the website: <http://www.nanotec.org.uk/finalReport.htm>.
- Uboldi C, Bonacchi D, Lorenzi G, Hermanns MI, Pohl C, Baldi G, Unger RE, Kirkpatrick CJ. 2009. Gold nanoparticles induce cytotoxicity in the alveolar type-II cell lines A549 and NCIH441. *Part Fibre Toxicol* 6: 18.
- Valberg PA, Long CM, Sax SN. 2006. Integrating studies on carcinogenic risk of carbon black: Epidemiology, animal exposures, and mechanism of action. *J Occupat Environ Med* 48: 1291-1307.
- Vallyathan V, Castranova V, Pack D, Leonard S, Shumaker J, Hubbs AF, Shoemaker DA, Ramsey DM, Pretty JR, McLaurin JL, Khan A, Teass A. 1995. Freshly fractured quartz inhalation leads to enhanced lung injury and inflammation - Potential role of free-radicals. *Am J Resp Crit Care Med* 152: 1003-1009.
- Vallyathan V, Shi XL, Dalal NS, Irr W, Castranova V. 1988. Generation of free-radicals from freshly fractured silica dust - Potential role in acute silica-induced lung injury. *Am RevRespir Dis* 138: 1213-1219.
- Verma A, Uzun O, Hu Y, Han HS, Watson N, Chen S, Irvine DJ, Stellacci F. 2008. Surface-structure-regulated cell-membrane penetration by monolayer-protected nanoparticles. *Nat Mater* 7: 588-95.
- Vippola M, Falck GCM, Lindberg HK, Suhonen S, Vanhala E, Norppa H, Savolainen K, Tossavainen A, Tuomi T. 2009. Preparation of nanoparticle dispersions for in-vitro toxicity testing. *Human Experiment Toxicol* 28: 377-385.
- Von Klot S, Wolke G, Tuch T, Heinrich J, Dockery DW, Schwartz J, Kreyling W, Wichmann HE, Peters A. 2002. Increased asthma medication use in association with ambient fine and ultrafine particles. *Eur Respir J* 20: 691-702.
- Vorbau M, Hillemann L, Stintz M. 2009. Method for the characterization of the abrasion induced nanoparticles release into air from surface coatings. *J Aerosol Sci* 40: 209-217.
- Wagner AJ, Bleckmann CA, Murdock RC, Schrand AM, Schlager JJ, Hussain SM. 2007. Cellular interaction of different forms of aluminum nanoparticles in rat alveolar macrophages. *J Phy Chem B* 111: 7353-7359.
- Wang H, Joseph JA. 1999. Quantifying cellular oxidative stress by dichlorofluorescein assay using microplate reader. *Free Radic Biol Med* 27: 612-6.

- Wang L, Wang KM, Santra S, Zhao XJ, Hilliard LR, Smith JE, Wu JR, Tan WH. 2006. Watching silica nanoparticles glow in the biological world. *Anal Chem* 78: 646-654.
- Wang PW, Henning SM, Heber D. 2010. Limitations of MTT and MTS-based assays for measurement of antiproliferative activity of green tea polyphenols. *PLoS One*, 5:1932-6203. (10pp). doi 10.1371/journal.pone.0010202.
- Wang XJ, Sun Z, Villeneuve NF, Zhang S, Zhao F, Li YJ, Chen WM, Yi XF, Zheng WX, Wondrak GT, Wong PK, Zhang DD. 2008. Nrf2 enhances resistance of cancer cells to chemotherapeutic drugs, the dark side of Nrf2. *Carcinogenesis* 29: 1235-1243.
- Warheit DB, Webb TR, Colvin VL, Reed KL, Sayes CR. 2007a. Pulmonary bioassay studies with nanoscale and fine-quartz particles in rats: Toxicity is not dependent upon particle size but on surface characteristics. *Toxicol Sci* 95: 270-280.
- Warheit DB, Webb TR, Reed KL, Frerichs S, Sayes CM. 2007b. Pulmonary toxicity study in rats with three forms of ultrafine-TiO₂ particles: Differential responses related to surface properties. *Toxicology* 230: 90-104.
- Wilson MR, Foucaud L, Barlow PG, Hutchison GR, Sales J, Simpson RJ, Stone V. 2007. Nanoparticle interactions with zinc and iron: Implications for toxicology and inflammation. *Toxicol App Pharm* 225: 80-89.
- Wilson MR, Lightbody JH, Donaldson K, Sales J, Stone V. 2002. Interactions between ultrafine particles and transition metals *in vivo* and *in vitro*. *Toxicol App Pharm* 184: 172-179.
- Wuelfing WP, Templeton AC, Hicks JF, Murray RW. 1999. Taylor dispersion measurements of monolayer protected clusters: A physicochemical method of nanoparticle size determination. *Abstracts Papers Am Chem So* 218: U139-U140.
- Xia T, Kovochich M, Brant J, Hotze M, Sempf J, Oberley T, Sioutas C, Yeh JI, Wiesner MR, Nel AE. 2006. Comparison of the abilities of ambient and manufactured nanoparticles to induce cellular toxicity according to an oxidative stress paradigm. *Nano Lett* 6: 1794-807.
- Xia T, Kovochich M, Liong M, Madler L, Gilbert B, Shi HB, Yeh JI, Zink JI, Nel AE. 2008a. Comparison of the mechanism of toxicity of zinc oxide and cerium oxide nanoparticles based on dissolution and oxidative stress properties. *Am Chem So Nano* 2: 2121-2134.

- Xia T, Rome L, Nel A. 2008b. Nanobiology: Particles slip cell security. *Nat Mater* 7: 519-20.
- Xie Y, Sherwood PMA. 1991. X-ray photoelectron-spectroscopic studies of carbon fiber surfaces. Part 13. Valence-band studies of oxidized fibers interpreted by X.alpha. calculations. *Chem Mater* 3: 164-168.
- Yamanaka N, Deamer D. 1974. Superoxide-dismutase activity in Wi-38 cell-cultures - Effects of age, trypsinization and Sv40 transformation. *Physiol Chem Phy* 6: 95-106.
- Yang G, Teague S, Pinkerton K, Kennedy I. 2001. Synthesis of an ultrafine iron and soot aerosol for the evaluation of particle toxicity. *Aerosol Sci Tech* 35: 759-766.
- Yang H, Liu C, Yang D, Zhang H, Xi Z. 2008. Comparative study of cytotoxicity, oxidative stress, and genotoxicity induced by four typical nanomaterials: the role of particle size, shape, and composition. *J App Toxicol* 29: 69-78.
- Yeganeh B, Kull CM, Hull MS, Marr LC. 2008. Characterization of airborne particles during production of carbonaceous nanomaterials. *Environ Sci Technol* 42: 4600-6.
- Yokel R, Florence R, Unrine J, Tseng M, Graham U, Wu P, Grulke E, Sultana R, Hardas S, Butterfield D. 2009. Biodistribution and oxidative stress effects of a systemically-introduced commercial ceria engineered nanomaterial. *Nanotoxicology* 3: 234-248.
- York JL, Maddox LC, Zimniak P, Mchugh TE, Grant DF. 1998. Reduction of MTT by glutathione s-transferase. *Biotechniques* 25: 622.
- Yu K, Grabinski C, Schrand A, Murdock R, Wang W, Gu B, Schlager J, Hussain S. 2009. Toxicity of amorphous silica nanoparticles in mouse keratinocytes. *J Nanopart Res* 11: 15-24.
- Yuan H, Miao J, Du YZ, You J, Hu FQ, Zeng S. 2008. Cellular uptake of solid lipid nanoparticles and cytotoxicity of encapsulated paclitaxel in A549 cancer cells. *Int J Pharm* 348: 137-45.
- Yueh MF, Tukey RH. 2007. Nrf2-Keap1 signaling pathway regulates human UGT1A1 expression *in vitro* and in transgenic UGT1 mice. *J Biol Chem* 282: 8749-8758.
- Zhang LW, Monteiro-Riviere NA. 2009. Mechanisms of quantum dot nanoparticle cellular uptake. *Toxicol Sci* 110: 138-155.

- Zhang Q, Kusaka Y, Zhu X, Sato K, Mo Y, Kluz T, Donaldson K. 2003. Comparative toxicity of standard nickel and ultrafine nickel in lung after intratracheal instillation. *J Occup Health* 45: 23-30.
- Zhang Z, Kleinstreuer C, Donohue JF, Kim CS. 2005. Comparison of micro- and nano-size particle depositions in a human upper airway model. *J Aerosol Sci* 36: 211-233.
- Zhu H, Itoh K, Yamamoto M, Zweier JL, Li YB. 2005. Role of Nrf2 signaling in regulation of antioxidants and phase 2 enzymes in cardiac fibroblasts: Protection against reactive oxygen and nitrogen species-induced cell injury. *Febs Lett* 579: 3029-3036.
- Zhu H, Jia ZQ, Misra BR, Zhang L, Cao ZX, Yamamoto M, Trush MA, Misra HP, Li YB. 2008. Nuclear factor E2-related factor 2-dependent myocardial cytoprotection against oxidative and electrophilic stress. *Cardiovas Toxicol* 8: 71-85.

APPENDIX A

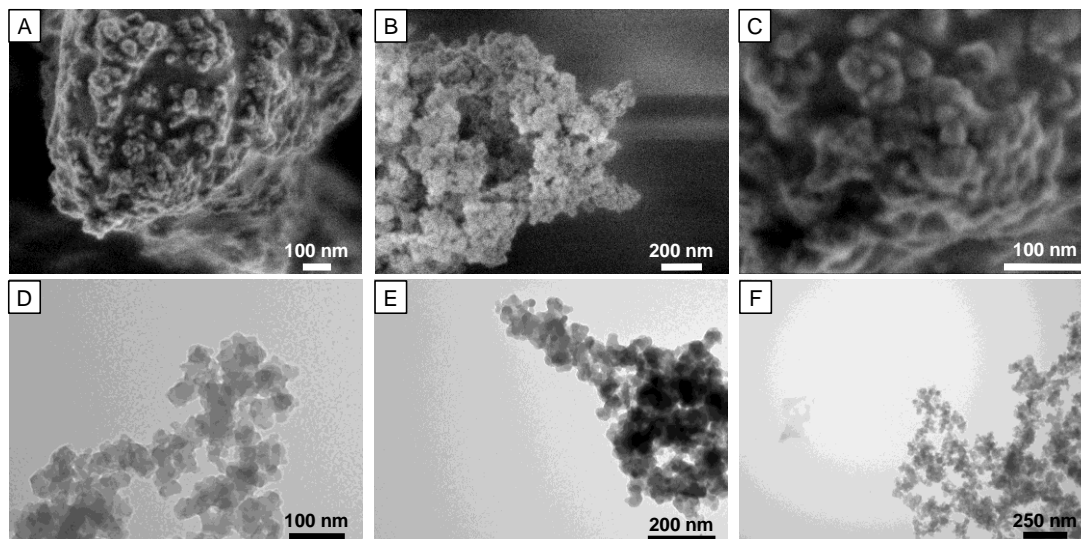


Figure A.1 Representative SEM and TEM images of SiO₂ nanoparticles. Scanning electron microscopy was performed on the SiO₂ nanoparticles in their powder form (A-C). Furthermore, transmission electron microscopy (D-F) of grid-deposited SiO₂ nanoparticles assisted in primary particle size determination.

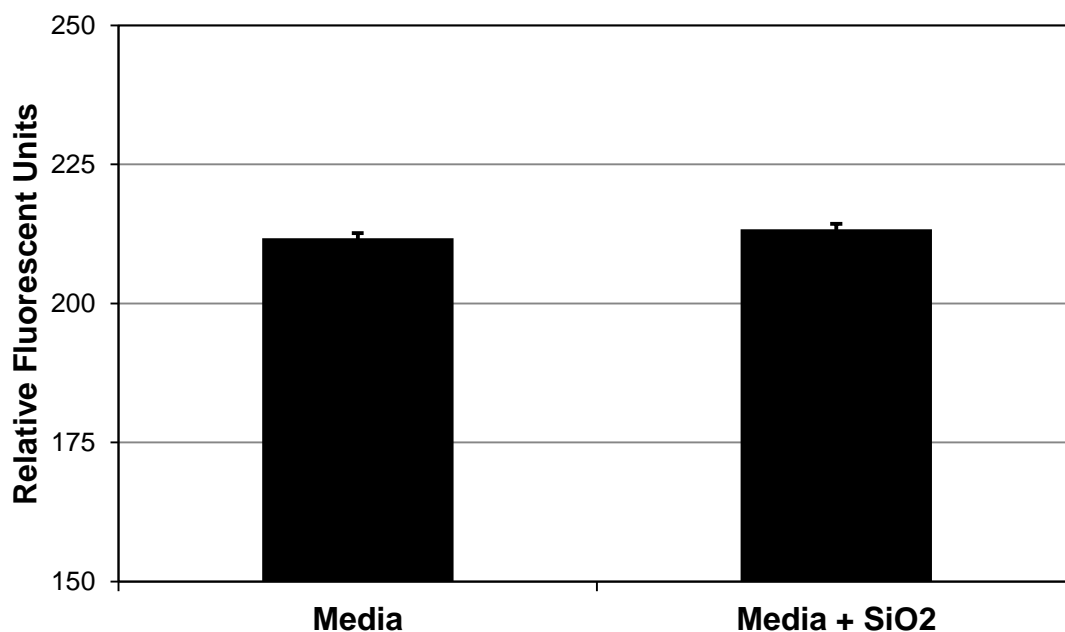


Figure A.2 SiO₂ nanoparticles do not interfere with the DCFH-DA assay. SiO₂ nanoparticles do not exhibit fluorescent properties that interfere with the DCFH-DA assay. Measurement of fluorescence in SiO₂-containing media did not differ significantly from media alone.

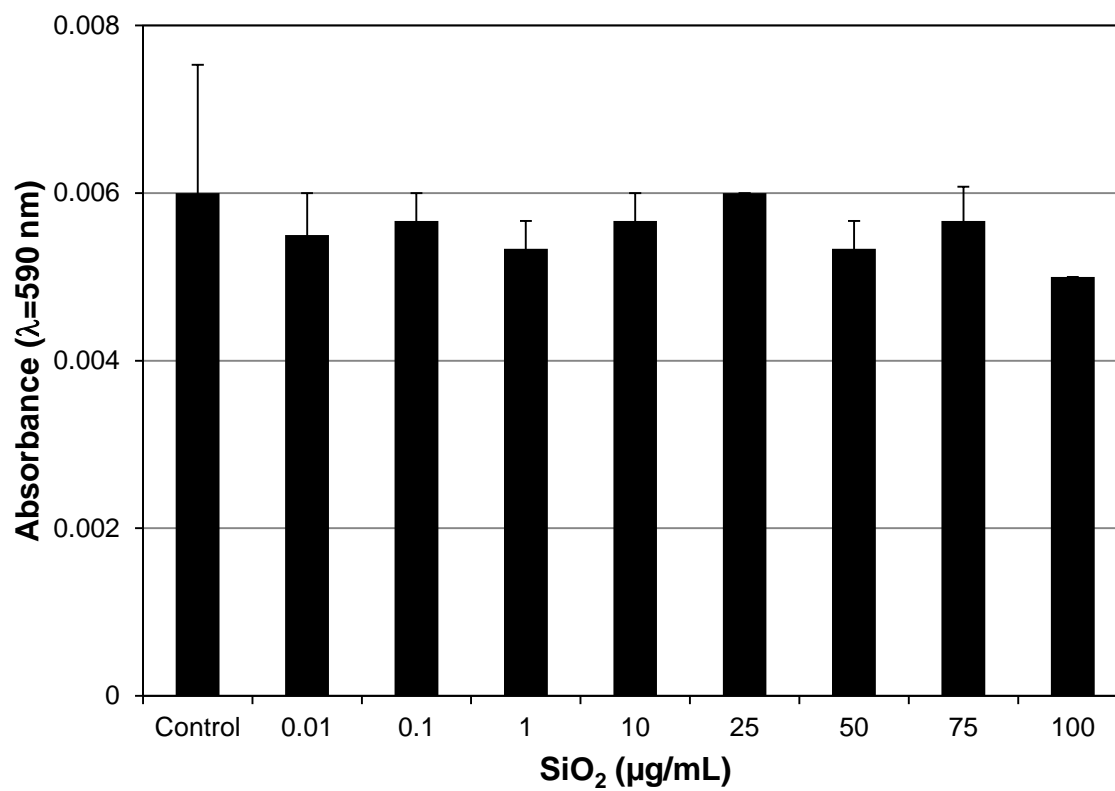


Figure A.3 SiO₂ nanoparticles do not interfere with the MTT assay. SiO₂ nanoparticles incubated at various doses (0.01 -100 mg/mL) did not cause altered media absorbance from that of control medium at 570 nm.

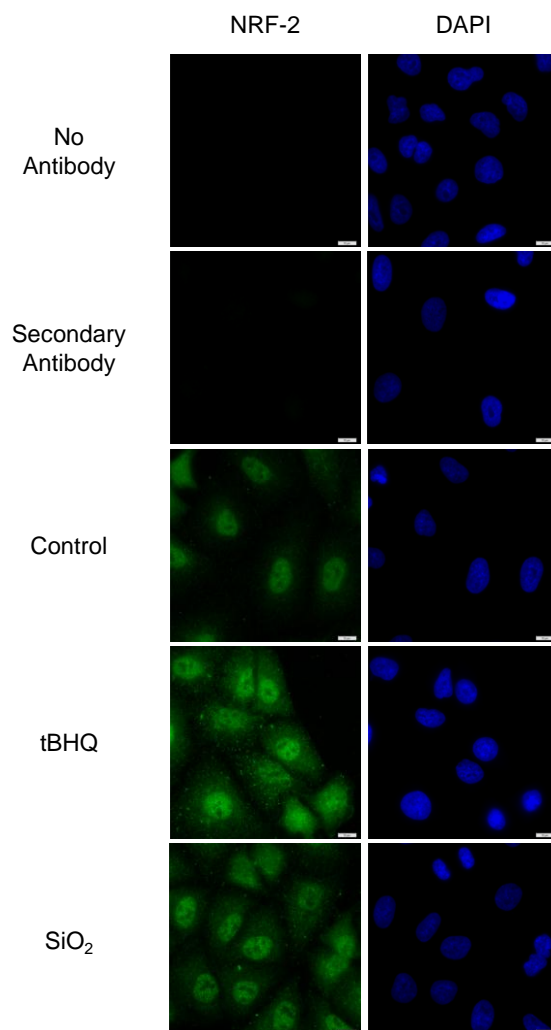


Figure A.4 Single channel micrographs of NRF2 translocation in A549 cells. Single channel micrographs indicate minimal cellular autofluorescence or non-specific antibody binding in the A549 cell line. Scale bar = 10 μ M.

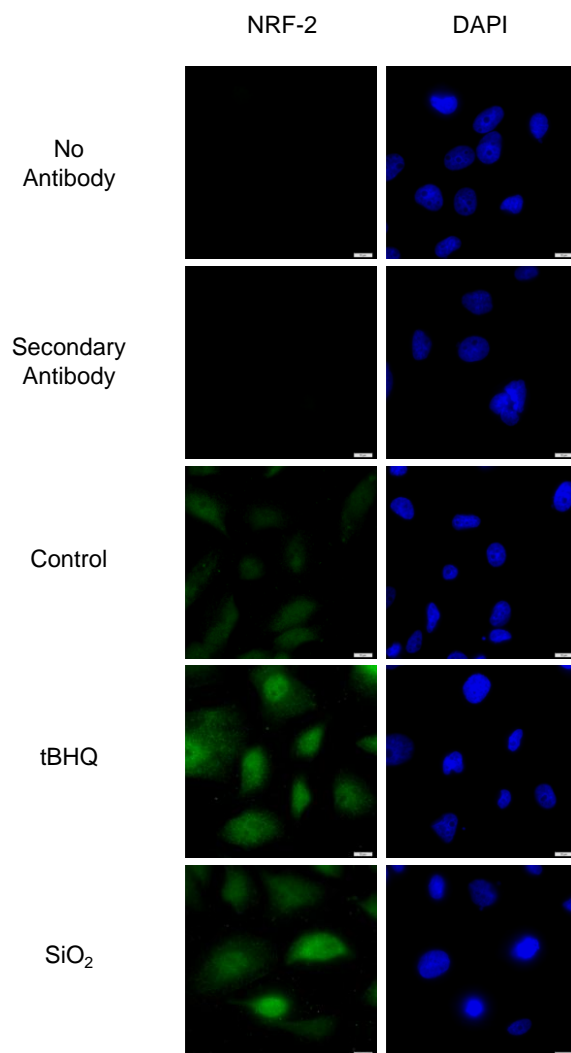


Figure A.5 Single channel micrographs of NRF2 translocation in MeT-5A cells. Single channel micrographs indicate minimal cellular autofluorescence or non-specific antibody binding in the MeT-5A cell line. Scale bar = 10 μ M.

VITA

James Michael Berg received his Bachelor of Science in Biology from Baylor University in 2007. Following graduation from Baylor, he entered the Toxicology Program at Texas A&M University where he completed his Doctoral degree in 2011. While at Texas A&M University, he published multiple peer-reviewed manuscripts with emphasis on nanoparticle characterization, nanoparticle mixtures and subsequent biological responses following nanoparticle exposure. His work has been featured in the journal *Nanotoxicology*, and on the cover of *Chemical Research in Toxicology*.

During his education at Texas A&M University, James Michael Berg served the Society of Toxicology on the Student Advisory Council, the Regional Chapter and Special Interest Group Graduate Committee, and as the Student Representative for the Gulf Coast Society of Toxicology. Through these roles, he helped to facilitate member coordination and communication at both the regional and national levels.

J. Michael Berg plans to utilize his background in toxicology as a health scientist in an effort to assess potential health risks associated with exposure to various chemicals.

J. Michael Berg can be reached at:

Department of Veterinary Physiology and Pharmacology

Texas A&M University MS4466

College Station, TX 77843

His email address is jmichaelberg@att.net